BROWN BOVERI REVIEW

RECEIVED
JUN 15 1960
INSTITUTE OF THE AERONAUTICAL SCIENCES

Celebrating the 18th CIGRE, Paris 1960

BOVERI REV. VOL. 47 No. 5/6 p. 281–372 BADEN, MAY/JUNE 1960

Printed in Switzerland

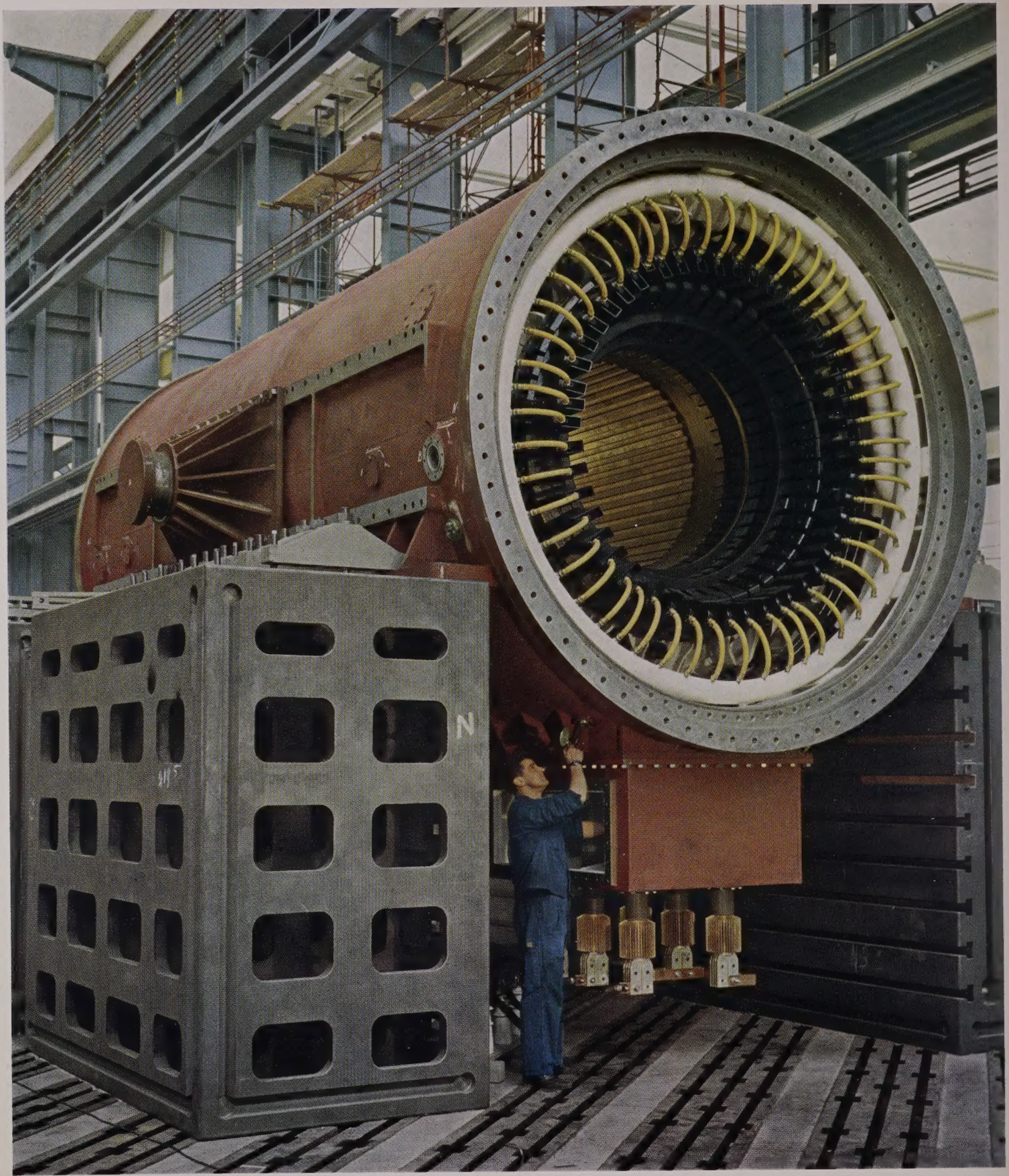

Stator of the 219-MVA three-phase alternator for Amer power station of the Noordbrabantsche Electriciteits Mij., Geertruidenberg (Holland), shown on test in the new Birrfeld factory. The connections for liquid cooling of the stator winding, also the terminals underneath the frame are clearly visible in the picture

Front cover: One of the three main single-phase auto-transformers for the Sils power station of the Kraftwerke Hinterrhein AG., Switzerland. Three such transformers with their regulating transformers form a three-phase bank rated 420/280/2 × 72·5 MVA. These transformers step up the output of Sils generating station to 220 and 400 kV, and at the same time provide a coupling between the 220 and 400-kV systems

THE BROWN BOVERI REVIEW

ISSUED BY BROWN, BOVERI & COMPANY, LIMITED, BADEN (SWITZERLAND)

VOL. 47 MAY / JUNE 1960 No. 5/6

The Brown Boveri Review appears monthly — Reproduction of articles or illustrations is permitted subject to full acknowledgement

CONTENTS:

	Page
H. Meyer: Celebrating the 18th CIGRE, Paris 1960	283
W. Frey: The Employment of Electronic Computers for the Solution of Problems Associated with the Generation and Distribution of Electricity	284
A. Edlinger: Auto-Transformers for 400/220 kV	292
H. Hartmann and B. Gänger: A New Design of Voltage Transformer for Extremely High Voltages	306
M. Christoffel and A. Kuster: Calculation of Short-Circuit Stresses in Transformer Windings with the Aid of Digital Computers	321
P. Baltensperger and E. Ruoss: The Short-Line Fault in High-Voltage Systems	329
R. Petitpierre: Airblast Circuit-Breakers for Extremely Heavy Duty	339
A. de Quervain and C. Hahn: Carrier Transfer for High-Speed Distance Protection	345
O. Wohlfahrt, M. Moravec, B. Doljak: Micadur—A New Insulation for the Stator Windings of Electrical Machines	352
A. Dudler: Tests on Various Methods of Voltage Control for Use with Large Generators	361

CELEBRATING THE 18TH CIGRE, PARIS 1960

THE INTERNATIONAL Conference of Large Electrical Systems, perhaps better known by its abbreviated French title CIGRE, is taking place between June 15th and 25th in Paris this year, for the eighteenth time in its history. Since the 1920s this biennial event has been the meeting-place of specialists from all over the world in the field of power engineering, especially those interested in generators, transformers, transmission lines, switchgear and protective gear. Here the plant and system engineers are joined by the research workers and the representatives of the manufacturers. It affords an excellent opportunity for them to discuss problems of mutual interest and to keep abreast of modern technical developments.

Since, for obvious reasons, the number of reports submitted to the Conference has to be limited, those published by members of this Company can only cover a few of the problems which have actually been investigated. Therefore we have selected some of the most interesting subjects which come in the sphere of CIGRE activity and publish reports on them in this special number of the Review. We feel sure that these will interest specialist readers, particularly those participating in this year's CIGRE meeting.

H. Meyer

(KME)

THE EMPLOYMENT OF ELECTRONIC COMPUTERS FOR THE SOLUTION OF PROBLEMS ASSOCIATED WITH THE GENERATION AND DISTRIBUTION OF ELECTRICITY

681.14:621.31

The problems which have to be faced in modern power systems demand thorough mathematical investigation. After reviewing their special structure, the author lays down methodical rules for the mathematical analysis of problems associated with the generation and distribution of electricity. It is evident that, to cope with the immense amount of numerical work involved, three different mathematical machines may be employed with advantage: namely an a.c. network analyser, an analogue computer and a digital computer. Examples of investigations performed with the two latter computers are given to illustrate the considerations put forward.

THE USES to which electronic computers can be put in the solution of problems associated with the generation and distribution of electricity are extremely varied, and are growing all the time. Brown Boveri, Baden, now have the following equipment at their disposal, listed in the order in which individual machines were taken into service:

An a.c. network analyser
An analogue computer
A digital computer

A description of these mathematical aids will be given in a later number of this journal. But it is worth considering the special structure of power systems as objects to which the three mathematical machines mentioned above can be applied.

For the purpose of the present article a power system is considered to cover all the equipment involved in the generation, transmission, distribution and utilization of electricity. Thereby all elements covered by the amalgamation of various subordinate networks must also be included in the combined system. The definition of a power system covers a technical creation of tremendous proportions, extending hundreds or even thousands of kilometres. The reason why such systems must be treated as single, uniform organisms, even though they comprise dozens of subsidiary notworks, which may be under separate management or even in different countries, is quite simple. It must be remembered that all generators belonging to these networks must run in synchronism, and that a sustained short circuit at a central point could lead to the total collapse of the system. This huge organization possesses some very sensitive elements (e.g. overhead power lines) and the individual can only gain a very general picture of the whole system. Nevertheless, the organization as a whole functions remarkably well.

It would not be out of place to study the reasons for this success, particularly because these considerations lead to a closer appreciation of the three different kinds of mathematical machine.

The most important reason, without doubt, is the hierarchical structure of the power system, that is to say, the system is held together by connecting lines operating at different voltage levels. Generally the area covered is greater, the higher the particular voltage. Moreover, the topological structure of the systems becomes simpler with increasing voltage.

This structural property is joined by an equally vital functional property. This could almost be termed the hierarchy of effects because phenomena at low voltages only have a limited effect on a higher stage. This limitation, however, is only able to persist on this scale as a result of advances which have been made in control and protection techniques. This applies to both normal and fault conditions.

A well conceived system can only be exposed to harm if faults occur in the highest voltage stage which governs all others—not allowing for exceptional, extraordinary faults, of course. It is interesting to note that similar structures may also be encountered in biological and social organisms.

These remarks may be considered as answering the question raised in the introduction. The hierarchical structure of the system, together with the limitation of effects, makes it unnecessary for the system to be analysed as a whole—it would be quite impracticable anyway. In practice this means that, for problems applying principally to a particular voltage stage, the effect on the stages above and below can be completely ignored in favourable circumstances or represented in a simplified manner, provided due care is taken. This rule applies to planning, to the design of the machines and other equipment, to operation and, what is even more interesting in this respect, to the mathematical analysis of the many different phenomena encountered in power systems.

Up to now only the material aspect of the power system has been dealt with. The occasion to which this special number is devoted affords an excellent opportunity for introducing the human element. For interconnected power systems to function successfully it is essential for the various electricity undertakings to collaborate closely and in harmony with the manufacturers, who in turn must often collaborate with one another. This cooperation has long since spread beyond national frontiers.

I. Methodical Rules for the Mathematical Analysis of Problems Associated with Power Systems

A. Problems Affecting the System on a Large Scale

Under this heading we may expect problems which demand the analysis—in severely simplified form—of the whole system, or at least of its larger sub-divisions; for instance, the calculation of short-circuit powers, the flow of active and reactive power, or the stability. Such problems always affect one voltage stage more than the others. Thus the question may concern the short-circuit power at a point in the highest stage, or the stability during rapid reclosure of a connecting line in the medium range. In the first case the effect on the network with the highest voltage will be taken into account, with appreciably simplified conditions at the junctions with the lower-voltage networks. The simplification becomes most obvious when the short-circuit powers of the lower-voltage networks at the junction points are known. These networks can then be represented simply by an electromotive force and a reactance.

Considering a simple example, the simplifications will now be described as encountered with a problem affecting the medium-voltage range. Fig. 1 a shows the circuit diagram, already greatly simplified

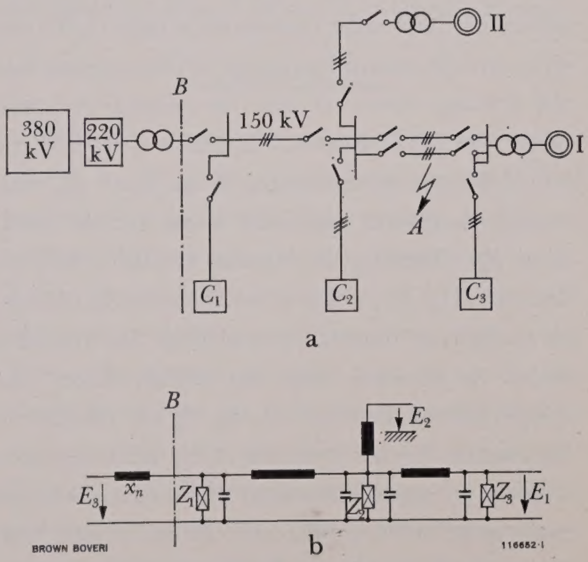

Fig. 1. – Equivalent circuit diagram for calculation of stability

a: Greatly simplified diagram of the part of the system being investigated

b: Equivalent circuit diagram

C_1, C_2, C_3 = Load centres

I, II = Generating stations

Z_1, Z_2, Z_3 = Equivalent impedances of the load centres

E_1, E_2, E_3 = Electromotive forces

The part of the system being investigated, as shown symbolically, is connected through a 220-kV system to a very powerful 380-kV system. The effect of those parts of the general system situated to the left of *B* can be represented by the reactance x_n and the e.m.f. E_3, there being no need for further knowledge of the 220 and 380-kV systems. Further relationships between *a* and *b* are obvious from the diagrams.

fied, of part of a large system. Only the immediately adjacent parts of the 380 and 220-kV systems are known, but we also know that the total installed capacity of the system is very large (infinite bus) compared with the outputs of the generating stations I and II. The question is whether the machines in station I will remain in synchronism when a short circuit in A is cleared with rapid reclosure. There is, of course, no need to stress that the exact details of such a fault have to be clearly defined.

Strictly speaking, the question is incorrectly posed. It is only permissible to speak of the stability of a single machine or generating station under special circumstances (see I. B. 2). In the present case it would be quite feasible for the generator II to fall out of step first, thereby hazarding generator I as well.

On account of the large capacity of the system it may be assumed that the phenomena in the subsidiary network under consideration fail to have any effect on the system frequency. Without going into the relevant theory it may be pointed out that, under the circumstances, the entire system to the left of B may be represented by an e.m.f. E_3, constant in magnitude and phase angle, and the reactance X_n. Omitting the details, attention may be drawn to Fig. 1 b, which shows the problem reduced to a system of impedances and three electromotive forces. As we know from the stability theory, the magnitudes of the e.m.f. E_1, E_2, E_3 are assumed to be constant for the duration of the fault condition and the subsequent transient phenomena, whereas their phase relationships vary in accordance with the rotor displacements. In the present case, however, due to the special assumptions which were made, the phase angle of E_3 is constant. By reducing the problem to one of three machines—the whole system may be treated as a machine with an infinitely large moment of inertia—it has been simplified to such an extent that analysis without the aid of computers, though laborious, is feasible without taking unduly long.

But conditions are not always so favourable, and it is sometimes necessary to take five or ten different machines into account, or even more. In such cases the use of a computer is essential. When employing computers, the procedure for which will be discussed later, it is important to consider the mathematical structure of the problem, as dealt with in this chapter.

Since the equivalent circuit diagram (Fig. 1 b) which has to be considered will always contain networks of varying degrees of complexity, these problems always involve a considerable amount of algebraic and arithmetical work. In stability calculations a system of high-order differential equations of simple structure has to be integrated.

B. Problems Affecting a Very Limited Part of the System

1. Fundamental problems

The engineer who has to deal with the problems of power systems uses a number of simplifying hypotheses. In the foregoing chapter it was demonstrated that, for instance, when investigating the stability, the machines concerned may be represented by an e.m.f. of constant amplitude and a series reactance. This hypothesis is based on precise knowledge of what occurs inside the machine. Moreover, it assumes that efficient voltage regulators are employed. With computers it is possible to check these hypotheses and obtain information regarding the influence of various parameters which do not appear at all in the simplified representation, for instance the short-circuit ratio of the generator and the response of the voltage regulators. No attempt will be made to list all the problems in this category, but it may be stated that many of the problems associated with overvoltages on transmission lines, produced by the operation of switchgear, are still waiting for a fundamental analysis.

2. Problems associated with specific phenomena in the system

In accordance with the considerations under I. A. let us assume that a synchronous motor is running in one of the load centres. The question to be answered is whether this machine will keep in synchronism during the fault or not, and whether the stability can be improved by super-excitation. The conditions closely resemble those of the stability problem discussed above. The motor is hardly likely to affect the voltage on the 150-kV side, therefore we may assume that it is connected through an equivalent reactance to an e.m.f. which, though not constant, varies according to a known function with time. But since the effect of voltage control also has to be investigated, the motor can no longer be represented by a simplified equivalent diagram. The complete system of equations for the machine will therefore have to be established. A similar investigation will be described briefly later (see III. A).

Another isolated problem of this kind arises in large systems when there is a surfeit of leading reactive power at times when the active power in the system is low, and this excess has to be absorbed by one or more machines. These machines are then severely under-excited, resulting in operating conditions which are only kept stable by the action of the voltage regulators. To assess the ability of a machine to absorb reactive power, a special kind of diagram was introduced not long ago, in which the entire system is normalized in an extraordinarily simple manner. These diagrams will be dealt with later in connection with the investigation of the effect of the damping winding on the special problem of stability.

In addition to the examples discussed, a brief reference may be made to the following problem: the variation of the terminal voltage of the synchronous machine under various operational conditions; above all, problems associated with the risk of self-excitation, in which the properties of the regulator are most important; the effect of overvoltages on power transformers, and so on.

A mathematical consideration which is important as regards these problems is that the algebraic portion rendered necessary by the network analysis is eliminated, but the system of differential equations which has to be dealt with is much more complex, owing to the fact that the machines and equipment have to be analysed more accurately than in the previous examples where, for instance for short-circuit calculations, they may be entirely algebraic. The analysis of large parts of the system requires an enormous amount of data, a complication which is not encountered with the problems dealt with in the previous chapter.

II. The Employment of Mathematical Machines

The fields of application of the three machines referred to at the beginning of this article overlap partly, so that it is not possible to allocate any single problem definitely to a particular machine. A brief summary of the main properties and limitations of the three types does, however, indicate how electronic aids can be rationally employed in this sphere. The following remarks are based on the equipment at present employed by Brown Boveri.

Network Analyser

Built as a single-purpose machine, this is employed, as its name suggests, for the analysis of problems associated with power systems, in particular those dealt with in the first chapter (see I. A.). From the mathematical aspect it is a machine which solves algebraic problems of a special nature. This is also a reason why this machine can be employed for certain problems not connected directly with networks. One the other hand it is incapable of integrating differential equations. For stability problems the equations have to be integrated step by step. But since it performs all the algebraic part of the work, the time it takes is not unduly long.

Analogue Computer

By nature the analogue computer is an analytical machine. Its strong point is the solution of ordinary differential equations; for algebraic problems, however, its use is rather limited. Its main sphere of activity is the group of problems dealt with earlier. One field for which it is exclusively reserved is simulation, e.g. of a synchronous machine. Since this application has already been described on more than one occasion [1, 2, 3][1], there is no need to give further details now.

Digital Computer and its Relationship to the Other Machines

This machine covers the widest range because it can solve algebraic and analytical problems. It thus competes with the two previously mentioned machines, with the exception of the simulation activity reserved for the analogue computer. But this does not necessarily mean that the digital computer is always superior to the other two machines. The questions arising out of this are at present the subject of lively discussion among the experts and can only be solved in full when sufficient experience has been gained in this still very new field. At this stage only two brief statements will be made: When the problem is to determine the transmission losses in a closely meshed system, the accuracy of the network analyser often does not meet the requirements, so that such problems usually have to be dealt with by the digital computer. The second case is the integration of systems of differential equations with partly discontinuous functions, such as are encountered in complicated control problems. These systems exhibit certain mathematical peculiarities for which the analogue computer is better suited.

Finally, the combined action of two machines may sometimes prove advantageous. This possibility was also allowed for when planning the new Brown Boveri computing centre (to be described in a later issue of this journal). For example, with stability problems, the algebraic part can be solved by the network analyser, the results yielding certain coupling coefficients and the initial conditions for the differential equations. Having obtained these data, integration can then be performed by the digital computer. Interesting possibilities are also offered by connecting the network analyser to the analogue computer. Each performs the task to which it is best suited; the analyser carries out the algebraic part, the computer copes with the differential equations.

III. Examples

A. An Investigation with the Analogue Computer

The investigation referred to in Section I. B. 1 is based on the following problem: As a result of a fault, the terminal voltage of a synchronous motor with a rating of 5000 kW drops to a certain level during a given time. The questions are:

How long may the system voltage drop to 0, 20, 40 or 60% of its nominal value without the motor losing synchronism?

To what sustained value may the voltage drop, regardless of duration, without the motor losing its synchronism?

For both questions the effect of super-excitation was also studied. The investigation was carried out on the analogue computer. For details of the procedure readers are referred to [3] in the bibliography. The results are tabulated below.

Time t_{max} during which the voltage may drop to ε% without the motor falling out of step

ε%	t_{max}		
	without super-excitation	with super-excitation	simplified calculation
0	0·41	0·42	0·42
20	0·63	0·64	0·59
26			∞
40	2·48	6·10	
42·5		∞	
56·6	∞		

The figures in the right-hand column were obtained with a simplified method of calculation, using the previously mentioned equivalent circuit diagram with an e.m.f. of constant amplitude and a series reactance. Above all, it is remarkable that, in the case of serious faults where the voltage drops to 0 — 20%, super-excitation has no effect on stability, whereas for the less severe faults its influence is pronounced. This result is explained by the fact that the duration of the serious faults in this case is of necessity the shortest, and naturally the super-excitation is unable to take effect.

---

[1] The figures in brackets refer to the bibliography on p. 291.

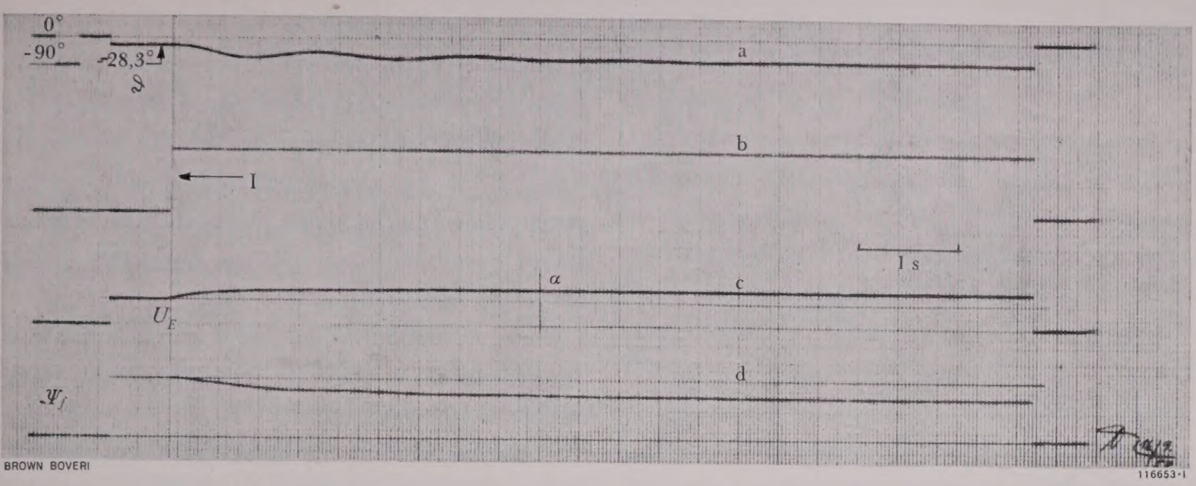

Fig. 2. – Investigating the stability of a 5500-kW synchronous motor, using an analogue computer

It is assumed that the terminal voltage of the motor drops to 42·5 % of its nominal value, due to a fault in the supply system.

a: Load angle of the motor δ
b: Marking the fault
c: Super-excitation voltage U_E
d: Flux linkage of the rotor winding Ψ_f

Despite the super-excitation, the flux linkage does not remain constant. For this reason, as explained in the text, the stability of the motor is not as good as expected from the calculation by the simplified method, as shown in the diagram in Fig. 1. By intensifying the super-excitation it is possible to prevent the drop in flux linkage. Thus the stability agrees closely to the result of the simplified calculation.

The last column of the table shows that, for very brief faults the result of the simplified calculation agrees with that given by the computer, or has an error of up to about 8%. But with the faults of infinite duration the difference is considerable. Calculation by the computer showed that with super-excitation the voltage may not drop below 42·5%, whereas the simplified method permits it to drop to 26%. The reason for this discrepancy is illustrated by Fig. 2. The lower trace shows the variation of the flux linkage of the rotor winding during the fault. In spite of super-excitation the flux linkage continues to decrease. The simplified method, however, assumes the flux linkage to be constant. From the oscillogram it can be seen that the super-excitation is not powerful enough to ensure constant flux linkage. Additional calculations carried out on the analogue computer showed that the super-excitation can be intensified to such an extent that the flux linkage remains constant. Then the agreement between the accurate and the simplified calculations is quite close.

The critical examination of the results contributed to the solution of the problems in the preceding chapter, by verifying the simplification hypotheses and the effect on the stability of one of the parameters.

B. Investigation with the Digital Computer

The problem to be investigated was the static stability of a turbo-alternator operating with severely reduced excitation. Particular interest was focussed on the effect of the damping winding. In the literature a standardized method has been adopted for the investigation of this problem. Firstly it is assumed that the machine is connected to an infinite bus through an external reactance x_e (Fig. 3), and that the voltage of the system does not agree with the value set on the voltage regulator. When the system voltage is high, the regulator causes the excitation of the generator to be reduced.

Fig. 4 shows one of the diagrams conventionally used for such problems. It is assumed that the terminal voltage of the machine is equal to the rated voltage. It is then clear that each point in the plane corresponds to an operating state of the machine. From every operating state illustrated by a point it is possible to state whether the machine is statically stable or not. To calculate the static stability various assumptions can be made. Consequently, various curves C can be plotted in the plane, separating the stable from the unstable states.

Curve C_1 applies when the terminal voltage is not controlled; in this case it represents the static stability with constant rotor current. In principle the damping winding has no effect on this stability.

Curve C_2 applies when the machine is controlled by an instantaneous regulator with proportional action. The curve represents the theoretical maximum attainable with this kind of control. Unexpectedly, the damping winding has practically no effect on the static stability defined in this manner. Curve C_2 is mainly interesting from the theoretical aspect. The states on it are in indifferent equilibrium and are therefore out of the question for practical operation.

The stability limit of the controlled machine was consequently re-calculated with changed assumptions. The new condition is based on the definition of synchronizing power

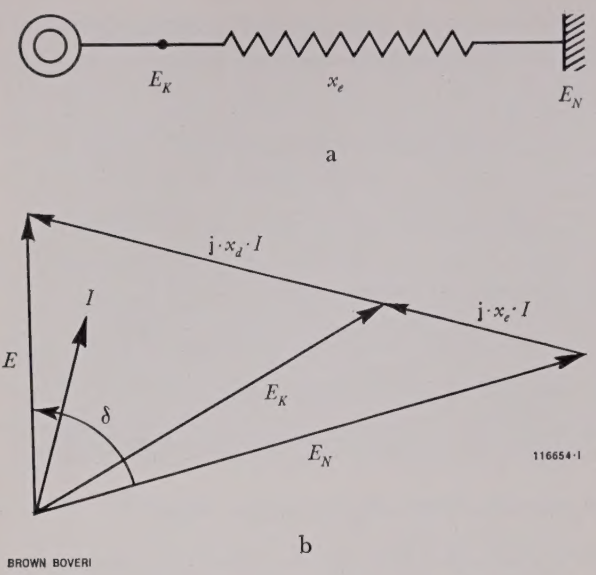

Fig. 3. – Stability of a turbo-alternator with severely reduced excitation, investigated with the aid of a digital computer

a: Schematic diagram
b: Vector diagram for the turbo-alternator
E_K = Terminal voltage
E_N = Voltage of the infinite bus (system)
E = Rotor voltage of the alternator
x_e = External reactance
x_d = Synchronous reactance
I = Stator current
δ = Displacement angle between E and E_N

When the voltage E_N of the system exceeds the rated terminal voltage E_K, the alternator runs under-excited.

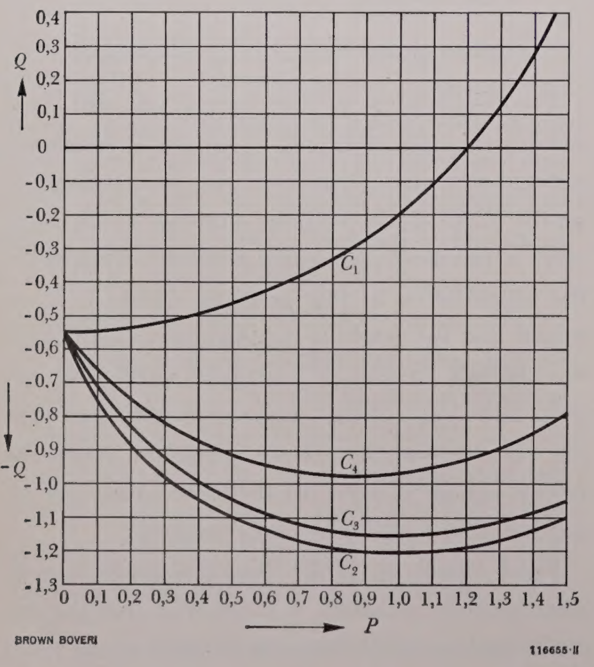

Fig. 4. – Diagram showing the states of the generator operating as in Fig. 3

P = Active power
Q = Reactive power
C_1 = Stability limit with constant rotor current
C_2 = Theoretical stability limit for the controlled machine
C_3 = Stability limit for the controlled machine assuming a non-vanishing synchronizing power $p_s = 0{\cdot}577$, as stated in the text
C_4 = As C_3, but for a machine with a damping winding

Above each curve operation is stable, below it is unstable.

Reactances: $x_d = x_q = 1{\cdot}8$
$x_e = 0{\cdot}4$
$x_d' = 0{\cdot}25$
$x_d'' = 0{\cdot}15$
$x_q'' = 0{\cdot}15$

Time constants: $T_d' = 0{\cdot}60$ s
$T_d'' = 0{\cdot}02$ s
$T_q'' = 0{\cdot}02$ s
$T_a = 10$ s

$$p_s = \frac{dP}{d\delta}$$

where P = active output

δ = displacement or load angle (see Fig. 3)

Generally p_s is only defined for the uncontrolled machine. It is nevertheless possible to define it for the controlled machine, as follows:

A displacement $d\delta$ produces a change in voltage at the terminals of the machine which, owing to the action of the regulator, changes the excitation current. Together with the angular change this produces a change dP in the active output, which will differ from that of the uncontrolled machine. It is, of course, assumed that all transients have decayed. Hence the above definition for p_s may be applied to the controlled machine with equal validity. If the active output is expressed to a per-unit basis, p_s becomes a mere number. For an uncontrolled solid-rotor machine producing rated output at a load angle of 60°, $p_s = \cot 60° = 0{\cdot}577$. Now it was assumed that the synchronizing power of the controlled machine was the same as that of the uncontrolled machine producing rated output at a load angle of 60°, i.e. $p_s = 0{\cdot}577$. Thus the curve C_3 is obtained for the machine with a damping winding, C_4 for one without.

In contrast to curve C_2, these show the pronounced effect of the damping winding. An attempt will not be made to explain the different effect of the damping winding, but it may be stated that, in the curves C_3 and C_4, the stability limit is defined by the action of the regulator provoking increasing oscillations of the synchronous machine. According to the results of the calculation the damping winding exerts an appreciable influence on the control system as a whole. In curve C_2 the stability is mainly governed by the properties of the synchronous machine, on which the damping winding has little influence.

(KME) W. FREY

Bibliography

[1] Brown Boveri Rev. 1957, Vol. 44, No. 1/2, p. 35.

[2] W. FREY: The Application of Theory and Electronic Computers to Automatic Control. Brown Boveri Rev. 1957, Vol. 44, No. 11, p. 468–72.

[3] P. COROLLER: Simulation of a Synchronous Machine with an Analogue Computer. Brown Boveri Rev. 1959, Vol. 46, No. 5, p. 299–306.

AUTO-TRANSFORMERS FOR 400/220 kV

621.314.223

The present article describes the design of the first 400-kV auto-transformers for mid-European e.h.v. systems. Following a brief reference to some of the fundamental problems and with the aid of illustrations of transformers already completed, the author explains the development which resulted in the design of these transformers after the introduction of solid earthing.

THE EMPLOYMENT of the "auto" connection for 400/220-kV coupling transformers has made it possible for e.h.v. transformers to be built in recent years with capacities not previously attained.

Having established a design of 220/150-kV auto-transformers [1],[1] and following successful development work in the sphere of 400-kV transformers [2, 3], Brown Boveri were in an excellent position to undertake the construction of such units and subsequently to turn out a remarkable number. As a result of the technical progress which has been made, auto-transformers are now just as dependable elements of power distribution systems as normal double-wound power transformers.

During this development programme it was possible to solve the technical problems associated with the complicated short-circuit conditions, regulation difficulties and the less favourable behaviour on impulse. These special features of the auto connection will now be dealt with briefly.

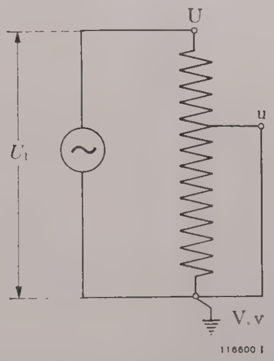

Fig. 1. – Auto-transformer, short circuit on the medium-voltage side

Short-Circuit Behaviour

Short-Circuit Flux Density

In contrast to normal transformers, the flux density produced in the iron core of an auto-transformer by a short circuit cannot be expressed directly in a very clear form. Let us consider a short circuit on the medium-voltage side[2] as illustrated, for instance, by Fig. 1. Obviously there is a very powerful leakage field present in this case, since, due to the short circuit, the full primary voltage is concentrated on the relatively small number of turns of the series winding. Therefore the opinion is frequently expressed that the iron core of an auto-transformer is considerably oversaturated in a system with infinite capacity, and there is no longer proportionality between the applied voltage and the short-circuit current.

It will now be demonstrated that this opinion is generally incorrect. For this purpose Fig. 2 shows the standard arrangement of the windings of an auto-transformer. They are arranged in natural order, that is, according to increasing potential. U and u denote the input terminals of the windings directly affected by the short circuit. In order that the flux density in the event of a short circuit may be expressed in a simple mathematical form, it is necessary to resort to the following artifice. The flux density is calculated by the roundabout route through the voltage induced in an imaginary, infinitely thin auxiliary winding immediately surrounding the core. The flux density in the yoke will be dealt with later.

---

[1] The figures in brackets refer to the bibliography on p. 305.

[2] In coupling auto-transformers the terms primary and secondary are unsuitable because they vary with the direction of flow of power. For the sake of clarity in this article the voltages are referred to as high, medium and low, respectively; e.g. 380/220/10 kV; also for transformers with no tertiary.

Supposing ε_{12} denotes the percentage reactance of the auto connection, referred to the throughput rating, ε_{N1}, ε_{N2} the associated system reactances to the same base, and ε_1, ε_2 the corresponding equivalent reactances of the three-winding transformer composed of 1, 2 and 4, the following relationships may be deduced, giving the flux density in the core during a three-phase short circuit, expressed as a percentage of the rated flux density:

$$p_1 = \frac{\bar{\varepsilon}_1}{\varepsilon_{N2} + \varepsilon_{12}}\, 100\,(\%) \qquad (1)$$

$$p_2 = \frac{\bar{\varepsilon}_2}{\varepsilon_{N1} + \varepsilon_{12}}\, 100\,(\%) \qquad (2)$$

where p_1 = percentage short-circuit flux density when the short circuit is on the high-voltage side,

p_2 = percentage short-circuit flux density when the short circuit is on the medium-voltage side.

A numerical example will help to clarify these conditions. In order to arrive at a statement which is generally applicable to the cases likely to be experienced, let us consider a transformer whose impedance voltage represents an average value, judging from units already produced. Such transformers have roughly the following data, related to one phase:

$$400/3 \text{ MVA}, \; 400/\sqrt{3} : 230/\sqrt{3} \text{ kV}$$

$$\varepsilon_{12} = 8{\cdot}5\,\%, \; \bar{\varepsilon}_1 = 9{\cdot}75\,\%, \; \bar{\varepsilon}_2 = -1{\cdot}25\,\%$$

Furthermore, we assume $\varepsilon_{N1} = \varepsilon_{N2} = 2{\cdot}6\,\%$, corresponding to fairly powerful systems. With these values the equations (1) and (2) yield the values

$$p_1 = 88\,\% \qquad |p_2| = 11\,\%$$

This somewhat unexpectedly favourable result implies that the flux density of the core remains *below* the rated figure, with both h.v. and m.v. short circuits.

Now let us examine the general relationship between normal and auto-transformers in this respect. For this we must compare units of the same internal rating and with the same winding geometry, it being immaterial in principle what voltage the series winding of the auto-transformer is allocated after conversion of the connections.

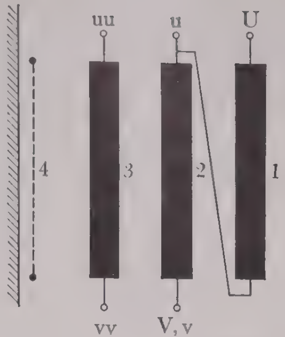

Fig. 2. – Arrangement of the windings in an e.h.v. auto-transformer

1 = Series winding
2 = Parallel winding
3 = Tertiary winding
4 = Imaginary auxiliary winding

A conversion of this kind is characterized by the following transformation equations, applicable to a three-winding transformer as in Fig. 2:

$$\begin{aligned}
\varepsilon_{12} &= \alpha \varepsilon'_{12} \\
\varepsilon_{13} &= \frac{1}{\alpha}\left[\varepsilon'_1 \alpha^2 + \varepsilon'_2\,(1-\alpha)^2 + \varepsilon'_3\right] \\
\varepsilon_{23} &= \frac{1}{\alpha}\,\varepsilon'_{23} \\
\varepsilon_1 &= \alpha\,\varepsilon'_{12} - \varepsilon'_2;\; \varepsilon'_1 = \frac{1}{\alpha}\,\varepsilon_{12} - \varepsilon_2 \\
\varepsilon_2 &= \varepsilon'_2 \\
\varepsilon_3 &= \frac{1}{\alpha}\,\varepsilon'_{23} - \varepsilon'_2 \\
\varepsilon_{N1} &= \frac{1}{\alpha}\,\varepsilon'_{N1} \\
\varepsilon_{N2} &= \frac{1}{\alpha}\,\varepsilon'_{N2}
\end{aligned} \qquad (3)$$

in which the auto fraction

$$\alpha = \frac{\text{Internal rating}}{\text{Throughput rating}}$$

$\varepsilon_{12}, \varepsilon_{13}, \varepsilon_{23}$ = winding
$\varepsilon_1, \varepsilon_2, \varepsilon_3$ = equivalent
$\varepsilon_{N1}, \varepsilon_{N2}$ = system
} reactances of the auto-transformer (referred to throughput rating)
$\varepsilon'_{12} \ldots \varepsilon'_{N2}$ = corresponding reactances of the normal transformer, referred to internal rating.

If the above transformation equations are now applied to the *normal (double-wound) transformer*, its short-circuit flux density can be expressed in terms of the quantities of the auto-transformer, the resultant ratio of the short-circuit flux densities being:

$$\frac{p'_1}{p_1} = \frac{100 - \alpha p_{20}}{100 - p_{20}} \cdot \frac{1 + \dfrac{\varepsilon_{N2}}{\varepsilon_{12}}}{1 + \alpha^2 \dfrac{\varepsilon_{N2}}{\varepsilon_{12}}} \tag{4}$$

$$\frac{p'_2}{p_2} = \frac{1 + \dfrac{\varepsilon_{N1}}{\varepsilon_{12}}}{1 + \alpha^2 \dfrac{\varepsilon_{N1}}{\varepsilon_{12}}} \alpha \tag{5}$$

in which p'_1, p'_2 are the flux densities with a short circuit on the h.v. or the m.v. side of the normal transformer

p_1, p_2 are the corresponding values for the auto-transformer

$p_{20} = \frac{\bar{\varepsilon}_2}{\varepsilon_{12}} 100$ is usually negative for conventional winding arrangements, and its absolute magnitude is very small.

The equations (4) and (5) yield the following remarkable result:

With normal transformation ratios and winding arrangements the behaviour of normal and auto-transformers with respect to the maximum short-circuit flux density (p_1 and p'_1) of the core in a system of infinite capacity is practically identical. In systems with limited capacity the short-circuit flux density of an auto-transformer is even smaller than that of a normal transformer.

Only with respect to the minimum short-circuit flux density of the core (p_2, p'_2) is the normal transformer more favourable than an auto-transformer. But then the densities experienced are so low that they lose all practical significance.

To explain this point let us consider the same transformer as above for a numerical example. The auto fraction $\alpha = 0{\cdot}425$. For the short-circuit flux density of the core with a short on the h.v. side (p_1, p'_1) and on the m.v. side (p_2, p'_2) we obtain the following values referred to the rated flux density:

	Auto	Normal
	transformer	
(a) Infinite system capacity	$p_1 = 115\%$ $\lvert p_2 \rvert = 15\%$	$p'_1 = 107\%$ $\lvert p'_2 \rvert \approx 6\%$
(b) Finite system capacity	$p_1 = 88\%$ $\lvert p_2 \rvert = 11\%$	$p'_1 = 101\%$ $\lvert p'_2 \rvert \approx 6\%$

In order to exclude any misapprehension, it may be pointed out that, due to its smaller impedance voltage, the *total* leakage flux of the auto-transformer is naturally greater than that of the normal transformer. But as is evident from the above argument, a considerable proportion of the leakage flux nevertheless spreads externally, i.e. surrounding the outer winding. Mathematically this can be demonstrated by the same method, considering an external auxiliary winding.

As will be explained later, the proportion of the flux obtained in this way may be considered as a second short-circuit leakage flux component of the auto-transformer. Whereas the flux component mentioned above as being only in the core is only linked with the inner winding (the common winding in the usual arrangement) and therefore only affects this winding, the second flux component only affects the outer winding (the series winding in the usual arrangement). To complete the picture these flux components are expressed as a percentage of the rated core flux by their linked amount, which only differs slightly from the true amount of the leakage flux, provided the radial dimensions of the winding are not too large. Then, depending on the position of the short circuit, the general expressions tabulated below apply:

	Short-circuit leakage flux linked with the	
	common winding	series winding
	expressed as % of rated core flux	
Short circuit on m.v. side (common winding short-circuited)	Zero (0 %)	$\frac{U_1}{U_s} \cdot \frac{100}{1 + \frac{\varepsilon_{N1}}{\varepsilon_{12}}}$ (180 %)
Short circuit on h.v. side	$\frac{100}{1 + \frac{\varepsilon_{N2}}{\varepsilon_{12}}}$ (77 %)	$\frac{U_2}{U_s} \cdot \frac{100}{1 + \frac{\varepsilon_{N2}}{\varepsilon_{12}}}$ (103 %)

(6)

where U_1, U_2 = Rated high and medium voltages

$U_S = U_1 - U_2$ = Rated voltage of series winding

ε_{N1}, ε_{N2} = System reactance referred to throughput rating

ε_{12} = Reactance of auto-transformer referred to throughput rating

The percentage values in brackets in the above table refer to the example quoted; for this transformer $\varepsilon_{12} = 8{\cdot}5\%$, $\varepsilon_{N1} = \varepsilon_{N2} = 2{\cdot}6\%$, $U_1 = 400$ kV, $U_2 = 230$ kV, $U_S = 170$ kV.

We observe that the magnitudes of the leakage fluxes of the common and series windings, which produce the short-circuit leakage field of the auto-transformer, differ appreciably from one another. In the cases considered in this article the short-circuit leakage flux linked with the common winding is below 100% (in the example 0 and 77%) whereas the series flux is over 100% (in the example 180 and 103%) referred to the rated core flux. Hence the behaviour of an auto-transformer with its series winding on the inside should be completely abnormal in the event of a short circuit on the m.v. side, but only in this case. The heavy flux surrounding the series winding would be driven through the core at full magnitude and would severely oversaturate it for practically the whole of its length. The outcome of this would be a much heavier current consumption and considerably higher short-circuit stresses in the series winding.

With the conventional winding arrangement however, the series winding is on the outside, so that its external field can now spread over a comparatively large area with parallel air and iron paths (yokes). This prevents the short-circuit flux density in the yokes of the auto-transformer from assuming inadmissibly high values.

From the above remarks it is apparent that the e.h.v. auto-transformer can be so designed that, as regards the short-circuit flux density in the core and yokes, its behaviour is not abnormal. With other winding arrangements, which will not be discussed here, the conditions can be determined exactly, using the procedure described.

Single-Phase Short Circuits

Auto-transformers experience no difficulties in handling three-phase short circuits. The share of the system in the total reactance then varies according to the impedance voltage and the throughput rating.

In solidly earthed systems, both normal and auto-transformers have also to reckon with earth faults which, as single-phase short circuits, can cause a severely unbalanced current distribution and may give rise to considerably heavier currents in the windings. These cases are dealt with by the well-known method of symmetrical components or with the aid of a network analyzer, if available.

These methods provide all the interesting quantities: the currents in the series, common and tertiary windings, as well as the current in the system and at the fault. Compared with the three-phase short circuit, however, the investigation of this kind of fault demands more complete knowledge of the system data, because in addition to the positive-sequence reactance, it is necessary for the negative-sequence and zero-sequence reactances to be known. If these values are not known such investigations naturally lose some of their value. The conditions in the system should at least be known approximately.

Owing to the large number of parameters the variety of short circuits is generally much greater than for three-phase faults. In 400- and 220-kV systems coupled through auto-transformers a primary condition is that both systems must be solidly earthed. Including the transformer being investigated, the state of the system is fixed provided the conditions on the l.v. (tertiary) side are known. In the latter case it is important to decide whether a tertiary supply source is available with an appreciable short-circuit capacity, or not. The latter is particularly true when the tertiary winding performs a purely balancing function. This is shown in Fig. 3 and 4.

The values quoted for the reactances of the system (positive, negative and zero-sequence reactances) correspond to three different sorts of short circuit on the h.v. and m.v. side referred to double, direct and indirect feed. The diagrams in Fig. 3 and 4 depict the different variants for finite and infinite short-circuit capacity of the system.

In order to stress the effect of the system data on the currents, the diagrams are augmented by the numerical values. These represent the sustained short-circuit currents in kA for the transformer mentioned above, assuming the positive-sequence and zero-sequence reactances are 3 and 6% respectively in the case in point.

Above all it may be seen that, both with direct and double feed and increasing short-circuit capacity in the system, the winding currents do not rise but

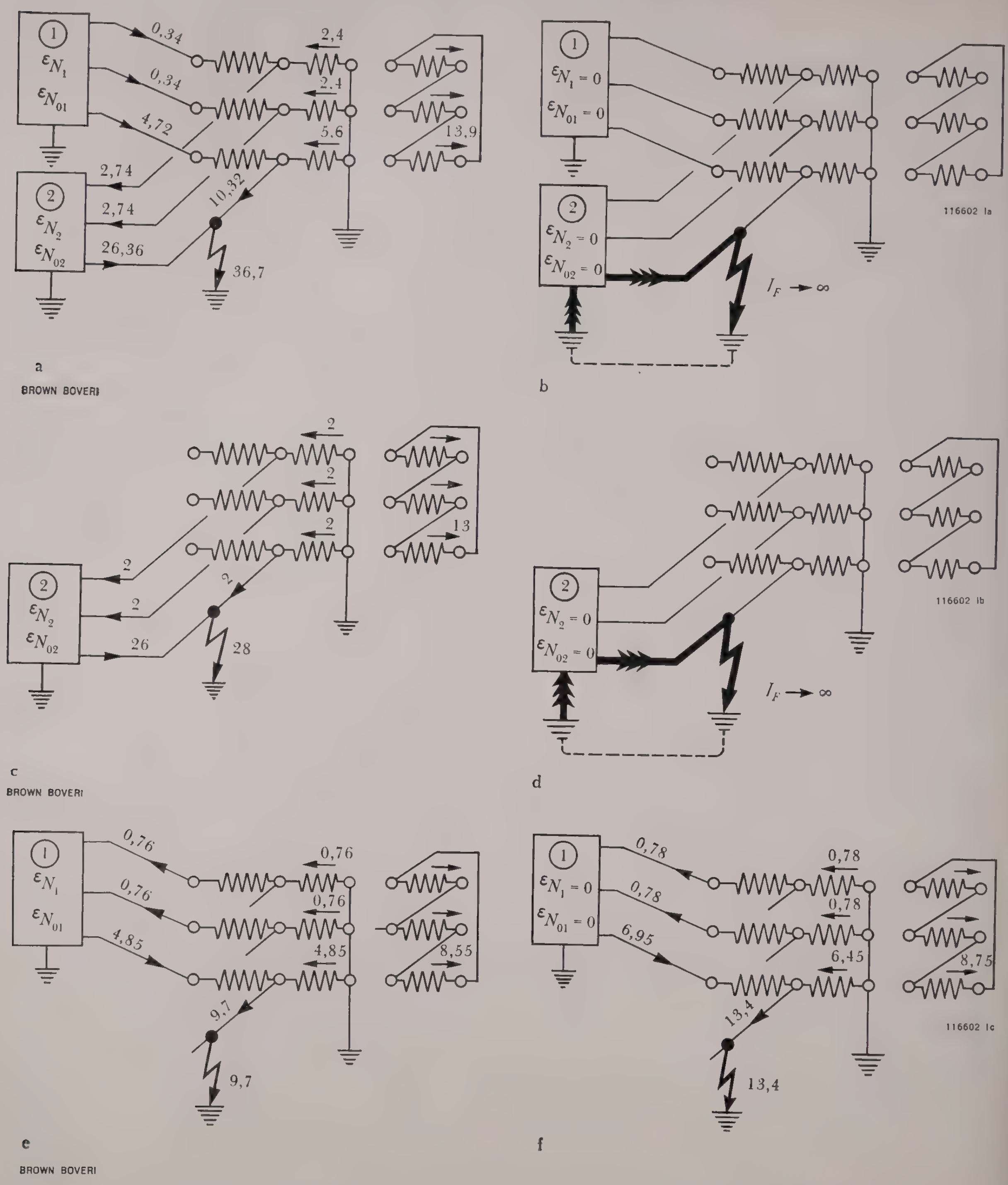

Fig. 3. – Single-phase earth fault on the m.v. terminal of an auto-transformer with negligible tertiary feed

Different kinds of short circuit and sustained fault currents (I_f) in kA with different system capacities.

Auto-transformer: 400 MVA, 400/230/20·5 kV
$\varepsilon_1 = 10{\cdot}25\,\%$
$\varepsilon_2 = -1{\cdot}75\,\%$
$\varepsilon_3 = 23{\cdot}75\,\%$
System: $\varepsilon_{N1} = \varepsilon_{N2} = 3\,\%$ or $0\,\%$
$\varepsilon_{N01} = \varepsilon_{N02} = 6\,\%$ or $0\,\%$
1, 2 = Power systems

a: double feed with finite short-circuit capacity in system
b: double feed with infinite capacity
c: direct feed with finite capacity
d: direct feed with infinite capacity
e: indirect feed with finite capacity
f: indirect feed with infinite capacity

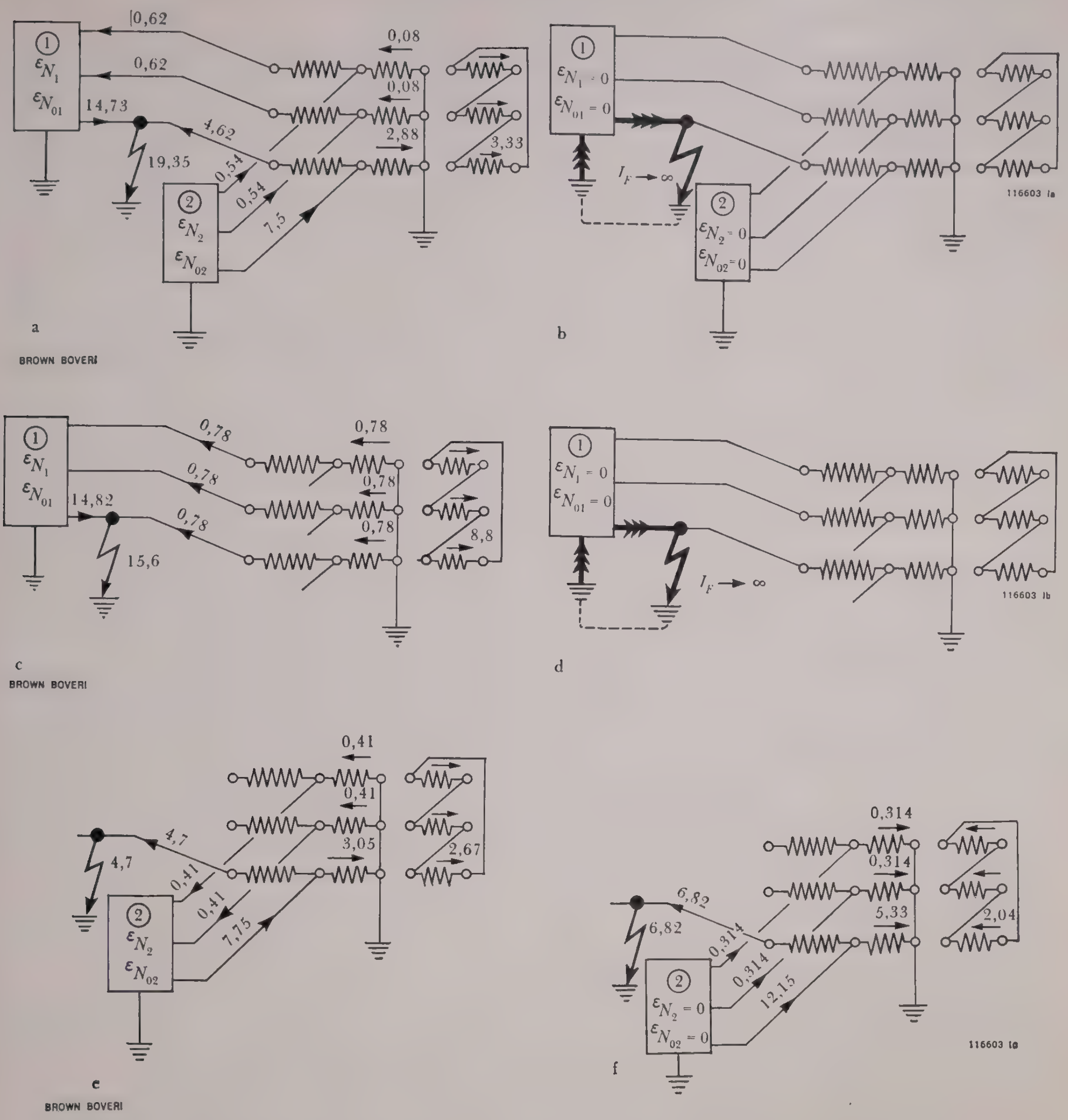

Fig. 4. – Single-phase earth fault at the h.v. terminal of an auto-transformer with negligible tertiary feed

Different kinds of short circuit and sustained fault currents (I_f) in kA with different system capacities.

Transformer and system data as in Fig. 3.

a: double feed with finite capacity
c: direct feed with finite capacity
e: indirect feed with finite capacity

b: double feed with infinite capacity
d: direct feed with infinite capacity
f: indirect feed with infinite capacity

drop towards zero (Fig. 3b, d; Fig. 4b, d). On the other hand the effect of infinite capacity with indirect feed is very clear (Fig. 3f and 4f). With finite capacity, however, the maximum current in the parallel winding occurs with a short circuit on the m.v. side and double feed (Fig. 3a). In all these cases the tertiary winding experiences only a small current, because the system is earthed on both sides.

With variable conditions in the system the current in the balancing winding is determined by the following expressions (7) and (8). These represent the current in its most general form and are thus applicable for double, indirect and direct feed and any earthing conditions. We thus obtain the current formulae applying in a limiting case, e.g. $\varepsilon_{N1} = \infty$, $\varepsilon_{N01} = \infty$ (h.v. system not feeding and unearthed), by simply forming limiting values:

(a) Single-phase short circuit on the h.v. side

$$I = \frac{100}{\varepsilon_{res1}} \cdot I_3 \cdot \frac{(\varepsilon_{N02} + \varepsilon_2)\, \varepsilon_{N01}}{(\varepsilon_{N01} + \varepsilon_{13})\,(\varepsilon_{N02} + \varepsilon_{23}) - \varepsilon_3^2} \qquad (7)$$

in which

$$\varepsilon_{res1} = 2\, \varepsilon_{N1} \cdot \frac{(\varepsilon_{N2} + \varepsilon_{12})}{\varepsilon_{N1} + \varepsilon_{N2} + \varepsilon_{12}} + \varepsilon_{N01} \cdot \frac{(\varepsilon_{N02} + \varepsilon_{23})\, \varepsilon_{13} - \varepsilon_3^2}{(\varepsilon_{N02} + \varepsilon_{23})\,(\varepsilon_{N01} + \varepsilon_{13}) - \varepsilon_3^2}$$

(b) Single-phase short circuit on the m.v. side:

$$I = \frac{100}{\varepsilon_{res2}} \cdot I_3 \cdot \frac{(\varepsilon_{N01} + \varepsilon_1) \cdot \varepsilon_{N02}}{(\varepsilon_{N01} + \varepsilon_{13})\,(\varepsilon_{N02} + \varepsilon_{23}) - \varepsilon_3^2} \qquad (8)$$

in which

$$\varepsilon_{res2} = 2 \varepsilon_{N2} \cdot \frac{(\varepsilon_{N1} + \varepsilon_{12})}{\varepsilon_{N1} + \varepsilon_{N2} + \varepsilon_{12}} + \varepsilon_{N02}\, \frac{(\varepsilon_{N01} + \varepsilon_{13})\, \varepsilon_{23} - \varepsilon_3^2}{(\varepsilon_{N01} + \varepsilon_{13})\,(\varepsilon_{N02} + \varepsilon_{23}) - \varepsilon_3^2}$$

In the above

I = Sustained short-circuit current in kA in the balancing winding

I_3 = Current in the balancing winding in kA, referred to load rating

$\varepsilon_1, \varepsilon_2, \varepsilon_3$ = Equivalent
$\varepsilon_{13}, \varepsilon_{23}$ = Winding
} reactances of the auto-transformer (referred to throughput rating)

$\varepsilon_{N1}, \varepsilon_{N2}$ = Positive-sequence
$\varepsilon_{N01}, \varepsilon_{N02}$ = Zero-sequence
} reactances of the systems (referred to throughput rating)

Voltage Regulation, Insulation

Especially for windings with graduated insulation it is most expedient for the voltage to be regulated at the neutral. The great disadvantage of the auto connection, however, is that it only permits this kind of control to a very limited extent, because it always involves a fairly large fluctuation in the flux density. It is this property of the auto-transformer which gives rise to most of its insulation problems.

In Fig. 5a the flux density attains its maximum (rated) value B_n and under the conditions shown in Fig. 5b drops to its minimum value βB_n. β denotes the reduction factor, u_R the rated voltage of the regulating winding while U and u are the two system voltages; then for step-up or step-down transformation

$$\beta = \frac{U_{min} - u_{max}}{U_{max} - u_{min}} \qquad (9)$$

$$u_R = \frac{U_{min}}{\beta} - U_{max} \qquad (10)$$

Suppose, for example $U_{max} = 420$ kV
$U_{min} = 380$ kV
$u_{max} = u_{min} = u = 230$ kV

then $\beta = 0{\cdot}79$
$u_R = 61$ kV

Thus, to correct a voltage fluctuation of only 10 % the flux density would have to vary by 21 % in the above case. Tapped windings as shown in Fig. 6b and c are therefore normally located at the high-voltage input.

An arrangement suitable for a wider range of regulation is shown in Fig. 6d. This kind of arrangement is known as direct control. Although in this case the regulating winding is at the input to the

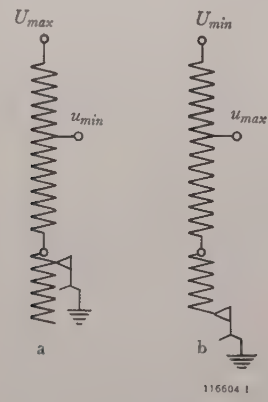

Fig. 5. – *Voltage regulation at the neutral point*

U_{max}, U_{min} High
u_{max}, u_{min} Medium
} service voltage limits

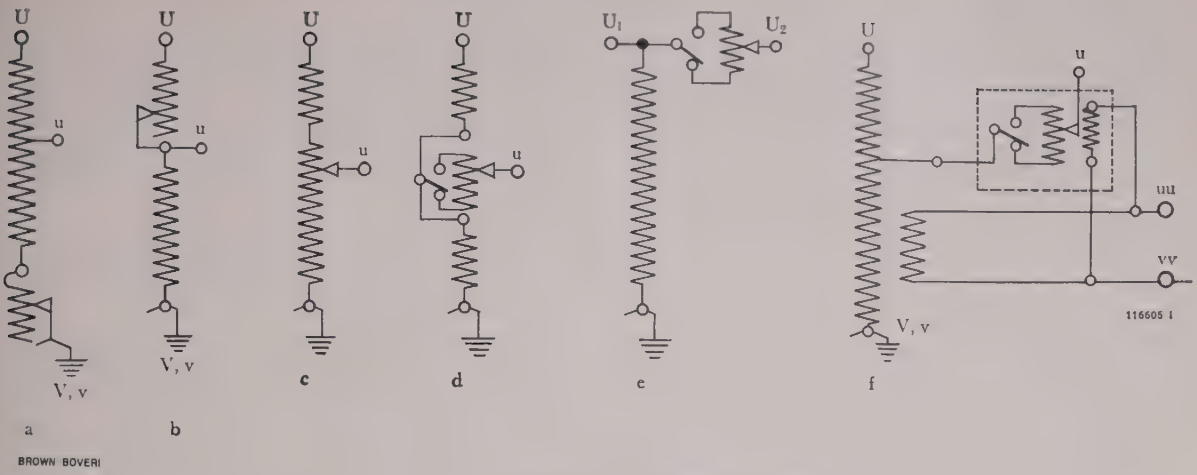

Fig. 6. – Arrangement of regulating winding

a: Regulation at neutral point
b, c, d, e: Direct regulation
f: Regulation by separate transformer (on-load tap changer at h.v. input)

transformer it is exposed to no greater surge stresses than with star-point regulation, provided it is correctly designed. Merely the potential to earth is somewhat higher, thus resulting in increased outlay for insulation. Brown Boveri employed this principle in the development of a design of single-phase regulating auto-transformer for 220/150 kV. These have given excellent results and 62 such units for a bank rating of 125 MVA have already been produced, the majority for installation in Swiss coupling stations, where the unit ratio is $250/\sqrt{3}:(202\text{-}140)/\sqrt{3}$ kV and the bank rating 125 MVA [1].

A special case of direct regulation is when the coupled systems have practically the same insulation level (as in Fig. 6e). In such cases, rare though they may be, a special form of tap-changer protection with a suitable lightning arrester connected across the regulating winding has been provided in almost every case so far. Impulse tests must then be carried out in conjunction with this protection. To observe the effect of the impulse it is convenient to employ the oil-pressure indicator [5].

Indirect regulation with a supplementary transformer (as in Fig. 5f) has the advantage of reducing the outlay for the main insulation and simplifying the design of the winding. Moreover, as a result of the division into a main and a regulating transformer, the transportability is also improved, provided the two are housed in separate tanks. Since this system of control can also be used for regulation with phase shifting, the above advantages become very important when dealing with transformers for very high capacities. The disadvantage is the greater amount of material involved. For very high ratings, in view of the very heavy current—which the on-load tap changer would hardly be capable of handling—it is advisable for the tap changer to be shifted from the low-voltage excitation circuit to the high-voltage input side, as shown in Fig. 6f.

Apart from regulation in the low-voltage excitation circuit as mentioned above, regulation by a separate transformer and direct regulation are roughly on a par as regards their behaviour on impulse. In both cases, even with a wide range of regulation, the stresses can be withstood up to the maximum level likely to be stipulated for the 220 kV terminal, i.e. 1050 kV, provided the transformer is suitably designed. Fig. 7 shows the outline of a high-capacity transformer with indirect regulation. The main and regulating transformers are both in one tank.

Completed 400/220-kV Transformers

The illustrations in Fig. 8–11 give some idea of the e.h.v. transformers produced by the Brown Boveri concern. As may be seen from the figures of insu-

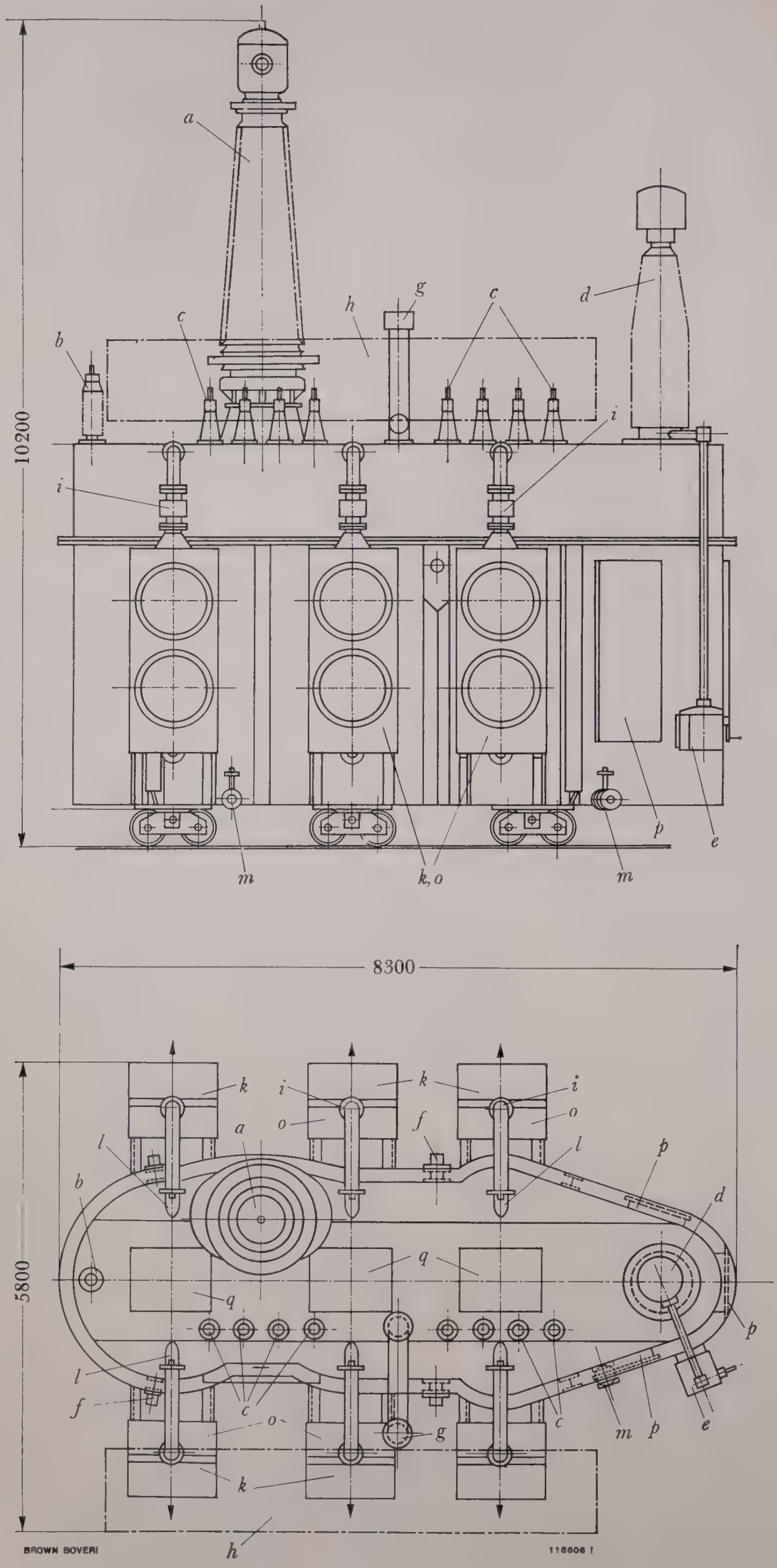

Fig. 7. – Single-phase auto-transformer with separate regulating transformer, on-load tap changer at the input to the 220-kV winding

Main and regulating transformer in one tank.

Bank rating: $\dfrac{600}{\dfrac{600}{60/60}}$ MVA,

$\dfrac{390}{\dfrac{289\text{–}204}{14/14}}$ kV;

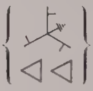
50 c/s

a = H. V. bushing (system)
b = H. V. bushing (earth)
c = L. V. bushings
d = M. V. bushing with tap changer
e = Tap changer mechanism
f = Lifting lugs
g = Safety valve
h = Oil conservator
i = Motor-driven pumps
k = Motor-driven fans
l = Stop valve
m = Oil drain valve
o = Oil cooler
p = Inspection doors
q = Withdrawal openings

lation strength (impulse tests up to 1900 kV with chopped wave) and rated capacity (up to 660 MVA), given in the captions, these are very impressive units. The transformers for the Sils power station in Switzerland will now be described in greater detail.

The 400-kV Regulating Auto-Transformers for Sils Power Station (Switzerland)

Brown Boveri were instructed to supply seven single-phase units to form two three-phase four-winding banks (with one unit as standby). The bank rating is 400/280/2 × 72·5 MVA, the transformation ratio being 420/306–200·8/10·5/10·5 kV.

These units are in fact a combination of generator transformer and coupling transformer. In each, two separate 10·5-kV windings are fed by two generators rated 72·5 MVA so that when acting as coupling transformers they can act at the same time as step-up or step-down transformers with capacities of 400 and 280 MVA, respectively.

The conditions stipulated regarding voltage regulation were particularly severe, and led to the wide range of ±20% of the mid-point tapping in the rated voltage range of 200·8–306 kV.

A further difficulty arose out of the stipulation that the 10·5-kV windings should be able to operate separately as well as independently at any power factor. Exacting conditions also had to be fulfilled in the voltage tests. The 400-kV winding had to be tested with an induced voltage of 680 kV and at 1550 kV with a full-wave 1/50 impulse; the corresponding values on the 220-kV side were 460 and 1050 kV. In addition, allowance had to be made for 9% overvoltage. Finally the units had to be transported on a narrow-gauge railway with severe restrictions regarding the load-carrying capacity and where small-radius curves forbid great length in the direction of the lines.

The best solution proved to be division of each single-phase unit into a main transformer with the ratio

$$\frac{10{\cdot}5 : 10{\cdot}5 : 250\,/\,\sqrt{3}}{420\,/\,\sqrt{3}}\ \text{kV}$$

and a regulating transformer energized from the 10·5-kV side with regulation at the input to the 220-kV winding as shown in Fig. 12. In operation the two water-cooled transformers are side-by-side and connected by cable; the impedance voltage when acting as an auto-transformer is about 9·5% referred to the mid-point tapping.

The main transformer has a single-limb radially laminated core with a disc-coil winding. Fig. 13 gives an impression of the harmonic appearance of the core. A remarkable feature is that, despite the less favourable conditions arising out of operation with four windings, a type rating of 100 MVA is attained. From all accounts, this is the largest single-core rating ever obtained with a transformer of this voltage range, suitable for transport by rail.

Like the main unit, the regulating transformer also has a radially laminated core. The regulating winding is situated at the input to the 220-kV winding and, since it is connected to two generators, is energized by two separate excitation windings in the main transformer. By locating the on-load tap changer at the 220-kV input it was possible to keep the tap-changer currents relatively small (at the most about 750 A) and at the same time to control with constant flux density, which is very desirable in view of the greater outlay for material resulting from indirect control.

The tap changer for varying the ratio in +17 and −15 steps is of the built-in type. It is accommodated in a container blanked off from the tank by a partition and containing the 220-kV cable end-box.

Close attention was paid to surge problems, upon which the reliability at extra-high voltages primarily depends. According to comprehensive mathematical investigations an optimum design was to be expected. Now it may be proudly stated that the measurements of voltage distribution on the completed unit, as well as the impulse tests, fully confirm the expected favourable performance. This is particularly true of the stresses on the regulating winding under all practical conditions. Fig. 14 shows some of the oscillograms recorded during these tests.

The measurements confirm that the maximum stresses imposed on the regulating winding by an impulse on the 400-kV terminal do not exceed 20%, and on the 220-kV terminal 30% of the amplitude of the incident wave.

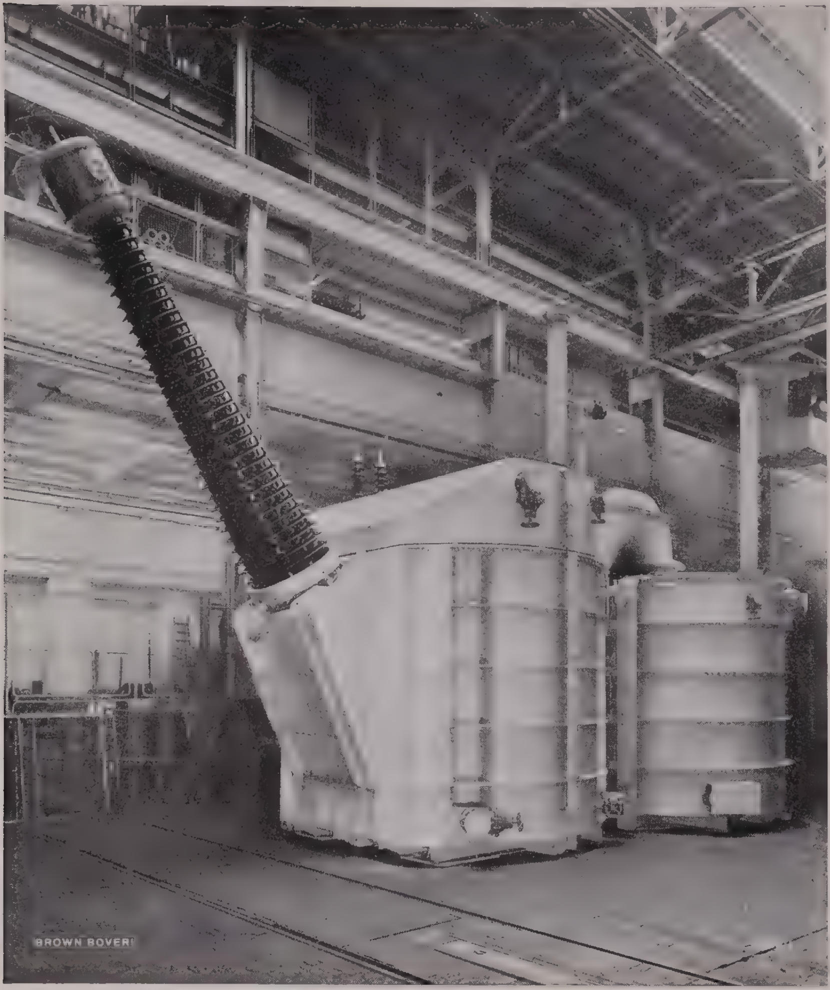

Fig. 8. – 400-kV single-phase auto-transformer with separate regulation for Sils power station in Switzerland

Main and regulating transformers in separate tanks, tap changer at the 220-kV terminal.

Bank rating:

$$\frac{400}{\frac{280}{72{\cdot}5/72{\cdot}5}}\ \text{MVA},\qquad \frac{420}{\frac{306\text{–}200{\cdot}8}{10{\cdot}5/10{\cdot}5}}\ \text{kV, 50 c/s}$$

7 units supplied (two three-phase banks and one reserve unit)

Test voltages:

H.V. winding:
induced voltage 680 kV
1/50 full-wave impulse 1550 kV

M.V. winding:
induced voltage and separate voltage (regulation transformer) 460 kV
1/50 full-wave impulse 1050 kV

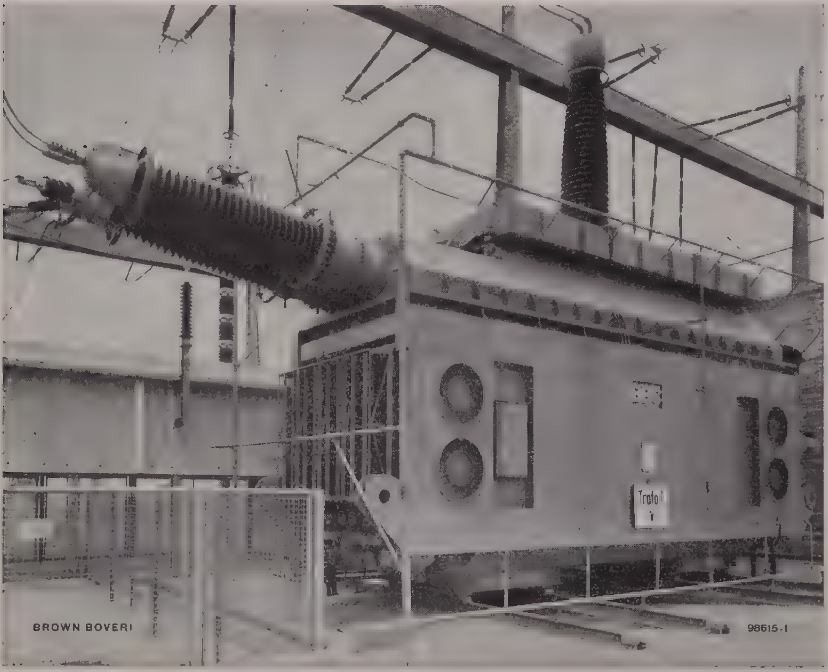

Fig. 9. – 660/3-MVA single-phase auto-transformer supplied to the Rheinisch-Westfälisches Elektrizitätswerk AG, Germany

Designed as mobile transformer with separate regulation; main and regulating transformers in one tank, on-load tap changer at the 220-kV terminal.

Bank rating:

$$\frac{660}{\frac{660}{200}}\ \text{MVA},\ \frac{400}{\frac{231 \pm 13 \times 3{\cdot}2}{30}}\ \text{kV, 50 c/s}$$

Two units supplied.

Test voltages:

H.V. winding:
induced voltage 640 kV

M.V. winding:
induced voltage 370 kV

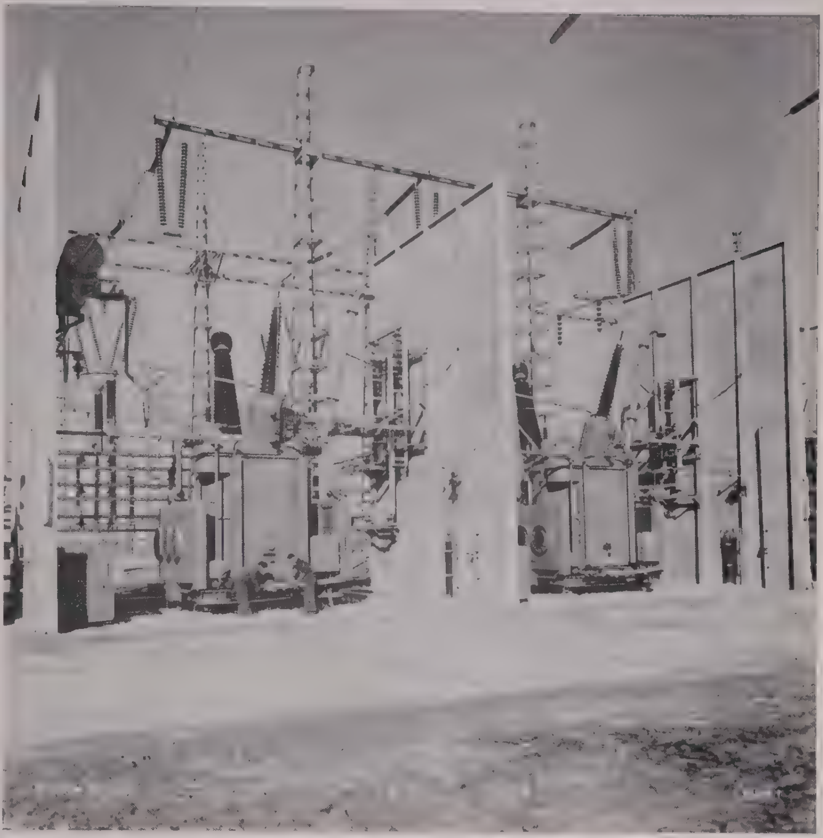

Fig. 10. – 300/3-MVA single-phase auto-transformer supplied to the Electricité de France

With neutral regulation by tap changer.

Bank rating:

$\begin{array}{c}300\\\hline 300\\\hline 90\end{array}$ MVA, $\begin{array}{c}362\text{–}380\text{–}400\\\hline 225\\\hline 11\end{array}$ kV, 50 c/s

Two three-phase banks supplied.

Test voltages:

H.V. winding:

induced voltage	630 kV
1/50 full-wave impulse	1450 kV

M.V. winding:

induced voltage	395 kV
1/50 full-wave impulse	900 kV

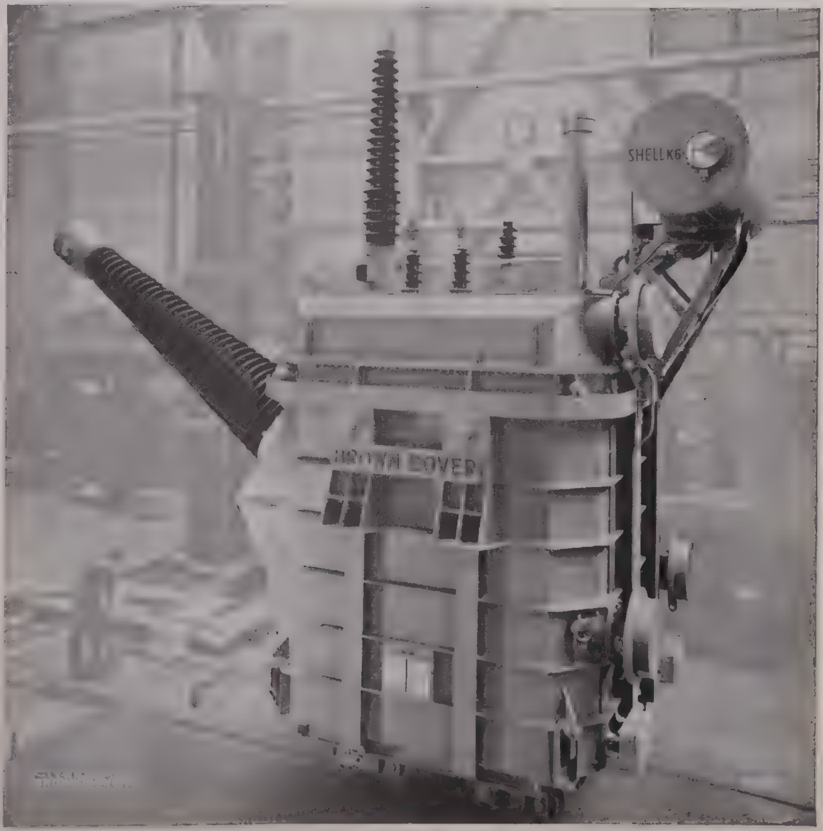

Fig. 11. – 420/3-MVA single-phase auto-transformer supplied to Imatran Voima Oy for their Hyvinkää substation in Finland

Bank rating:

$\begin{array}{c}420\\\hline 420\\\hline 165\end{array}$ MVA, $\begin{array}{c}380\\\hline 238\\\hline 20\end{array}$ kV, 50 c/s

One three-phase bank and one spare unit supplied.

Test voltages:

H.V. winding:

induced voltage	725 kV
1/50 full-wave impulse	1650 kV
chopped-wave impulse	1900 kV

M.V. winding:

induced voltage	455 kV
1/50 full-wave impulse	1050 kV

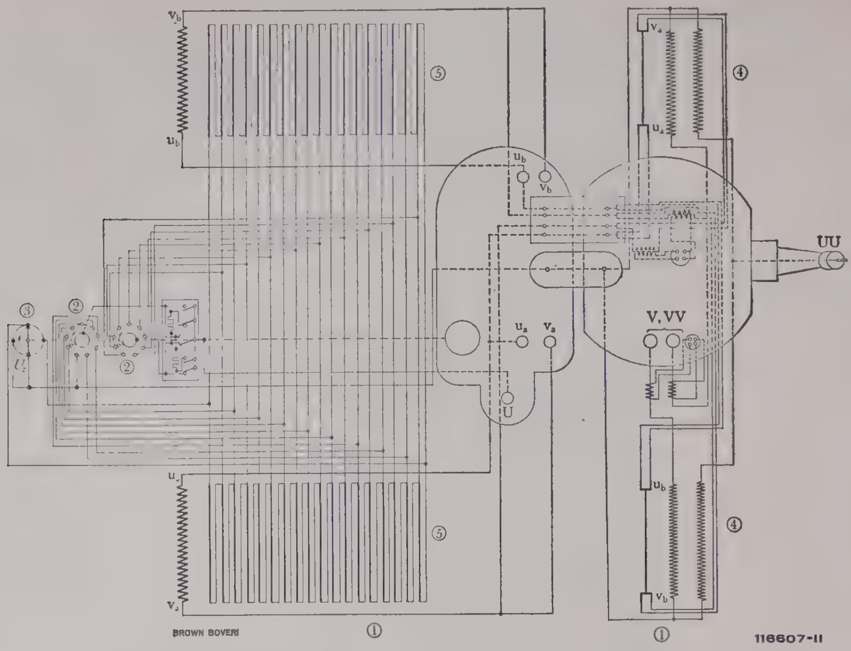

Fig. 12. – Circuit diagram of the 400/220-kV auto-transformer for Sils, Switzerland (see Fig. 8)

1 = Transformer windings
2 = Tapping selector
3 = Reversing switch
4 = Main transformer
5 = Regulating transformer
UU, VV = High voltage
UV = Medium voltage
u_a, v_a, u_b, v_b = Tertiaries (low voltage)

The secondary voltage increases in the direction of the arrow.

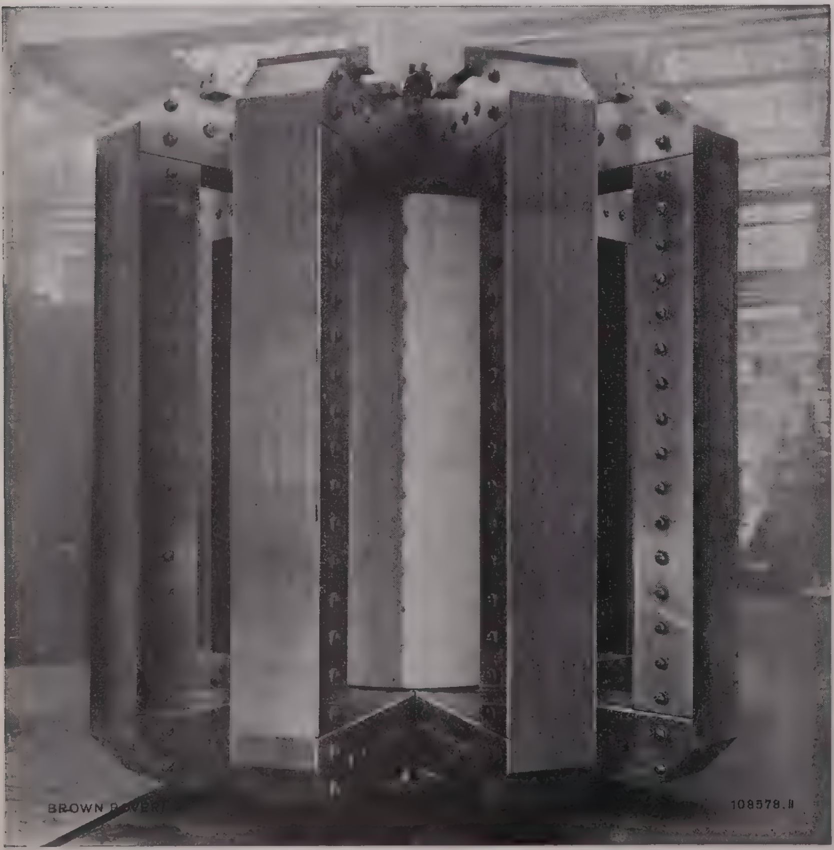

Fig. 13. – Iron core of the main transformer of the unit illustrated in Fig. 8

With this radially laminated core the power transformed is about 100 MVA which, to all accounts, is a record for a single limb of an e.h.v. transformer.

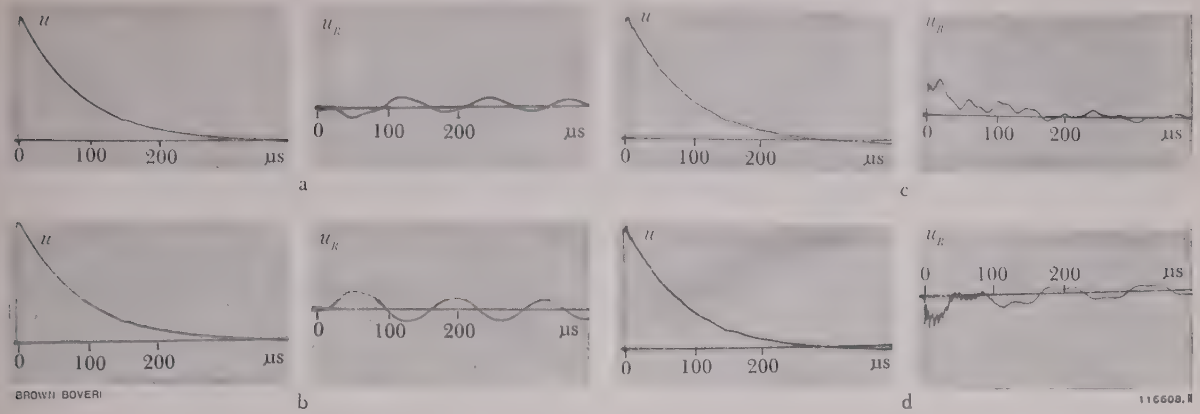

Fig. 14. – Oscillograms of the impulse voltages measured across the regulating winding of the 400/220-kV transformer illustrated in Fig. 8

$u = 1/50$ impulse voltage
u_R = Voltages across the regulating winding

a: Impulse on the 400-kV terminal
M.V. winding earthed through 500 Ω
Tertiary terminals shorted and earthed
Neutral terminal earthed direct
Tap changer position 1 (420/306 kV)

b: Impulse on the 400-kV terminal
M.V. windings earthed through 500 Ω
Tertiary terminals shorted and earthed
Neutral terminal earthed direct
Tap changer position 33 (420/200·8 kV)

c: Impulse on the 220-kV terminal
H.V. winding earthed through 500 Ω
Tertiary terminals shorted and earthed
Neutral terminal earthed direct
Tap changer position 1 (420/306 kV)

d: Impulse on the 220-kV terminal
H.V. winding earthed through 500 Ω
Tertiary terminals shorted and earthed
Neutral terminal earthed direct
Tap changer position 33 (420/200·8 kV)

These values are so low that a special means of external protection for the regulating winding (lightning arrester) could be dispensed with by a wide margin—a record for such large transformers.

(KME) A. EDLINGER

Bibliography

[1] M. CHRISTOFFEL: Auto-Transformers with Direct Regulation for Extra-High Voltages. Brown Boveri Rev. 1956, Vol. 42, No. 6, p. 187–95.

[2] M. CHRISTOFFEL and M. ITSCHNER: 380-kV Transformers. Brown Boveri Rev. 1955, Vol. 41, No. 9, p. 330–6.

[3] B. GÄNGER: Impulse Testing of E.H.V. Transformers with 1775 kV. Brown Boveri Rev. 1956, Vol. 42, No. 12, p. 525–32.

[4] K. SCHLOSSER: Grosse Spartransformatoren. Elektrotech. Z. Edn. A, 1960, Vol. 8, No. 2, p. 59–67.

[5] B. GÄNGER: The Brown Boveri Oil-Pressure Detector Employed for Fault Detection During Impulse Tests on Transformers. Brown Boveri Rev. 1957, Vol. 44, No. 8, p. 336–42.

A NEW DESIGN OF VOLTAGE TRANSFORMER FOR EXTREMELY HIGH VOLTAGES

621.314.222.8.027.8

Following a reference to the main designs of e.h.v. voltage transformers and the specific conditions they have to fulfil, the authors describe a new design of hermetically sealed unit for a rated voltage of 345 kV, constructed of two parts in cascade with bar-type cores. The article concludes with an account of the numerous tests and measurements which have been successfully carried out with these transformers.

AMONG the items of high-voltage equipment which designers regard with particular affection, a special place is held by instrument transformers. Their constructional evolution has made great progress in recent years, and now they are highly developed units, specially designed for their specific task, which demands absolute reliability with hardly any maintenace during long periods.

Particularly in the instrument transformer field there is a wide variety of basic insulation systems and an abundance of different constructional forms. This variety is partly the result of adhering to long-established design principles which have in due course been joined by new ideas based on more extensive knowledge or new materials, partly also to the wide range of rated voltages. An item of equipment for a high voltage cannot merely be derived by proportionally increasing the insulation distances and retaining the general arrangement suitable for much lower voltages. This would lead to designs which, besides being uneconomical, might not even be able to withstand the voltage. The problem can only be satisfactorily solved when a design is specially prepared for the particular voltage range in question.

For a long time only oil in conjunction with solid material was used to insulate voltage transformers. Unlike current transformers, in which only the main insulation between the h.v. (primary) winding and the secondary winding or earth is highly stressed, voltage transformers experience appreciable potentials between adjacent parts of windings (turns, layers, coils). But with oil, which has a high impulse ratio, these spaces are very efficiently insulated against the severe short-time overvoltages. Hence the range of high and extremely high voltages is mostly reserved for single-phase oil-filled bushing-type voltage transformers. Their basic design is assumed to be well-known from previous publications [1].[1]

However, on account of certain drawbacks of oil, there is a tendency nowadays either to get away from it altogether or, if this is impracticable, to limit its quantity to the bare minimum. The latter is particularly true at higher voltages, where its replacement proves far more difficult than at lower ratings. However, the limit has shifted in recent years, increasingly to the disadvantage of oil; in the future, too, still further progress is expected in this direction.

Therefore, before deciding on the basic design of the voltage transformer for a rated line voltage of 345 kV, which will subsequently be described, the possibility of using compressed air instead, or possibly other gases or vapours was investigated. Also, the good results obtained with moulded resin transformers might possibly have been considered sufficiently encouraging for the use of resin to be extended to higher voltages than at present. For the 345-kV transformer, however, it was decided that only materials which had been tested at extremely high voltages and have long proved reliable in service should be employed. Hence oil-impregnated paper insulation was retained.

---

[1] The figures in brackets refer to the bibliography on p. 320.

Special Requirements for E.H.V. Voltage Transformers

The bushing-type transformers referred to above, with oil insulation, have been in service for twenty years in all parts of the globe, from the tropics to the far north with ambient temperatures down to −40 °C. Their rated voltages extend from 72·5 to over 300 kV. Prototypes have also been made for 420 kV and subjected to very severe tests [2]. For these very high voltages the size of the object for transport is often a deciding factor in the design because, where possible, it is preferable for the transformers to be assembled in the factory and despatched ready for immediate commissioning. Extensive assembly work on site and particularly drying out the active part and filling with oil should be avoided. But since the impulse test voltage for 420-kV equipment is around or sometimes above 1500 kV, requiring a flashover distance of over 3 m in the surrounding air, it is not difficult to realize that, if the metal fittings at the top and bottom of the transformer are included, the height is very close to the rough figure of 4·5 m which is allowed for the railway loading gauge. Tilting or even laying flat during transport is generally undesirable for mechanical and electrical reasons. Therefore, to simplify the transport problem, the transformer was divided into *two independent units*. Owing to the favourable arrangement of the transformer, the height of each section is reduced to about half. Furthermore, the new arrangement of internal capacitance has greatly improved the resistance of the transformer to high-speed transients.

Insulation Problems

With e.h.v. instrument transformers the problem of insulation, particularly its thickness, becomes supremely important. An effort will, of course, always be made to keep the effective field strength approximately constant by proportionally enlarging the insulation distances with increasing voltage, but even at the best the withstand voltage only increases with the thickness of the material. The larger these distances are made, the more difficult it generally becomes to realize the quasi-homogeneous electrical field stipulated for technical designs. Even small projections, edges, inadequate rounding off, and so on, can give rise to disturbing field concentrations and thus to internal ionization or premature breakdown. The primary consideration behind the new design was that it should be free from end effects and possess a quasi-homogeneous field.

Since the electrical field in e.h.v. transformers extends over a very wide area, great care must be taken. Considering the insulation system as a large number of supposedly identical elementary cells connected in parallel, it is the one which is weakest which breaks down. Thus it was discovered that with increasing electrode area the breakdown voltage of both oil and solid insulation decreases logarithmically [3, 4]. Therefore on account of the statistical fluctuation in the nature of the dielectric it is only permissible to allow for reduced maximum field strengths for high-voltage equipment where electrodes of large area are necessary. This is particularly true of short-time voltage stresses, such as insulation tests or transient voltage rises. With sustained voltage it is also necessary to observe the limit of thermal breakdown. This is determined by the internal temperature rise due to dielectric losses and the heat dissipated at the edges of the dielectric. Continuous operation is only feasible so long as the steady-state flow of heat is sufficient to prevent overheating inside the dielectric. At high ambient temperatures the critical voltage U_k is naturally lower. Its magnitude also depends to a considerable extent on the absolute value and rate of rise σ of the loss factor $\tan\delta$ with temperature, as well as on the thermal conductivity λ, as may be seen from the formula of a plate dielectric cooled on both sides:

$$U_k = 2510 \sqrt{\frac{\lambda}{f \varepsilon \sigma \tan\delta}} \qquad (\text{kV})$$

$$= \frac{\log_e \tan\delta - \log_e \tan\delta_0}{\vartheta - \vartheta_0} \qquad ({}^\circ\text{C}^{-1})$$

where $\tan\delta$ and $\tan\delta_0$ are the loss factors at the temperatures ϑ and ϑ_0 of the cooling medium.

For oil-impregnated paper the specific thermal conductivity λ is approx. $2 \times 10^{-3} \frac{\text{W}}{\text{cm °C}}$

The dielectric constant ε is approx. 3·6

f is the frequency

When heat is only dissipated on one side the critical voltage is reduced by half; it is independent of the thickness of the dielectric. This means that, with a given dielectric, it is pointless to increase the insulation distance by using more material; certainly the resistance to brief voltage stresses is increased, but not to sustained voltage. The critical voltage can only be improved by incorporating cooling spaces or by choosing a better dielectric, preferably one in which the loss is small and only increases slightly with rise in temperature. This demands the use of very high-grade materials and extremely careful preparation, using the best method of drying and a sufficiently high vacuum during the process of impregnation. Hence, with oil-impregnated paper for single-thickness insulation, it is not difficult to obtain values for the critical voltage which are several times the operational voltage. In view of the very high voltage for which the present unit had to be designed, it was considered desirable for the safety margin to be increased still further and the critical voltage for the whole unit to be raised to a very high level. This was achieved by adopting the cascade connection which, from the dielectric aspect, corresponds to distributing the voltage drop between two quite separate layers of insulation; in other words, for the same quality of material the critical voltage is doubled.

But it is not sufficient for this excellent insulation property to be attained merely while the transformer is new; it must also be maintained over a long period in service. For this to be achieved, it is firstly important to prevent the surrounding atmosphere from exerting any harmful influence on the oil filling, and secondly to prevent this influence from extending to the solid dielectric.

As regards the deterioration of the oil, the conditions in an instrument transformer are considerably more favourable than in a power transformer, because the temperature rise in service is much smaller and occurs less frequently. Thus the oil never reaches a high temperature, consequently tends to oxidize less, and therefore does not form dipole substances which would increase tan δ. The entry of atmospheric moisture can be prevented by the insertion of a dehumidifier or by hermetically sealing the transformer. This can be effected, for instance, by a gas cushion above the surface of the oil, which is compressed when the oil expands and relieved when the temperature falls again. The change in pressure takes place in a very limited range and so slowly that there is no risk of gas dissolved in the oil being released when the pressure drops, thereby producing bubbles at points which may be highly stressed, as might happen in power transformers with such a buffer [5]. If all contact is to be eliminated between the oil and the air or gas cushion, the transformer enclosure must be completely filled with oil and hermetically sealed. A flexible element then has to take up the change in volume of the oil. Such hermetically sealed transformers at constant (atmospheric) pressure have gained a certain amount of popularity in recent years, despite the fact that perfectly good results have been obtained with "breathing" designs, in which dehumidified air is allowed to have access to the oil and, in the opinion of this Company, there is no compelling reason for departing from this well-proved system, especially when the rated voltage is not unduly high. For this flexible element Brown Boveri employ an oil-filled bellows fixed to the head of the transformer. This appears to be the best solution, in view of its almost unlimited life and the completeness with which the air is excluded. Bellows of a similar kind have been used for over ten years for the joints between the radiators and tanks of large air-cooled power transformers.

Constructional Problems

Apart from the high-voltage problems there are other features of no less importance. Conventional instrument transformers are noted for their relatively high output capacity compared with the very modest requirements of the meters connected to them. To mention an example, the power capacity of a Brown Boveri unit, allowing for maximum admissible temperature rise, is more than 10 kVA at $245/\sqrt{3}$ kV, whereas the power actually utilized by the meters is often less than 100 VA. Hence with every transformer the purchaser obtains a high inherent power capacity which is wasted. It is therefore obvious that another solution is desirable, enabling the transformer to fulfil its metering task without such disproportionality between the installed and utilized power. One method which has been well-known for a long time is the *capacitive voltage divider* with a resonant low-voltage circuit. In contrast to the magnetic transformers, the potential distribution of the h.v. coupling capacitor is completely uniform even when the voltage changes rapidly, thus affording a high electric strength in the face of surges. In most cases it is employed anyway for the power line carrier telephone service. Disadvantages are its dependence on frequency, the effect on the metering accuracy of ageing in the dielectric or adverse weather conditions, the tendency to generate subharmonic oscillations [6] and unsatisfactory communication to the secondary side of rapid changes on the primary side (switchgear operation).

Another possibility is to use a *straight iron core*, to which the lines of force return through space (Fig. 1), instead of a closed magnetic circuit with very low reluctance. The advantages of simpler design and reduced weight are then offset by an increase in the no-load current and reduction of the power capacity. But, as previously stated, the latter is no disadvantage, with regard to economic utilization of the active materials, provided the output power and accuracy of the transformer meet the requirements. By re-designing the core it was also possible to keep the magnetizing current within reasonable limits.

The New Design

Having decided to use oil-impregnated paper insulation, and having settled the special requirements of e.h.v. voltage transformers, the main features of the new design are fairly clear. The transformers consist of a cascade of two otherwise separate units, each having a bar-shaped core and each hermetically sealed.

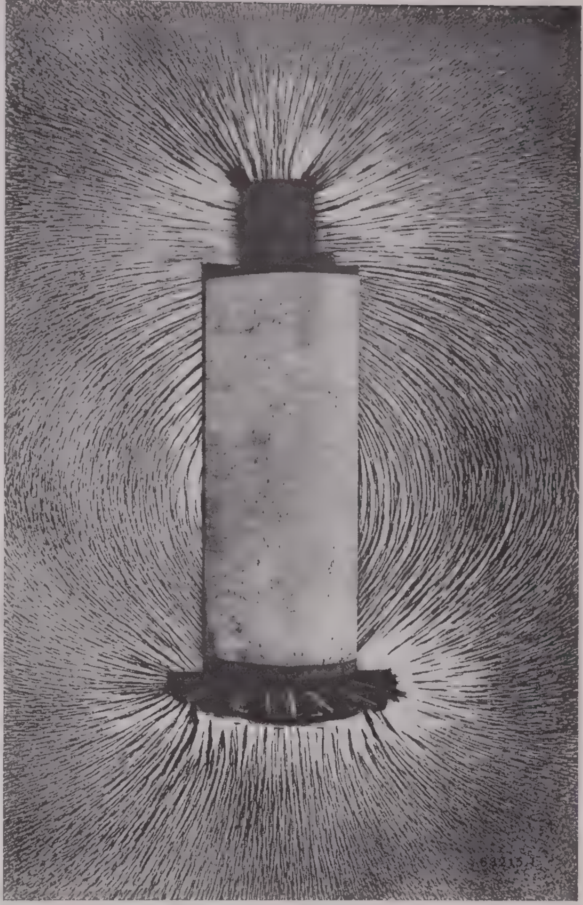

Fig. 1. – Magnetic field of a bar core as shown by iron filings

The concentration of the lines of force at the points where they leave the iron provides the design with the best opportunity of reducing the magnetizing power, whereas the dispersion of the lines at the centre indicates that little power is required there to guide the flux.

The maximum admissible service voltage was fixed at $345/\sqrt{3}$ kV. Accordingly, each half has to carry $172{\cdot}5/\sqrt{3}$ kV.

The basic circuit arrangement is shown in Fig. 2. The primary (h.v.) winding is equally divided between the two parts of the cascade. Hence the two cores 4 and 4′ are at half potential and are correspondingly insulated against earth and against the secondary (l.v.) winding 1 and the input to the h.v. winding. A coupling winding 3/3′ next to the

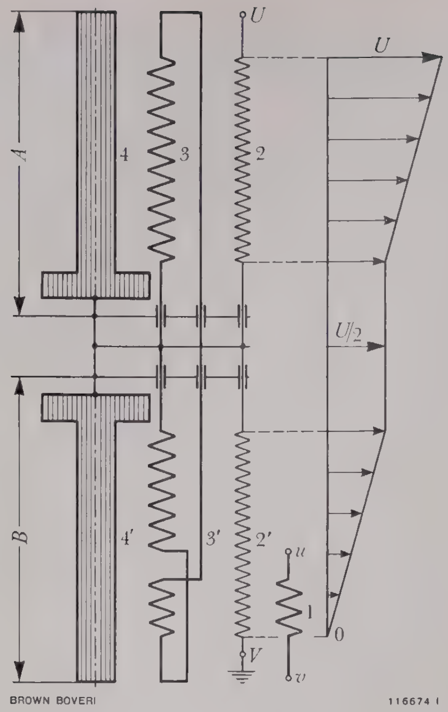

Fig. 2. – Schematic diagram of the cascade

A = Upper section
B = Lower section
U = Mains voltage
1 = Secondary winding u, v
2, 2′ = Primary winding U, V
3, 3′ = Coupling winding
4, 4′ = Iron cores

Spreading the primary (h.v.) winding over the entire flashover distance of the transformer improves potential control. The mechanical parts at the middle of the unit, as well as the iron core and the coupling windings are at half potential.

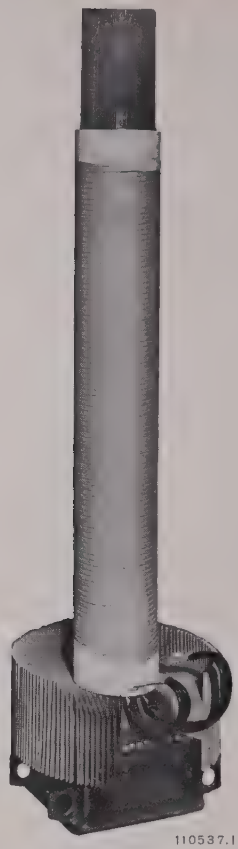

Fig. 3. – Iron core with coupling winding

To improve the conductivity with regard to the flux, the flange ends are fitted with a number of radial guide-vanes.

iron cores and at the same potential as them transfers the power from the upper to the lower half, thereby helping to reduce the short-circuit voltage and limiting the error produced by the variable burden.

During transients the iron cores connected to the mid-point of the h.v. winding (see Fig. 2) are also raised to about half the total potential. Steep surges cause a heavy displacement current to flow from the input end of the upper half, through the core to the part of winding near the end of the lower half, producing in each of these parts the well-known initial distribution with voltage drops concentrated at the beginning and end of the h.v. winding. If no counter-measures were taken, the first and last coils would be very heavily stressed. In the present case this is avoided by adopting a special means of control with capacitively coupled rings placed over the winding and connected to suitable points on it. In the lower part an appropriate arrangement of the earthed secondary winding achieves the same result without special control capacitors.

The iron cores are radially laminated in the well-known Brown Boveri manner which, while permitting good utilization of the circular cross-section, enables draw-bolts to be dispensed with. The inner ends of the two cores terminate in flanges which are fastened to fixing plates. In addition to the flanges, a large number of radial guide vanes are provided (Fig. 3) to improve the conductivity for the magnetic flux. The surface at the other end,

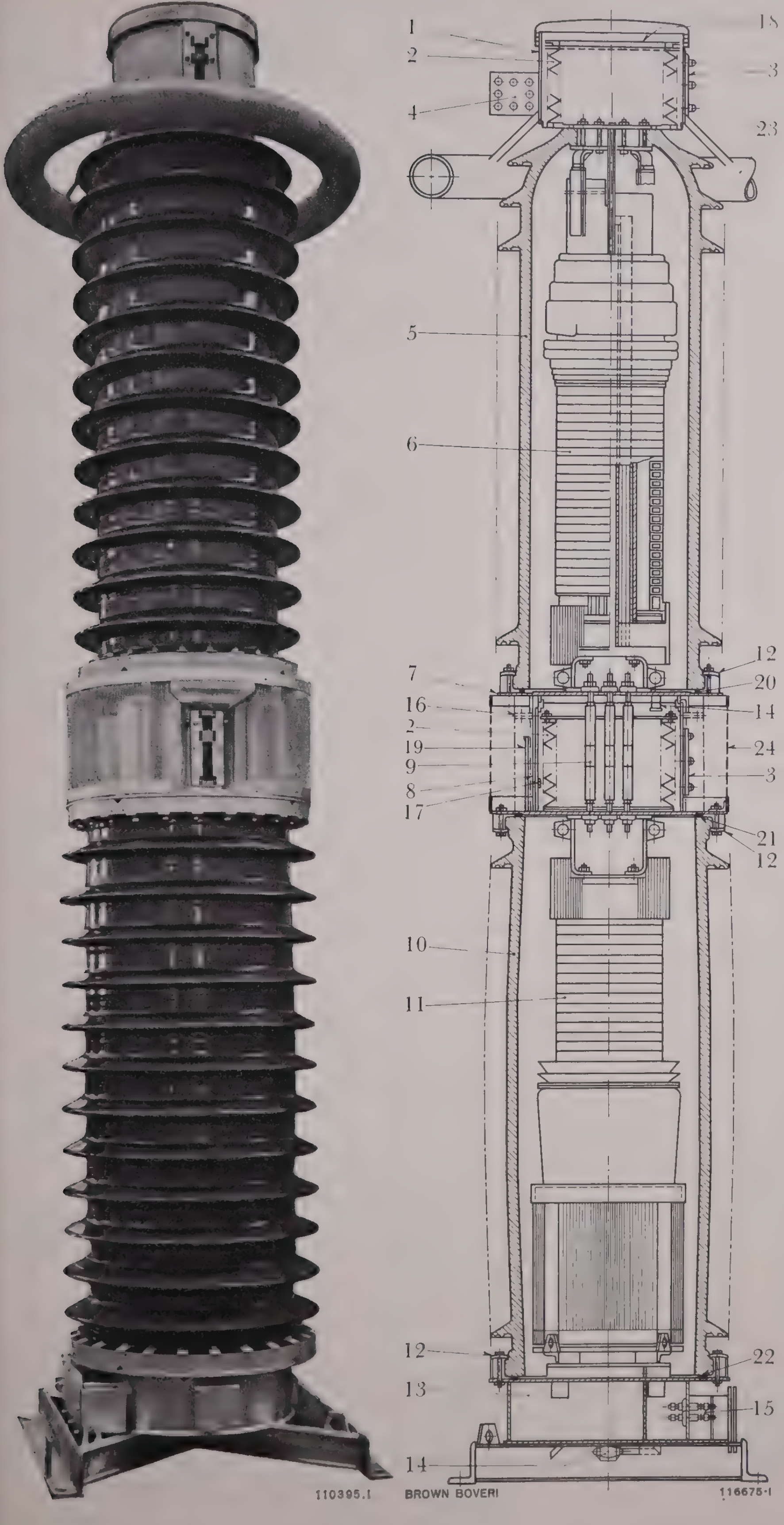

Fig. 4. – Design of the cascade

Right: Section
Left: Perspective view

1 = Terminal head
2 = Membrane
3 = Oil-level gauge
4 = Primary terminal
5 = Insulator (upper part)
6 = Active part (upper part)
7 = Base (upper part)
8 = Head (lower part)
9 = Connections between the two active parts
10 = Insulator (lower part)
11 = Active part (lower part)
12 = Clamps
13 = Tank
14 = Oil drain device
15 = Terminal box
16 = Bolted joint between the two halves
17 = Potential connection screw
18 = Oil filler cap (upper part)
19 = Oil filler cap (lower part)
20 = Gasket
21 = Gasket
22 = Gasket
23 = Anti-corona ring
24 = Grille

The internal design of the active parts conduces to the attractive appearance of the transformer. Thus the primary winding also controls the potential on the outer surface.

which is exposed to a powerful electrical field, is rounded off by a hood placed over the core.

Each core carries its coupling winding on a sheath of presspahn. (For the design of the cascade see Fig. 4.) Above it the main insulation is wound on with constant thickness throughout, and cut off square towards the flange. To even out the stress on the dielectric and to force the magnetic field to assume a fundamentally radial path, the head so formed (at the top of the upper section, the bottom of the lower section) is covered with a layer of conducting material which at the top is at high voltage, at the bottom at earth potential.

The h.v. winding consists of a number of identical coils in series, each of which contains an extremely large number of turns of thin varnished wire in layers. Only the bottom and uppermost layers are wound from thicker wire to improve control of the voltage along the coil and to improve its mechanical strength. Each coil is separately wrapped with several thicknesses of paper. The measuring (secondary) winding is outermost at the end of the h.v. winding and separated from it by an insulating sleeve and paper wrapping with a splayed flange turned over at the upper end.

The active parts are bolted to base-plates. That of the lower is simultaneously the transformer tank and contains the terminal box with the l.v. bushings, also the feet and lifting loops for the whole transformer. When they have been dried out for several days at 105 °C and a low oven pressure, the active parts are inserted in the insulators and impregnated with transformer oil under vacuum. Then the terminal head is fitted on each section. As already mentioned, this contains the flexible sealing member (bellows), which is filled to the level indicated by the oil gauge and immediately closed with a cover, preventing the access of atmospheric gas to the oil. This also renders oil sampling superfluous. The bellows are protected by the cylindrical jacket of the terminal head. The oil level can be easily checked by inspecting the level of the bellows cover through a window in the jacket. The upper bellows is given extra protection by an additional cover.

To prepare the transformer for service, the upper part is placed on the lower and the two bolted together. Then three leads have to be connected between the two sections. To obtain a neat appearance the centre portion of the transformer, formed by the terminal head of the lower section and the base-plate of the upper section, is surrounded by a screening grille.

Tests and Results

Tests and measurements were performed to determine the most favourable dimensions, to establish the measuring accuracy and strength values, and to assure full dependability during power-frequency and transient phenomena in the system.

The proof of uniform distribution of an incident impulse wave between the upper and lower sections was established, because the distribution is somewhat modified by the ever-present earth-leakage capacitance, in that the stress at the top becomes slightly higher. However, in view of the fact that this disturbing capacitance is at the most 50 pF, while the initial capacitance of each section on impulse is about 20 times as large, it is obvious that the distortion will be kept in modest limits. Nevertheless the conditions were checked by a special test (see Fig. 5 and the accompanying details). Even at voltages up to 800 kV and with wavefronts steeper than the standard impulse the maximum deviation from a fifty-fifty distribution was less than 5%.

Several models were made to test the most suitable shape for the closed part of the insulating sleeve surrounding the main insulation. Of the many possibilities: open or closed head, with or without projecting and insulated grading electrodes, slack or tightly pressed insulation, the one which gave the best results when tested at power frequency and on impulse and, at the same time, was compact, was finally chosen. The final design of a half-

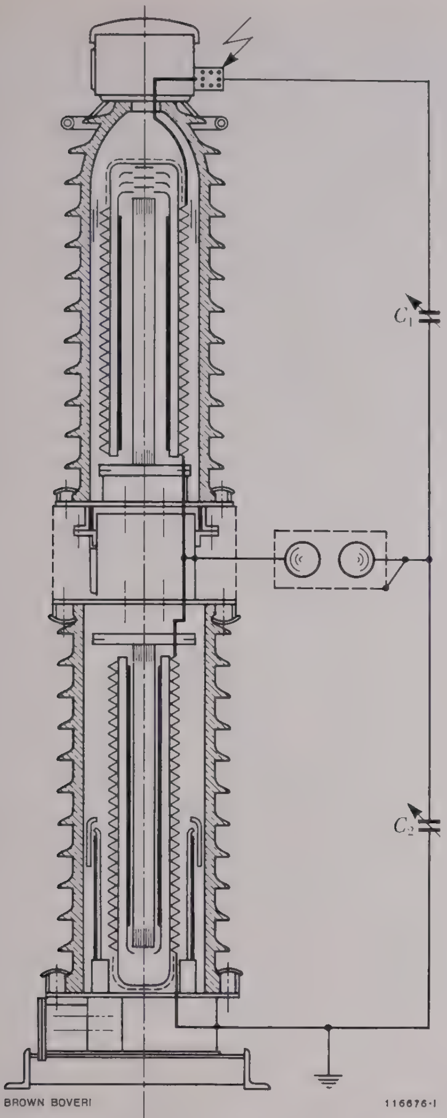

Fig. 5. – Determination of the potential at the middle of the cascade with high impulse voltages

Left, the cascade; right, the capacitive voltage divider with adjustable capacitances ($C_1 \approx C_2 \approx 500$ pF). The screened measuring spark gap is used to establish equality of potential between the middle of the cascade and the divider tapping. The deviation from a 50:50 distribution was 5% at the most. The internal arrangement of the active parts is reflected in the harmonious appearance of the transformer. Hence the primary winding also controls the potential across the external surface.

transformer withstood the following 50-c/s voltages applied successively for 1 min: 380, 420, 460, 510 and 550 kV. Breakdown finally took place at 563 kV. Since the whole transformer has *two* such insulating sleeves in series, the overall safety factor is correspondingly higher.

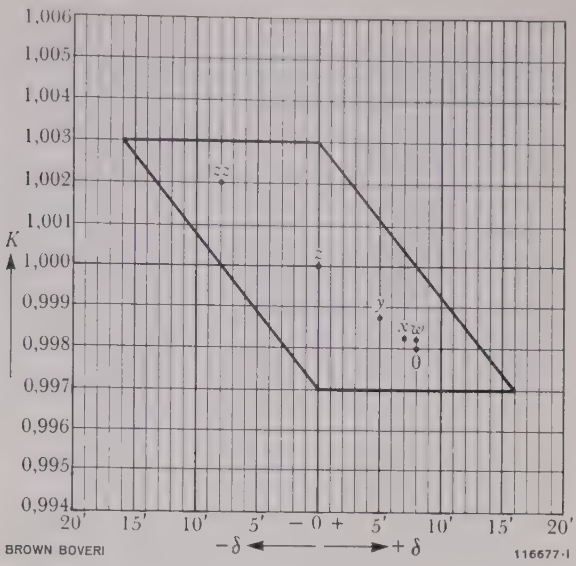

Fig. 6. – Voltage error and angle error of a cascade voltage transformer type TMCS 345. Max. service voltage 345 kV, ratio 172 500/69 V (2500:1), frequency 60 c/s, rated burden W, X, Y, Z, ZZ; accuracy ASA class 0·3

$W = 12{\cdot}5$ VA, $\cos\beta = 0{\cdot}1$
$X = 25$ VA, $\cos\beta = 0{\cdot}7$
$Y = 75$ VA, $\cos\beta = 0{\cdot}85$
$Z = 200$ VA, $\cos\beta = 0{\cdot}85$
$ZZ = 400$ VA, $\cos\beta = 0{\cdot}85$
0 = No-load
K = Ratio correction factor

For the average burden ($Z = 200$ VA) the voltage error and angle error are zero. At all stipulated burdens these figures are well within the admissible limits.

Measuring Accuracy

From results of tests on the completed transformers, those relating to its measuring accuracy will be dealt with. The network in Fig. 6 is drawn in accordance with the ASA specifications, the heavy parallelogram showing the permissible locus of the voltage and angle error for ASA class 0·3%. The error points for different burdens (at different power factors) are well inside the prescribed parallelograms, even beyond the specified burden of 400 VA. For the mean burden of 200 VA the error is zero. The question may arise, whether and in what way the error of the transformer will vary when its location differs, particularly when there are ferromagnetic objects in its vicinity. To check this point, sheet-steel cylinders were placed at distances of 20 (provided the voltage permitted), 50

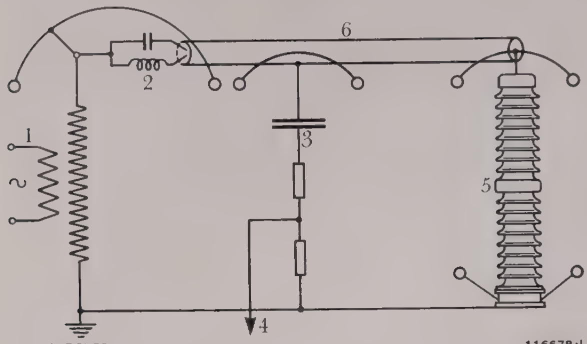

Fig. 7. – Experimental circuit for testing the freedom from ionization

1 = Laboratory transformer
2 = Tuned trap
3 = Coupling capacitor (2000 pF)
4 = To noise meter
5 = Test object with screening
6 = Connecting lead of large diameter, free from corona

Switching on the test object 5 did not increase the noise, thereby proving the freedom from ionization.

and 100 cm, and measurements carried out on transformers standing alone and close to one another. The resultant changes in the error were at all times within the accuracy of the measuring system. It may therefore be stated that, due to the good design of the magnetic circuit, even ferromagnetic objects close to the transformer do not affect its accuracy.

Dielectric Properties

The dielectric properties of the new type of transformers were very thoroughly investigated, first using models of the head insulation, then on the assembled active parts of each half, i.e. with windings in position, and finally on complete transformers.

From Schering bridge measurements of the loss factor of the head insulation, both at room temperature and after heating to 90 °C, it was verified that the preparation of the main insulation is first-class. The thermal breakdown voltage deduced with the aid of the formula for the critical voltage (see page 307) offered an ample safety margin against failure in service.

The transformer was also tested for freedom from internal discharge by measuring the amount of radio interference (RIV). Fig. 7 shows the circuit used, which has been standard practice in America (NEMA No. 107) for some time. Between the voltage source 1 and the coupling capacitor 3 there is a radio-frequency trap, the task of which is to keep away from the measuring device all disturbances originating in the power system or produced in the test transformer, as well as to prevent any disturbance generated in the test object from flowing away through the test transformer. External corona was prevented by effectively rounding off all edges and corners in the high-voltage circuit, i.e. at the lines, the coupling capacitor and the test object, with the aid of anti-corona fittings, shielding rings, etc. The test frequency used was 1 Mc/s.

During the measurements the background noise amounted to $8\,\mu$V. From 0 to 15 % above the maximum service voltage ($1{\cdot}15 \times 345/\sqrt{3} = 230$ kV), switching on the test object did not cause this noise to increase, thereby proving the complete freedom from ionization of the main insulation, as well as of the longitudinal insulation (coils and turns). The combined results of loss angle and radio interference measurements are therefore conclusive proof of the excellent quality of the dielectric.

Electric Strength of the Cascade

As regards the electric strength of the transformer, the figures stipulated were 690 kV for the power-frequency voltage, and 1550 and 1780 kV for full-wave and chopped impulses, respectively.

To prevent heavy predischarges taking place between the head of the test object and earth, a coil of thin wire bent into a ring was fitted (see the left-hand half of Fig. 8). Consequently, not only could the very high test voltage be held for the full duration of the test (48 s corresponding to 150 c/s), but it was actually raised to 765 kV during a subsequent test.

The test was performed with a 1200-kV transformer fed with a voltage of elevated frequency from a motor-generator set, to keep down the flux density of the magnetic circuit of the test object. The right-hand half of Fig. 8 gives some idea of the

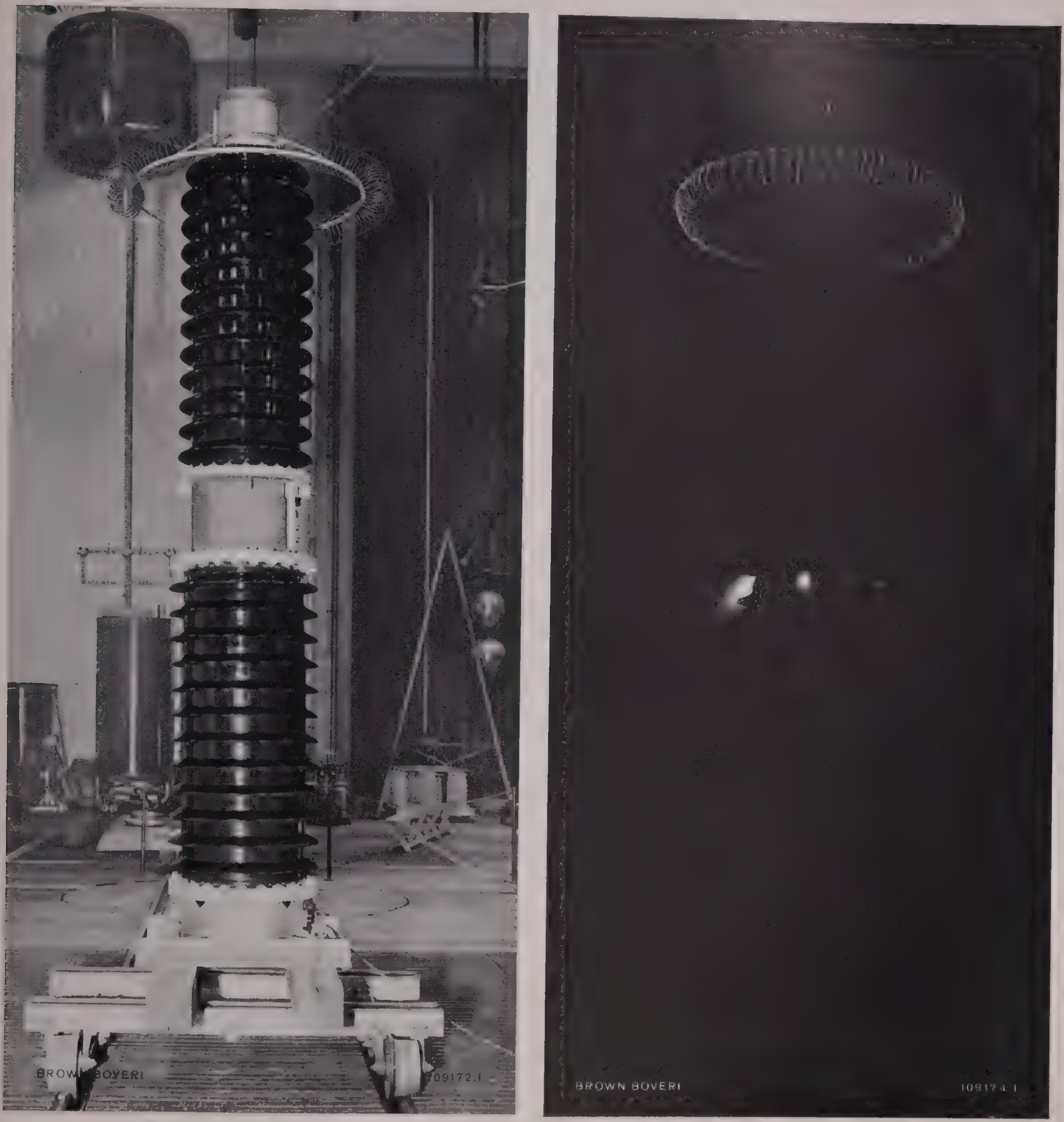

Fig. 8. – Power-frequency voltage test on the transformer

Left: transformer ready for testing, with wire loop at top, middle grille removed.
Right: during the test at 765 kV.

Discharges with an appreciable current are only produced at the middle, but these are eliminated when the grille is replaced.

luminous phenomena in the high-voltage circuit. Powerful discharges only occurred around the middle of the transformer, i.e. where the two sections are joined, but these were overcome by the grille referred to earlier (see Fig. 4, left), which was fitted to the finished unit.

Since the capacity of the test set-up was inadequate for testing the whole cascade, the two halves were separately tested henceforth. The upper section then withstood 380, 420, 460 kV (at 150 c/s for 48 s each); at 510 kV flashover occurred across the porcelain insulator without damaging the inside.

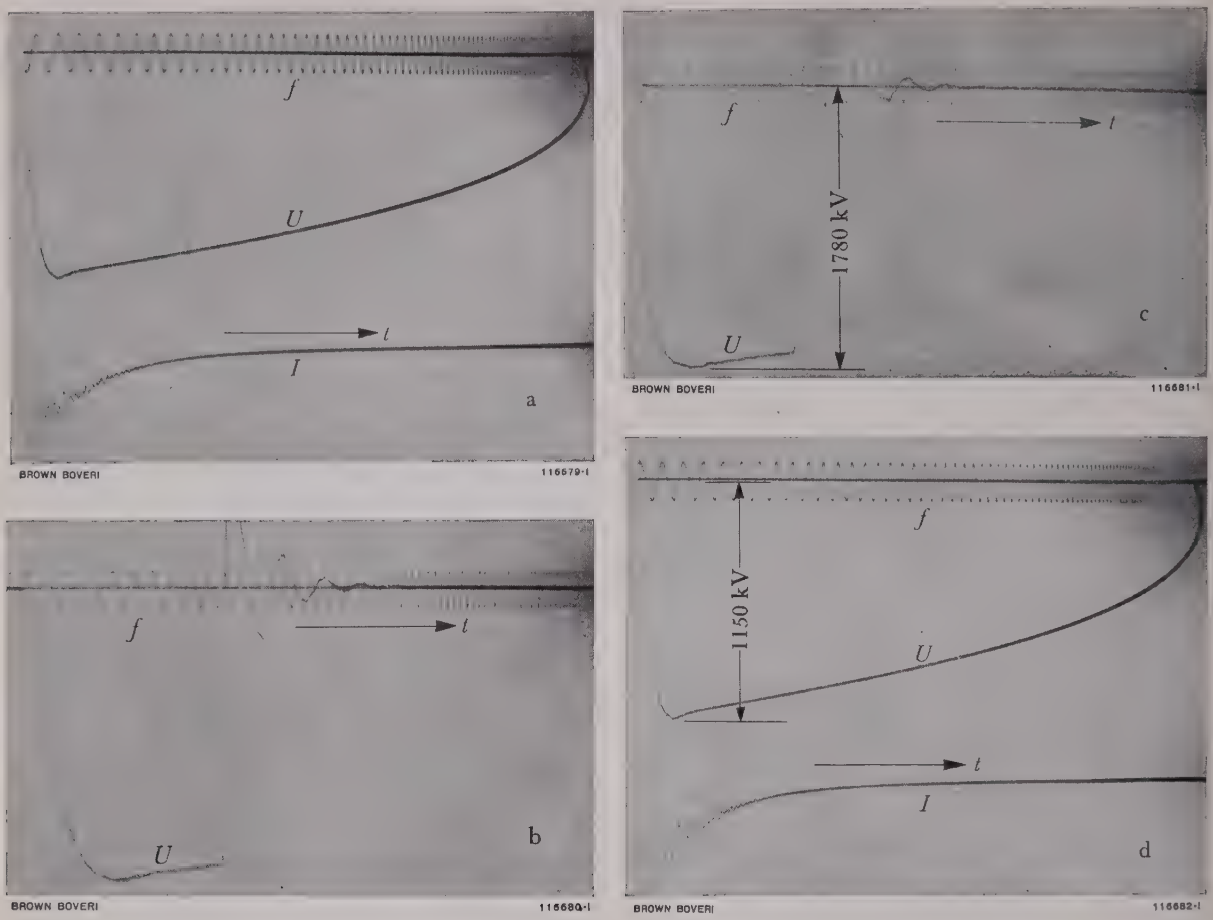

Fig. 9. – Oscillograms of impulse tests

(a) Reference shot at half voltage. Calibration frequency $f = 1$ Mc/s; voltage U and earth current I recorded

(b, c) Chopped-wave impulse at 115% of full-wave voltage. Calibration frequency 2·5 Mc/s

(d) Full-wave shot 1550 kV, values recorded as in (a) but with reduced deflection sensitivity of the oscillograph, in order to obtain curves approximately equal in height.

420 and 460 kV were induced in the lower section. At the latter value external flashover occurred; hence this section was immersed in an oil-filled insulated tank. Then the following voltages were induced: 460, 510, 560 and 610 kV (all for 48 s corresponding to 150 c/s) and satisfactorily held. In view of the high flux density in the test object, the voltage at 150 c/s could not be increased above 610 kV. Nevertheless it had already been proved that each half of the transformer could withstand

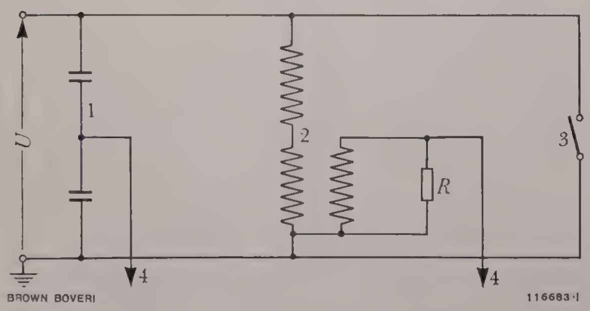

Fig. 10. – Test circuit to establish the behaviour of the cascade when the system voltage changes suddenly

U = Supply voltage (175 kV, 60 c/s)
R = Burden
1 = Capacitive voltage divider, measuring capacitance on h.v. side 2200 pF
2 = Cascade voltage transformer
3 = Circuit-breaker producing the sudden short circuit
4 = To oscillograph

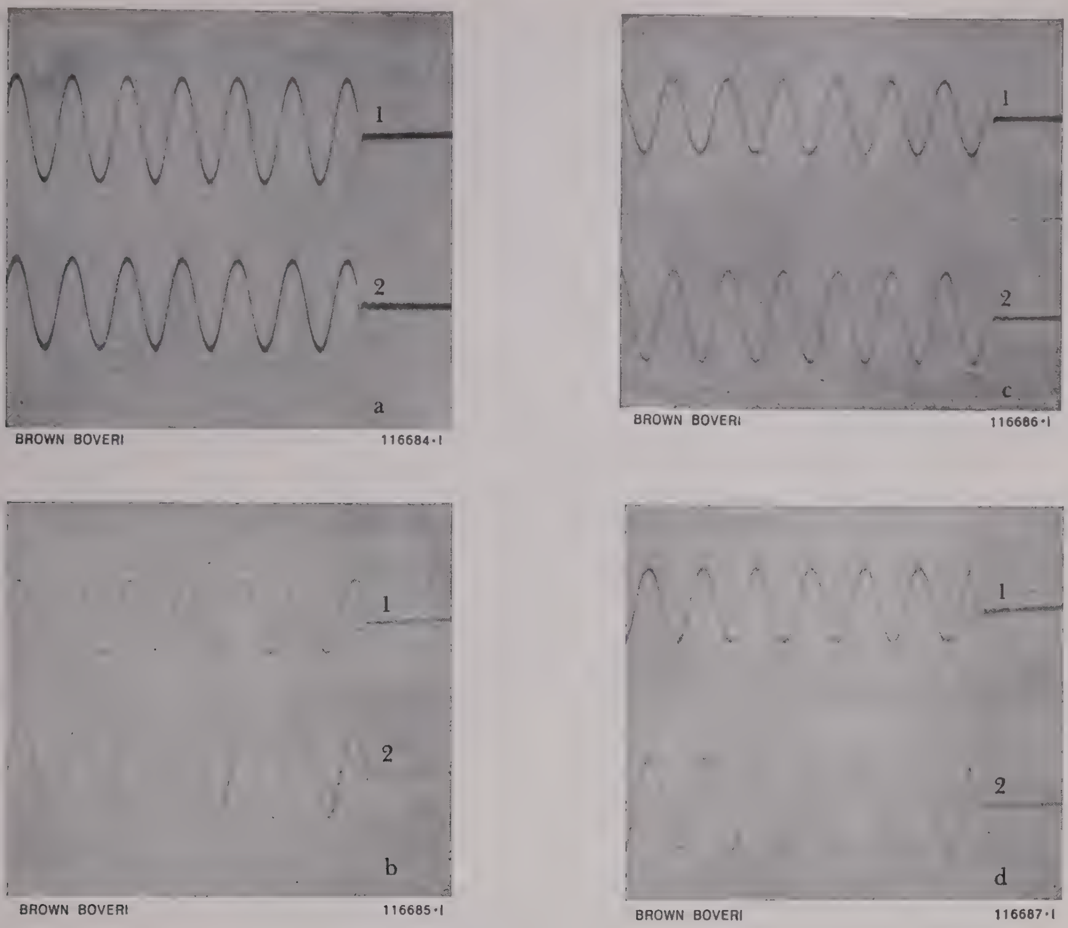

Fig. 11. – Oscillograms of short-circuit tests
(see Fig. 10)

1 = Recorded with capacitive voltage divider
2 = Recorded with conventional voltage transformer
3 = Recorded with cascade voltage transformer

(a) Burden 0 VA: short circuit shortly before voltage zero
(b) Burden 0 VA: short circuit in the region of voltage peak
(c) Burden 400 VA, $\cos \varphi \approx 1$: short circuit shortly after voltage zero
(d) Burden 400 VA, $\cos \varphi \approx 1$: short circuit in the region of voltage peak

The cascade voltage transformer gives a true reproduction of the primary voltage, even when it changes suddenly.

twice the full line voltage for a short time. Further tests at a higher frequency no longer gave a clear picture of the actual conditions.

Some of the results obtained during an impulse test in the presence of the customer may be seen in the oscillograms in Fig. 9. Following a shot at about half the stipulated voltage, two 1780-kV shots were applied, chopped after 3 μs, immediately followed by a full-wave impulse at 1550 kV. The fast-sweep oscillograph was used to record the impulse voltage tapped off the voltage divider, and the current to earth. To obtain curves of equal height, thereby simplifying comparison, the full-wave impulses were recorded with a correspondingly changed deflection sensitivity of the oscillograph. As can be seen by comparing the chopped-wave oscillograms with one another, and with the full-wave shot, the curves of voltage and current exhibit no changes which can be attributed to an insulation weakness. At this point the test was considered passed. After acceptance, the full-wave impulses were taken up to 1850 kV without incident. Not until the maximum voltage

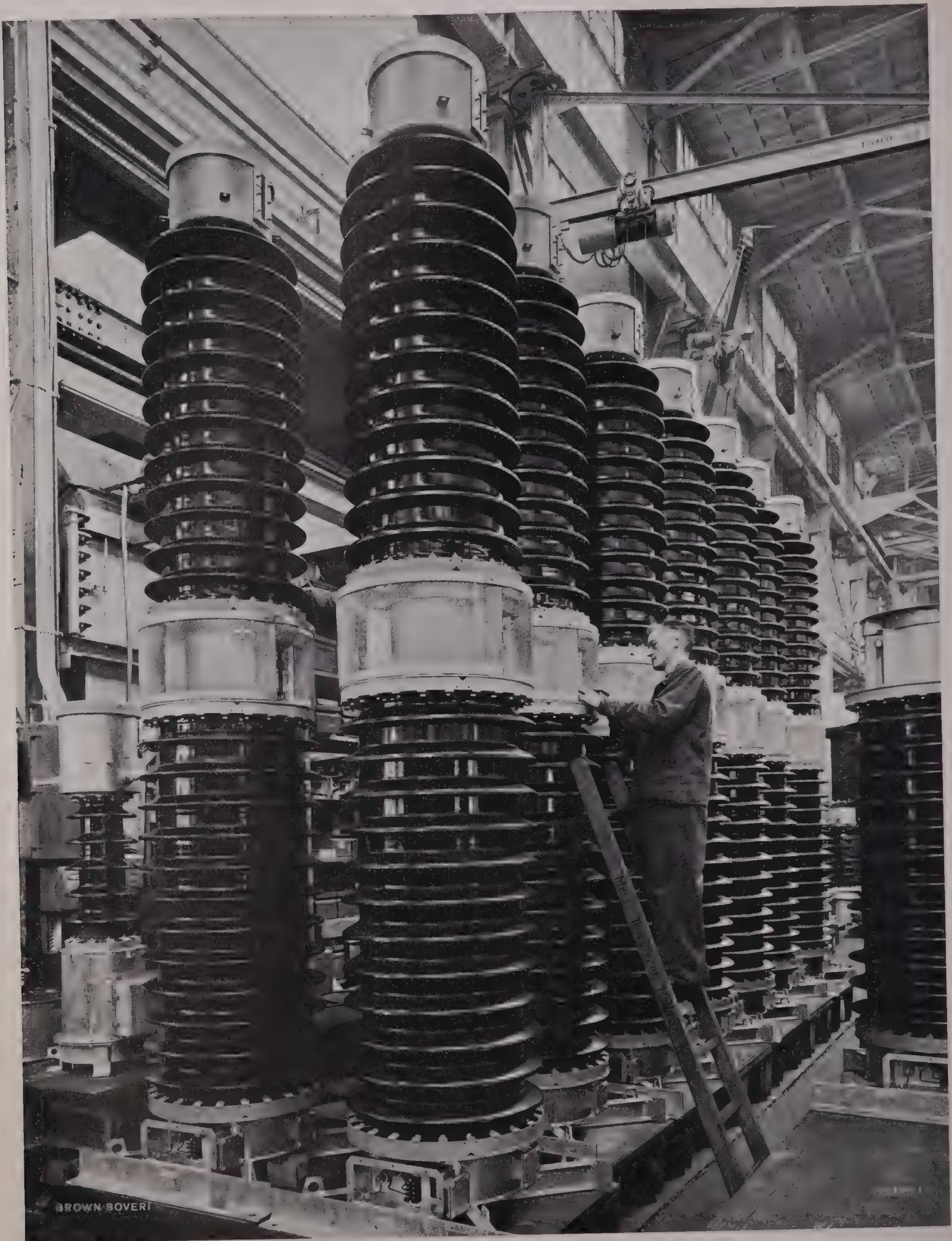

Fig. 12. – Single-phase hermetically sealed cascade voltage transformers type TMCS 345, *for outdoor installation and connection between phase and earth*

Max. service voltage 345 kV, 60 c/s; tested to 690 kV at 150 c/s; impulse withstand voltage 1550 kV; ratio 172 500/69 V; rated burden 400 VA, WXYZZ; accuracy ASA class 0·3.

Temperature rise of the cascade

	Part	Temperature rise in °C		
		at rated conditions $345/\sqrt{3}$ kV 0·4 kVA	at max. burden $300/\sqrt{3}$ kV 12·5 kVA	earth fault 300 kV and rated burden
Upper section	Oil, top	20	26	28
	Oil, bottom	13·7	17	18·9
	Primary winding (resistance method)	32	46·1	27·6
	Coupling winding, hottest point	33	50	44·1
	Iron, hottest point	30·7	49·8	39·4
Lower section	Oil, top	24·3	33	31·7
	Oil, bottom	20·3	26·6	20·9
	Primary winding (resistance method)	32	46·1	27·6
	Coupling winding, hottest point	26·7	36	32·9
	Secondary winding (resistance method)	27·8	55	34·4
	Iron, hottest point	25	35·5	29·8

of 1930 kV was attained did a defect occur and this, as subsequent dismantling established, was a flashover between the lower part of the primary winding and the secondary winding.

A model of the lower section of the cascade transformer was tested separately with a large number of positive and negative shots at 800 kV, and with chopped waves at 900 kV, without breaking down.

Reproduction of Rapid Voltage Changes

Particularly interesting is the transformer's behaviour when the voltage of the supply network changes rapidly. In general, the present tendency is for faulty parts of installations to be completely isolated as quickly as possible to reduce the repercussions on the interconnected network. The rapidity of protective systems has been progressively increased, culminating in the one-cycle distance relay. Within one cycle of the supply frequency this relay registers the occurrence and nature of a fault, measures the distance to the seat of the trouble and issues the command to the circuit-breaker. In order to avoid erroneous operation it is essential that the protective system should always receive the exact characteristic values (current and voltage) from the instrument transformers. Even voltage collapse, for instance in the immediate vicinity of the transformer, should be reproduced faithfully with respect to shape and time. In the capacitive transformers this requirement encounters grave difficulties owing to the tuned resonance and employment of circuits containing iron. Whether and to what extent the cascade transformers are at a disadvantage in this respect had to be established by suitable tests. Employing a sudden short circuit on the h.v. side, the secondary voltage of the cascade was compared with that of a voltage divider which functions without error and thus produces a true image of the high voltage (see the circuit diagram in Fig. 10, the caption of which explains all the important features).

For a few special cases (zero or very high burden, switchgear operation at peak or zero voltage) Fig. 11 shows some of the many oscillograms recorded during the tests performed. The results obtained with the capacitive divider may be considered free of any error. Even when the short circuit occurred at the voltage peak, the results obtained with the transformer resemble them very closely. This proves that the cascade voltage transformer is ideal for operation in conjunction with protective systems with extremely rapid response.

Temperature Rise

The Table above shows the figures of temperature rise under normal operating conditions ($345/\sqrt{3}$ kV, 0·4 kVA) at maximum burden ($300/\sqrt{3}$ kV, 12·5 kVA) and in the event of an earth fault (300 kV, rated burden) at all of which the temperature rise is within the permissible limits.

Summary

Since these tests were carried out a large number of voltage transformers of this design have been taken into operation. They may, with all confidence, be expected to render many years' reliable service under all conditions likely to occur.

H. HARTMANN
(KME) B. GÄNGER

Bibliography

[1] H. HARTMANN: The Low-Oil-Capacity Bushing Voltage Transformer. Brown Boveri Rev. 1946, Vol. 33, No. 4/5, p. 95–7.

[2] B. GÄNGER and H. HARTMANN: Impulse Strength of Brown Boveri High-Voltage Instrument Transformers. Brown Boveri Rev. 1955, Vol. 42, No. 6, p. 196–208.

[3] K. H. WEBER and H. S. ENDICOTT: Electrode area effect for the electrical breakdown of transformer oil. Pwr App. & Syst. 1957, No. 31, p. 393–8.

[4] H. KAPPELER: Réalisations récentes de traversées pour transformateurs 380 kV. CIGRE Report No. 126/1958.

[5] W. I. DEGNAN, G. G. DOUCETTE and R. I. RINGLE: An improved method of oil preservation and its effect on gas evolution. Pwr App. & Syst. 1958, No. 38, p. 657–63.

[6] R. ZAHORKA: Unterschwingungen kapazitiver Spannungswandler. Elektrotech. Z. Edn. A, 1959, Vol. 80, No. 4, p. 108–12.

CALCULATION OF SHORT-CIRCUIT STRESSES IN TRANSFORMER WINDINGS WITH THE AID OF DIGITAL COMPUTERS

621.3.014.32:621.314.21:681.14

The present article describes a method of computing the forces occurring in transformer windings, without having to make appreciable simplifications. Due to their cyclic structure the formulae are ideal for numerical evaluation in a digital computer. The practical scope of the application of the method is illustrated by a simple example.

1. Presenting the Problem and the Assumptions

UNDER external short-circuit conditions the windings of large power transformers are subjected to extremely severe stresses. The problem of computing the forces occurring is essentially one of ascertaining the sense and magnitude of the leakage flux density in the winding space, while the other factor, i.e. the value of the short-circuit current in the windings, is determined by the reactance of the transformer and the power system, which can be easily calculated.

In transformers with concentric windings—this arrangement being employed almost exclusively by Brown Boveri for large units—the main short-circuit forces act in the radial direction and are taken up by the copper of the windings. Calculation of these forces is not difficult since the maximum value of the axial component of the leakage flux density can be determined by simple formulae. Calculation of the forces acting in the axial direction, however, is much more difficult since the slightest asymmetry in the arrangement of the winding can exert a considerable influence on the magnitude of the radial component of the leakage flux density. Hitherto it was standard practice for these forces to be calculated with the aid of radical simplifying assumptions [1, 2, 3].[1] Among these assumptions the most serious may be considered to be the neglect of the winding curvature, and the fact that the influence of the iron core is, at the most, only considered to a very limited extent. The unsatisfactory aspect of these methods is not so much the inaccuracy of the results, but rather the inability to estimate the error resulting from the simplifications. Experimental verification is only possible in isolated cases.

Only one method [4] is known which takes these two effects into consideration. Yet as was pointed out in a more recent paper [5], it is very hard to apply this method even when a digital computer is available. The authors were therefore content to consider only the two-dimensional case (neglecting the curvature of the winding). A further report dealing with the determination of the reactance of transformers with very asymmetrical windings described another method of evaluating the field. Investigation of this method has been continued and it has been found to be very suitable for the determination of the forces.

The problem is illustrated in Fig. 1. In the window of the transformer frame there are h current-carrying windings. The force acting on the shaded rectangular part of the winding s is required.

In order that we may come to grips with the problem and find its solution, we make the following assumptions:

1. Cylindrical symmetry is assumed. The limb is therefore represented by a perfect cylinder, the horizontal yoke by a plane of infinite length and, finally, the vertical yoke for the return flux path by a hollow cylinder with an inside radius r_2, as is more or less the case with single-phase transformers of the radial-core type. The solution must also permit the boundary transition $r_2 \rightarrow \infty$.

---

[1] The figures in brackets refer to the bibliography on p. 328.

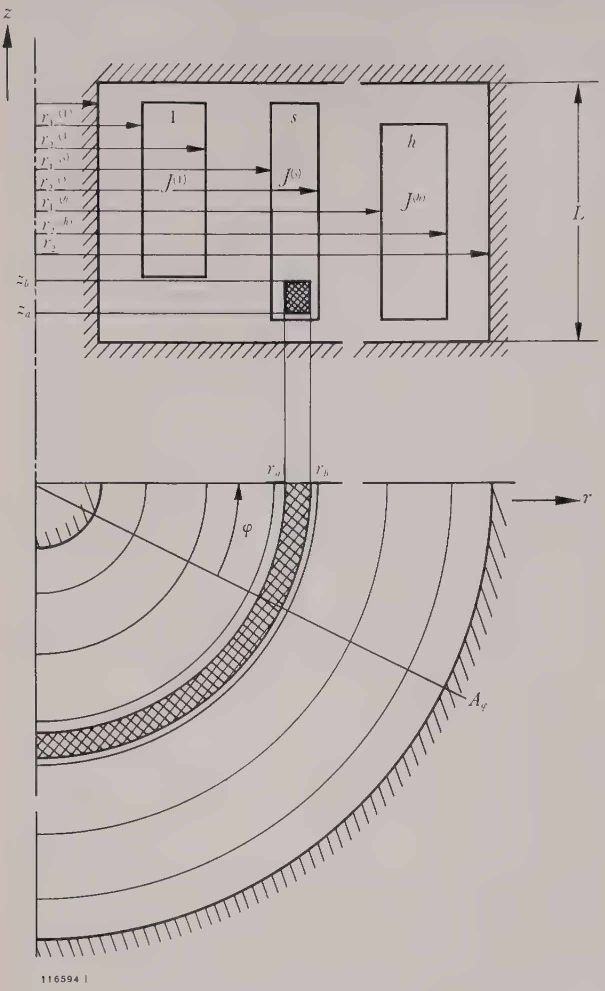

Fig. 1. – Cross-section of the window of a transformer with h windings

r, z, φ = Cylindrical coordinates
r_1 = External radius of the limb
r_2 = Internal radius of the shell for the return flux path
$r_1^{(s)}$ = Internal radius of the s-th winding
$r_2^{(s)}$ = External radius of the s-th winding
$s = 1$ to h = Numerical notation of the windings
L = Height of transformer window
$J^{(s)}$ = Current density in the s-th winding
r_a, r_b, z_a, z_b = Limits of the part of the winding for which the force is to be calculated
A_φ = Reference axis for φ

2. The permeability of the iron is assumed to be infinite, i.e. the lines of magnetic force are perpendicular to the boundary surface between iron and air at all points. Equally important is the assumption that the integral of the current density vanishes if extended over all windings (the sum of the ampere-turns is zero).

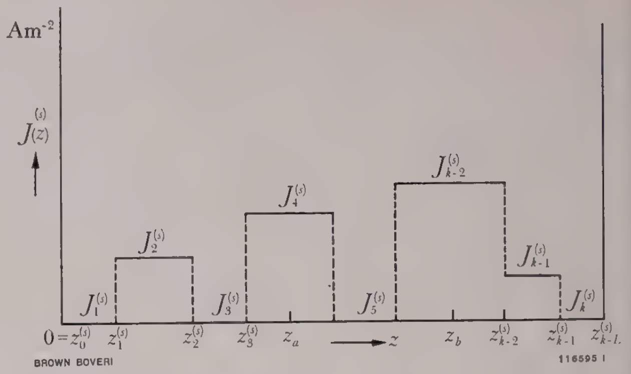

Fig. 2. – Current density $J(z)^{(s)}$ in the s-th winding, as a function of the z coordinate

3. Every winding is assumed to be rectangular in cross-section, i.e. there is assumed to be no variation in the radial dimensions of the winding along the axis.

4. The current density in every winding is assumed to be constant in the radial direction (i.e. from $r_1^{(s)}$ to $r_2^{(s)}$). Hence we can define a current density $J(z)^{(s)}$ in every winding, which is independent of the radius. For each winding the value is constant in parts, so that the overall representation can be in the form of a stepped curve (Fig. 2). This last assumption greatly facilitates integration, as will be demonstrated in the next two chapters. On the other hand, this assumption is sufficiently general to cover all cases occurring in practice. In the calculations it is merely necessary to ensure that the winding is adequately subdivided.

With these four assumptions an exact solution is derived in the next two chapters. It may be expected that the error resulting from the idealization of the conditions, i.e. the ideal distribution of the iron, infinite permeability of the iron, neglect of the winding insulation, will be insignificant.

2. Differential Equation for the Magnetic Field and its Solution

The cylindrical system of coordinates (r, φ, z) is used, as shown in Fig. 1. The vector $\vec{J}$ of the current density has a φ component only, the same being true of the vector potential $\vec{V}$; these components are denoted by J and V. From Maxwell's equations the following partial differential equation can be derived:

$$\frac{\partial^2 V}{\partial r^2} + \frac{1}{r}\frac{\partial V}{\partial r} - \frac{V}{r^2} + \frac{\partial^2 V}{\partial z^2} = \mu_0 J \qquad (1)$$

where $\mu_0 = 0{\cdot}4\,\pi\,10^{-6}\ \mathrm{H\,m^{-1}}$

Once the solution for the vector potential has been found, the components of the magnetic flux density can then be obtained from it in the following way:

$$B_r = -\frac{\partial V}{\partial z}\,;\ B_z = \frac{1}{r}\frac{\partial (rV)}{\partial r}\,;\ B_\varphi = 0 \qquad (2)$$

Moreover the solution must satisfy the following boundary conditions (the lines of force are perpendicular to the boundary surfaces between iron and air):

$$B_r(r, 0) = B_r(r, L) = 0 \qquad (3\text{a})$$

$$B_z(r_1, z) = B_z(r_2, z) = 0 \qquad (3\text{b})$$

With the tentative solution:

$$V(r, z) = R(r).Z(z) \qquad (4)$$

we obtain the next relationship from equation (1) for the *homogeneous* part:

$$\frac{R''}{R} + \frac{1}{r}\frac{R'}{R} - \frac{1}{r^2} = -\frac{Z''}{Z} = m^2 \qquad (5)$$

Since the first expression depends only on r, the second only on z, then m must be constant. Taking into account the boundary conditions (3a), we then obtain the characteristic functions:

$$Z(z) = \cos mz \qquad (6)$$

where $m = \frac{n\pi}{L}$ $(n = 0, 1, \ldots)$

These, however, are exactly the characteristic functions of the Fourier expansion of an even function in the interval $(0{\cdot}2L)$. By substituting (4) and (6) in (1) we therefore obtain the following ordinary differential equation:

$$\left(\frac{\mathrm{d}^2}{\mathrm{d}r^2} + \frac{1}{r}\frac{\mathrm{d}}{\mathrm{d}r} - \frac{1}{r^2} - m^2\right) R_n(r)\cos mz =$$
$$= -\mu_0\, j_n \cos mz \qquad (7)$$

where R_n or j_n respectively denote the n-th term of the Fourier expansion of:

$$V(r, z) = \sum_{n=0}^{\infty} R_n(r)\cos\frac{n\pi}{L}z$$

$$\text{or}\quad J(z) = \sum_{n=0}^{\infty} j_n \cos\frac{n\pi}{L}z$$

Noting the distribution of the current density according to Fig. 2 (for the sake of briefness and clarity the index s is omitted), we readily obtain:

$$\left.\begin{aligned} j_0 &= \frac{1}{L}\int_0^L J\,\mathrm{d}z = \frac{1}{L}\sum_{\nu=1}^{k-1}(J_\nu - J_{\nu+1})\,z_\nu \\ j_n &= \frac{2}{L}\int_0^L J\cos\left(\frac{n\pi}{L}z\right)\mathrm{d}z = \\ &= \frac{2}{n\pi}\sum_{\nu=1}^{k-1}(J_\nu - J_{\nu+1})\sin\frac{n\pi}{L}z_\nu \end{aligned}\right\} \qquad (8)$$

If merely the radial component of the leakage flux density is of interest, we only need to consider the case for $n > 0$ ($n = 0$ makes only a contribution to the axial component). The general solution for the case $n > 0$ is as follows:

$$R_n(r) = C_n I_1(mr) + D_n K_1(mr) - \frac{\pi}{2\,m^2}\cdot\mu_0 j_n L_1(mr) \quad (9)$$

The first two terms on the right-hand side represent the general solution of the homogeneous equation (7). C_n and D_n are the constants of integration, I_1 and K_1 are modified Bessel functions of the first and second kind. The third term is a particular integral of the inhomogeneous differential equation (7). In this case $L_1(mr)$ represents the Struve function [7, 8]. From the foregoing we finally obtain the following expression for the radial component of the flux density:

$$B_r(r, z) = -\frac{\partial V(r, z)}{\partial z} =$$
$$= -\frac{\partial}{\partial z}\sum_{n=1}^{\infty} V_n(r)\cos mz = \sum_{n=1}^{\infty} m\,V_n(r)\sin mz \qquad (10)$$

Here we shall not enter into the details of the lengthy and tedious problem of determining the constants of integration by means of the boundary conditions. Instead we confine our remarks to the following:

The boundary conditions (3a) are already satisfied by the tentative solution (6) with the characteristic values

$$m = \frac{n\pi}{L}.$$

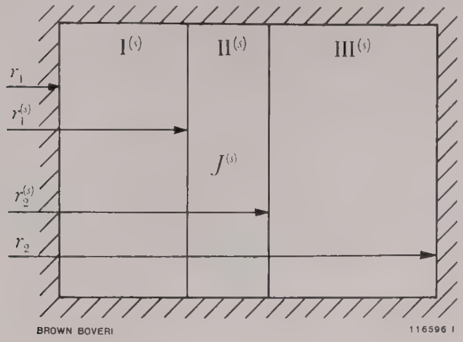

Fig. 3. – Subdivision of the transformer window into the regions I$^{(s)}$, II$^{(s)}$, III$^{(s)}$ *by the s-th winding*

A different integration constant is valid for each of these regions.

Let us first consider that contribution to the vector potential *A*, which is produced by the currents in the *s*-th winding. It may be seen from Fig. 9 that the transformer window is divided by the *s*-th winding into three regions I$^{(s)}$, II$^{(s)}$ and III$^{(s)}$. In each of these regions different values are valid for the constants of integration C_n and D_n. Meanwhile, in addition to the boundary condition (3b), another requirement still has to be taken into account, namely: the solutions must permit a smooth transition from one region to the next. To derive the system of linear equations necessary for the determination of the constants of integration we also need the solution for the axial component of the flux density. For the sake of simplicity, however, this is omitted here. It may be pointed out that for that purpose the following functional relationships between the Bessel and Struve function should be used:

$$\left.\begin{aligned}
&\frac{\mathrm{d}}{\mathrm{d}x}\left[x I_1(x)\right] = x I_o(x)\\
&\frac{\mathrm{d}}{\mathrm{d}x}\left[x K_1(x)\right] = -x K_o(x)\\
&\frac{\mathrm{d}}{\mathrm{d}x}\left[x L_1(x)\right] = x L_o(x)\\
&I_o(x)\,K_1(x) + I_1(x)\,K_o(x) = \frac{1}{x}\\
&x\left[L_1(x)\,K_o(x) + L_o(x)\,K_1(x)\right] = \frac{2}{\pi}\int_0^x \xi K_1(\xi)\,\mathrm{d}\xi\\
&x\;\left[L_1(x)\,I_o(x) - L_o(x)\,I_1(x)\right] = -\frac{2}{\pi}\int_0^x \xi I_1(\xi)\,\mathrm{d}\xi
\end{aligned}\right\}\quad(11)$$

Finally we obtain the following expression for the radial component of the flux density in the region of the winding *s* ($s = 1 \ldots h$):

$$\left.\begin{aligned}
&B_r^{(s)}(r, z) =\\
&\frac{2\mu_0}{\pi^3}\sum_{n=1}^{\infty}\frac{1}{n^2}\left\{\left[\sum_{\sigma=1}^{s-1} A_n^{(\sigma)} R_{3n}^{(\sigma)} + A_n^{(s)} R_{2n}^{(s)} + \sum_{\sigma=s+1}^{h} A_n^{(\sigma)} R_{1n}^{(\sigma)}\right]\cdot\right.\\
&\cdot I_1(x) + \left[\sum_{\sigma=1}^{s-1} A_n^{(\sigma)} S_{3n}^{(\sigma)} + A_n^{(s)} S_{2n}^{(s)} + \sum_{\sigma=s+1}^{h} A_n^{(\sigma)} S_{1n}^{(\sigma)}\right] K_1(x)\\
&\qquad\left. - \frac{\pi}{2} A^{(s)} L_1(x)\right\}\sin mz\\
&\text{where:}\quad m = \frac{n\pi}{L}\\
&\qquad\qquad x = m\,r\\
&A_n^{(\sigma)} = \sum_{\nu=1}^{k^{(\sigma)}-1}\left(J_\nu^{(\sigma)} - J_{\nu+1}^{(\sigma)}\right)\sin m z_\nu^{(\sigma)}\\
&R_{3n}^{(\sigma)} = \frac{I_0(x_1)\cdot K_0(x_2)}{D}\int_{x_1^{(\sigma)}}^{x_2^{(\sigma)}} x K_1\,\mathrm{d}x +\\
&\qquad\qquad + \frac{K_0(x_1)\,I_0(x_2)}{D}\int_{x_1^{(\sigma)}}^{x_2^{(\sigma)}} x I_1\,\mathrm{d}x\\
&R_{2n}^{(\sigma)} = R_{3n}^{(\sigma)} + \int_0^{x_2^{(\sigma)}} x K_1\,\mathrm{d}x\\
&R_{1n}^{(\sigma)} = R_{3n}^{(\sigma)} + \int_{x_1^{(\sigma)}}^{x_2^{(\sigma)}} x K_1\,\mathrm{d}x\\
&S_{1n}^{(\sigma)} = \frac{I_0(x_1)\,K_0(x_2)}{D}\int_{x_1^{(\sigma)}}^{x_2^{(\sigma)}} x I_1\,\mathrm{d}x +\\
&\qquad\qquad + \frac{I_0(x_1)\,I_0(x_2)}{D}\int_{x_1^{(\sigma)}}^{x_2^{(\sigma)}} x K_1\,\mathrm{d}x\\
&S_{2n}^{(\sigma)} = S_{1n}^{(\sigma)} - \int_0^{x_1^{(\sigma)}} x I_1\,\mathrm{d}x\\
&S_{3n}^{(\sigma)} = S_{1n}^{(\sigma)} + \int_{x_1^{(\sigma)}}^{x_2^{(\sigma)}} x I_1\,\mathrm{d}x\\
&D = K_0(x_1)\,I_0(x_2) - I_0(x_1)\,K_0(x_2)
\end{aligned}\right\}\quad(12)$$

3. Computation of the Axial Forces

With the expression thus obtained for the radial component of the flux density, there are no longer difficulties in the way of calculating the force exerted on the shaded part of the winding in Fig. 1. This is equal to:

$$F_z^{(s)} = -\int_{r_a}^{r_b}\int_{z_a}^{z_b}\int_{0}^{2\pi} J^{(s)}(z)\,B_r(r,z)\,\mathrm{d}\varphi\,\mathrm{d}z\,r\,\mathrm{d}r \qquad (13)$$

On carrying out the triple integration we arrive at the final expression

$$\left.\begin{aligned} F_z^{(s)} = {} & 4\mu_0\left(\frac{L}{\pi}\right)^4 \sum_{n=1}^{\infty}\frac{B_n^{(s)}}{n^5}\,\cdot \\ & \cdot\left\{\left[\sum_{\sigma=1}^{s-1} A_n^{(\sigma)} R_{3n}^{(\sigma)} + A_n^{(s)} R_{2n}^{(s)} + \sum_{\sigma=s+1}^{h} A_n^{(\sigma)} R_{1n}^{(\sigma)}\right]\int_{x_a}^{x_b} x I_1\,\mathrm{d}x + \right. \\ & + \left[\sum_{\sigma=1}^{s-1} A_n^{(\sigma)} S_{3n}^{(\sigma)} + A_n^{(s)} S_{2n}^{(s)} + \sum_{\sigma=s+1}^{h} A_n^{(\sigma)} S_{1n}^{(\sigma)}\right]\int_{x_a}^{x_b} x K_1\,\mathrm{d}x - \\ & \left. - \frac{\pi}{2} A_n^{(s)} \int_{x_a}^{x_b} x L_1\,\mathrm{d}x\right\} \end{aligned}\right\} \qquad (14)$$

where: $B_n^{(s)} = \sum\limits_{z_a < z_\nu < z_b} J_\nu^{(s)}\,(\cos m z_{\nu+1} \cos m z_\nu)$

The meaning of the other symbols is either given with expression (12) or is obvious from Fig. 1.

Formula (14) gives the desired expression for the axial force F_z in a transformer as shown in Fig. 1. For practical applications it is important to note that it is quite possible to pass to the limits $r_2 \rightarrow \infty$ (no exterior yoke for the return path of the flux) and $r_1 \rightarrow 0$ (ironless coil).

On the other hand it is, of course, not admissible to pass to the limit $L = \infty$ (no horizontal yoke), as L represents the interval of the period in the Fourier expansion of the vector potential. If the influence of the horizontal yoke on the axial forces is to be investigated, it is sufficient to make L large in comparison with the axial length of the windings, and thus eliminate its effect almost entirely.

The final expression which has been found for the axial force is evidently too complicated to be used for calculations with a desk calculator or with tables of functions. But on the other hand, due to its cyclic structure, this expression is very suitable for numerical evaluation by means of a digital computer. In the following chapter the structure of this expression is analysed and the procedure explained for calculation by the digital computer.

4. Programme for the Digital Computer

Let us now examine the calculation procedure as actually carried out by the digital computer, using the flow diagram in Fig. 4 to help us. The boxes are numbered consecutively from 1 to 19. Box 1 stores the input data, i.e. the geometrical dimensions as shown in Fig. 1, also the distribution of the current density in each of the windings (as in Fig. 2) and finally the data characterizing the part of the winding for which the particular force is to be computed.

The axial force F_2 according to expression (14) is represented as an infinite series with the summation index n. In practice we only need to continue with summation until the error due to neglecting the subsequent terms has become sufficiently small. In box 2 the summation index is set to zero, and a zero is also introduced into the storage cell reserved for the partial sums s_n. The evaluation of a single term a_n of this series takes place in boxes 4 to 16. The summation index is first increased by 1 in box 3, whereupon the quantities which are independent of r are determined in box 4. In box 5 the Bessel and Struve functions, their integrals and the factors ${R_1}_n^{(s)}$ to ${S_3}_n^{(s)}$—composed of the former quantities—are computed. In box 6 a new summation variable σ is given the initial value s. In box 7 the quotas of the investigated windings are calculated. After increasing by 1, box 9 checks whether there are any more windings to the right of s (if $s = h$, as in Fig. 3, there are no more windings present in the region $\mathrm{III}^{(s)}$). In this case the quotas involved are first computed in box 10 and then added directly to what is already present. But if the winding in question is the outermost, or if the addition is finished, the programme will jump from box 9 to 11. This, in analogy to the procedure mentioned above, checks whether there are any more windings to the left of the investigated winding. If so, the contributions involved are calculated and totalled in box 13. If not, the programme will jump directly from 11 to 16. Here the term a_n is completely evaluated and, in the following box 17, finally added to the partial sum s_n already present. Box 18 checks whether the ratio of the newly calculated term a_n to the partial sum s_n is smaller than a given error limit ε. If this is not the case, the calculation of the next term is started in box 3. If the error of the calculation has passed below the error limit ε the required force is computed in the final box by multiplying the newly calculated partial sum with the constant factor

$$4\,\mu_0 \left(\frac{L}{\pi}\right)^4.$$

The flow diagram in Fig. 4 merely shows a rough outline of the actual calculation procedure. Yet it gives a visual idea of how a calculation programme for a digital computer is set up. The greatest difficulties in setting up the calculation programme were presented by the computation of the Bessel and Struve functions and their integrals. As a digital computer has no table of functions at its disposal, it is obliged to calculate all the values of these functions itself. This is done with the aid of power or asymptotic series. A paper in a later issue of this journal will deal with the problems involved in these calculations.

5. Applications

The method for the calculation of forces, described in the foregoing sections, finds a wide range of application. Its usefulness will now be illustrated by means of a simple example.

Fig. 5 (top left) shows the cross-section of a two-winding transformer with windings. The total of the contraction forces, F_1 and F_2 respectively, each of which acts on one of the winding halves 1 and 2, was calculated. Here the clearance d between the winding and the horizontal yokes was varied; the graphs in Fig. 5 show the forces F_1, F_2 and their sum $F_1 + F_2$ as a function of the distance d between the winding and the horizontal yoke. Moreover the influence of the distance between the exterior winding and the vertical yoke for the return path of the flux was investigated; $e = 20$ corresponds to a

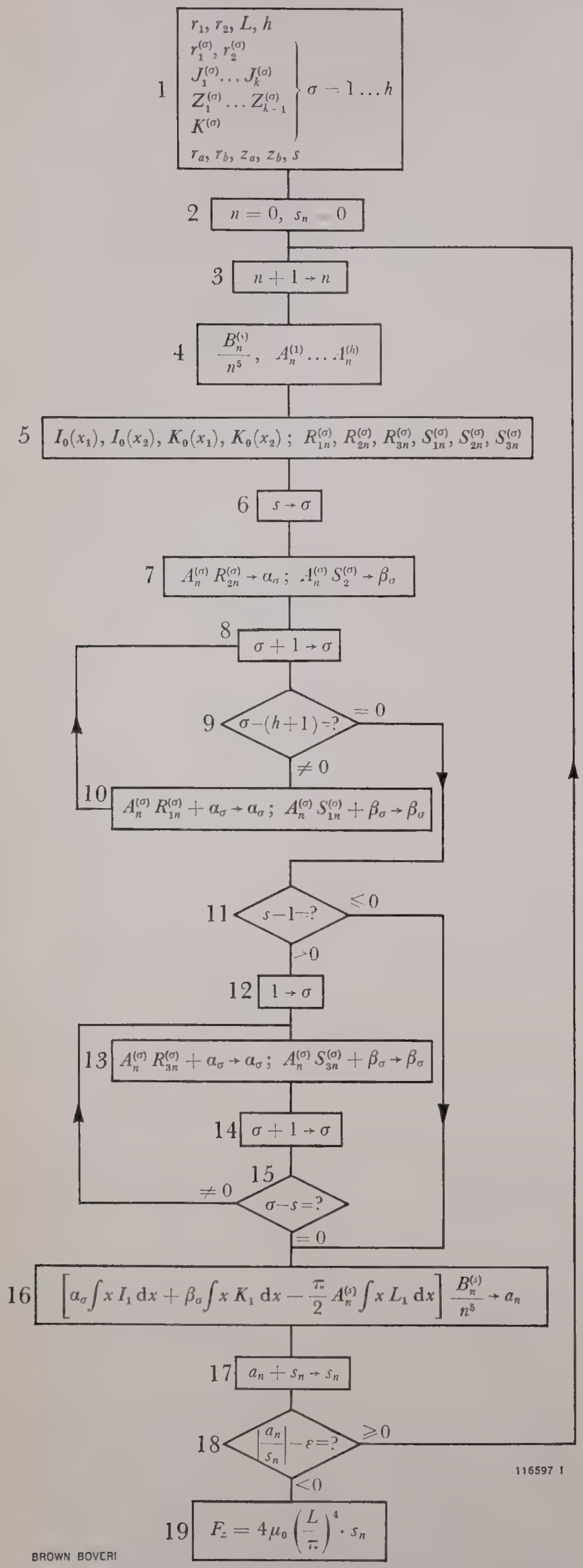
1
r_1, r_2, L, h
$r_1^{(\sigma)}, r_2^{(\sigma)}$
$J_1^{(\sigma)} \dots J_k^{(\sigma)}$
$Z_1^{(\sigma)} \dots Z_{k-1}^{(\sigma)}$
$K^{(\sigma)}$
$\sigma = 1 \dots h$
r_a, r_b, z_a, z_b, s
2
$n = 0,\ s_n = 0$
3
$n + 1 \rightarrow n$
4
$\frac{B_n^{(s)}}{n^5},\ A_n^{(1)} \dots A_n^{(h)}$
5
$I_0(x_1), I_0(x_2), K_0(x_1), K_0(x_2);\ R_{1n}^{(\sigma)}, R_{2n}^{(\sigma)}, R_{3n}^{(\sigma)}, S_{1n}^{(\sigma)}, S_{2n}^{(\sigma)}, S_{3n}^{(\sigma)}$
6
$s \rightarrow \sigma$
7
$A_n^{(\sigma)} R_{2n}^{(\sigma)} \rightarrow \alpha_\sigma;\ A_n^{(\sigma)} S_2^{(\sigma)} \rightarrow \beta_\sigma$
8
$\sigma + 1 \rightarrow \sigma$
9
$\sigma - (h+1) = ?$
$= 0$
$\neq 0$
10
$A_n^{(\sigma)} R_{1n}^{(\sigma)} + \alpha_\sigma \rightarrow \alpha_\sigma;\ A_n^{(\sigma)} S_{1n}^{(\sigma)} + \beta_\sigma \rightarrow \beta_\sigma$
11
$s - 1 = ?$
≤ 0
> 0
12
$1 \rightarrow \sigma$
13
$A_n^{(\sigma)} R_{3n}^{(\sigma)} + \alpha_\sigma \rightarrow \alpha_\sigma;\ A_n^{(\sigma)} S_{3n}^{(\sigma)} + \beta_\sigma \rightarrow \beta_\sigma$
14
$\sigma + 1 \rightarrow \sigma$
15
$\sigma - s = ?$
$\neq 0$
$= 0$
16
$\left[\alpha_\sigma \int x\, I_1\, dx + \beta_\sigma \int x\, K_1\, dx - \frac{\pi}{2} A_n^{(s)} \int x\, L_1\, dx\right] \frac{B_n^{(s)}}{n^5} \rightarrow a_n$
17
$a_n + s_n \rightarrow s_n$
18
$\left|\frac{a_n}{s_n}\right| - \varepsilon = ?$
≥ 0
< 0
19
$F_z = 4\mu_0 \left(\frac{L}{\pi}\right)^4 \cdot s_n$
116597 I

Fig. 4. – Flow diagram for the computation of the axial force F_z using equation (14)

For explanation see text.

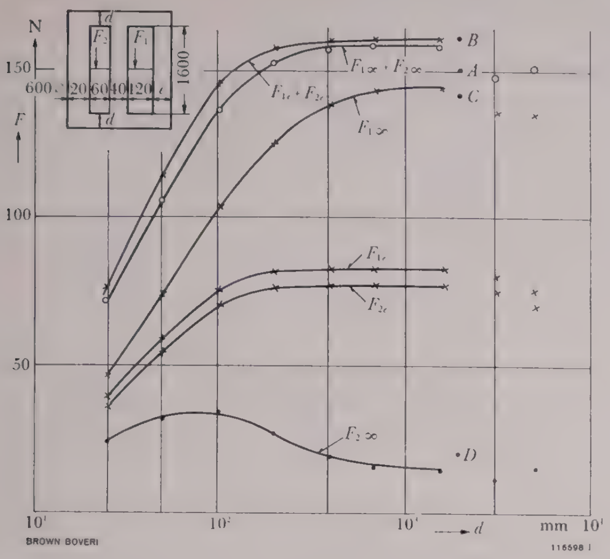

Fig. 5. – Compression forces F_1 and F_2 in the inner and outer windings of a two-winding transformer with symmetrical windings, as a function of the distance d between the windings and the horizontal yoke with and without an outer yoke for the return flux path

With yoke $e = 20$, the forces are F_{1e} and F_{2e}

Without yoke $e = \infty$, the forces are $F_{1\infty}$ and $F_{2\infty}$

The points *A* to *D* represent the values computed by simple manual calculating methods, and with radical simplifications:

A: $F_1 + F_2$	computed without allowance for the iron
B: $F_1 + F_2$ C: F_1 D: F_2	the limb taken into account by considering the mirror image of the windings

near yoke for the return path of the flux, $e = \infty$ to a very distant one. The forces plotted (in Newton) refer to an arbitrarily chosen value for the ampere-turns per unit length of 31 250 A/m.

The conclusions of these investigations are not surprising; yet they are valuable for the numerical results obtained. It is noticed that, with increasing clearance *d* between the winding and the horizontal yoke, the forces rise rapidly at first, then more gradually, reaching a certain limit value for $d \rightarrow \infty$. Further the well-known fact is observed that, due to the proximity of the iron core, the inner winding is subjected to substantially higher stresses than the external one. This is only true, however, as long as the outer yoke for the return path of the flux is remote. The force $F_{2\infty}$ reaches a maximum value in the region of $d = 100$ mm. The occurrence of a maximum is explained by the fact that, on the one hand, the axial forces tend to be zero for $d = 0$ while, on the other, the lines of the leakage flux have the tendency to close towards the limb with increasing *d*. This affords relief for the outer winding.

The points *A*, *B*, *C*, *D* represent values calculated by hand using simple methods. The winding curvature was neglected. Moreover the iron was neglected in case *A*, whereas in cases *B–D* the influence of the iron in the limb was taken into account.

This example is highly appropriate as a test case for the digital computer. It is, however, less suitable for demonstrating the advantages of, and the necessity for using an electronic computer, since results can be obtained with manual calculating methods which are at least of the same order of magnitude. The problem, however, assumes a quite different aspect if not only the total sum of the forces is to be determined, but also their distribution along the axis. Fig. 6 shows the results of this calculation for the parameter values: $d = 200$ and $e = \infty$. For the evaluation of these curves each half of the winding was divided into twenty equal parts.

In transformers with symmetrically arranged windings and constant ampere-turns per unit length, it will be observed that the axial forces act mainly at

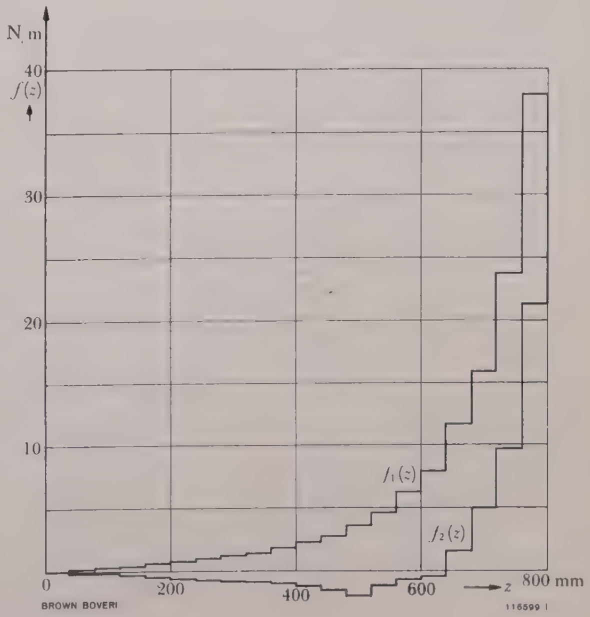

Fig. 6. – Forces per unit length $f_1(z)$ and $f_2(z)$ for the transformer in Fig. 5 and for the parameter values $d = 200$ and $e = \infty$

$z = 0$ denotes the axial mid-point of the winding the ends of the winding. This picture of the forces would certainly alter if the constancy of the ampere-turns per unit length were disturbed, for instance if a number of coil groups were disconnected.

It is interesting to note that the force per unit length $f_2(z)$ of the outermost winding has a zero point relatively near the end of the winding. This means that the maximum value of the compressive force does not appear in the middle of the axial length of the winding, but at two points near the ends, i.e. one at the bottom and the other at the top. This phenomenon has already been mentioned elsewhere (see Fig. 4 on page 12 of [9]). This always occurs in the outer winding of two-winding transformers situated a long way from the yoke for the return flux path.

Finally it is also interesting to study the time taken in calculation. The following may serve as an indication of the time involved. The results required for plotting the curves in Fig. 5 were furnished by a digital computer type S & H 2002 in less than one hour, whereas their evaluation using formula (14) would take many weeks by ordinary methods.

6. Conclusions

The method described for calculating the axial short-circuit forces in transformer windings has proved to be very effective. Its main feature is that calculations can be carried out in a routine manner. The transformer designer only needs to fill out a prepared sheet, stating the data of the windings and marking those parts of the winding for which the forces have to be determined. The digital computer then supplies the desired values in a remarkably short time.

M. CHRISTOFFEL
(Tan) A. KUSTER

Bibliography

[1] F. MÜLLNER: Stromkräfte in Transformatorwicklungen. Elektrotech. u. Maschinenb. 1924, Vol. 42, p. 679.

[2] W. KNAACK: Schubkräfte bei axial verschobenen Transformatorwicklungen. Elektrotech. Z., Edn A, 1955, Vol. 76, p. 217.

[3] W. KNAACK: Mechanical Stresses in Transformer Windings upon Short Circuit. CIGRE Report No. 135/1956.

[4] E. ROTH: Inductance due aux fuites magnétiques dans les transformateurs à bobines cylindriques et efforts exercés sur les enroulements. Rev. gén. Elect. 1936, Vol. 40, p. 259–68, 291–303, 323–336.

[5] A. PICHON, B. HOCHART and F. SALGUES: Problèmes de tenue au court-circuit de transformateurs. CIGRE Report No. 142/1958.

[6] L. RABINS: Transformer Reactance Calculations with Digital Computers. Trans. Amer. Inst. elect. Engrs 1956, Vol. 75/I, p. 261–7.

[7] R. COURANT and D. HILBERT: Methoden der mathematischen Physik I, 2nd edn., publ. by Springer, Berlin 1931.

[8] N. W. MACLACHLAN: Bessel Functions for Engineers, 2nd edn., publ. by Clarendon Press, Oxford 1955.

[9] M. WATERS: The Measurement and Calculation of Axial Electromagnetic Forces in Concentric Transformer Windings. E.R.A. Report Q/T 134, 1953.

THE SHORT-LINE FAULT IN HIGH-VOLTAGE SYSTEMS

621.3.064.1:621.315.1

Following a description of the principal features of the short-line fault, the article explains the effect of the circuit-breaker and its breaking capacity on such faults. Methods for testing the individual interrupters of a breaker with multiple interruption are described. Finally a review is given of tests with short-line faults carried out in h.v. systems.

THE REQUIREMENTS which modern high-voltage circuit-breakers have to fulfil have become increasingly severe in recent years. On the one hand enormous short-circuit powers have to be reliably interrupted in a very short period. On the other hand the breakers must be able to withstand extremely high voltage stresses, such as may occur if a system falls out of step. They must also be capable of interrupting small inductive and capacitive currents reliably without producing inadmissible overvoltages. A modern breaker is also expected to cope with evolving faults. With the rapid growth of short-circuit powers, in particular the short-circuit currents, the short-line fault has also become an important problem. The present article is exclusively devoted to this kind of fault, others having been amply described in previous publications.

I. Principal Features of Short-Line Faults

A short-line fault is a fault occurring a short distance from a breaker on a power line. Fig. 1 shows schematic circuit diagrams of the most important cases. In case *a*, for example, the power source *G* drives a short-circuit current through the three line phases (Z_1, Z_2, Z_3) and, under asymmetrical conditions, through the earth-wire (Z_e) too. When the first phase has been interrupted, a state resembling case *c* is produced; and after the interruption of the second phase, like *e*. But it is not immaterial whether the phases not affected by the short circuit are closed or open. If, due to asymmetry in the system, current is driven through the earth-wire, the potential at the short circuit rises relative to earth potential at the breaker.

Subsequent considerations will refer only to simplified single-phase diagrams. Supposing, in case *e*, the two "sound" phases are ignored, as well as the length of line between the short circuit and the end of the line (Z'_3, Z'_e), and the impedances Z_e and Z_3 are added to form a single impedance Z, the circuit then assumes the form shown in Fig. 2. This case has already been dealt with in the literature on more than one occasion [1, 3],[1] so that it is sufficient to confine present remarks to the most important conditions in the system when the circuit is interrupted.

During the short circuit, the voltage U_n drives the current I through the circuit. The voltage drop across the input impedance is then

$$U_{Z_n} = I \cdot Z_n = U_n \frac{Z_n}{Z_n + Z} \tag{1}$$

and along the line

$$U_Z = I \cdot Z = U_n \frac{Z}{Z_n + Z} \tag{2}$$

At the instant the current is interrupted, when the current is zero at its normal service frequency, the voltage to earth of the line terminal of the breaker – ignoring the resistive component of the line and the breaker arc – attains its peak value at the service frequency:

$$U_Z \sqrt{2} = U_n \sqrt{2} \cdot \frac{Z}{Z_n + Z} \tag{3}$$

---

[1] The figures in brackets refer to the bibliography on p. 339.

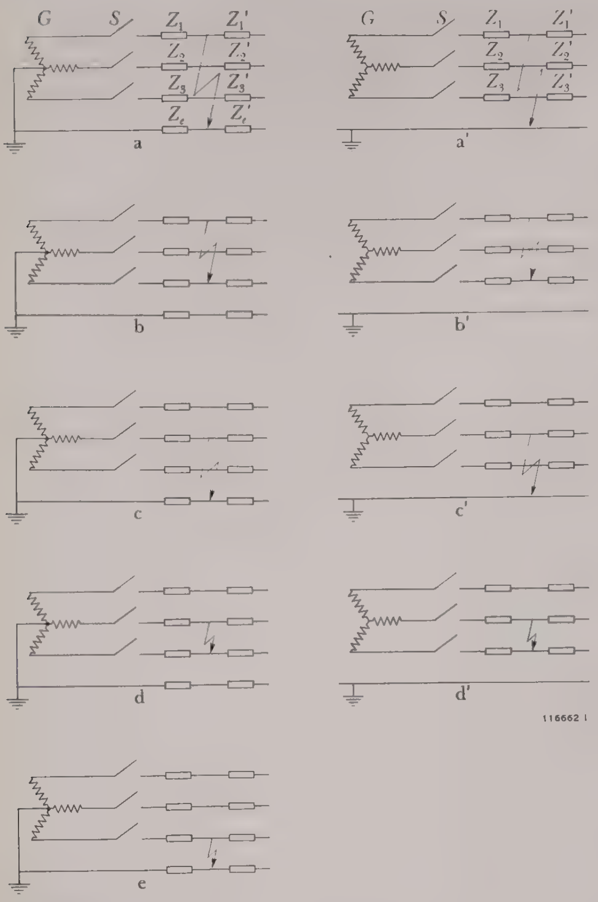

Fig. 1. – The most important forms of short-line fault occurring in h.v. systems

↯ = Short circuit
G = Source of power
S = Circuit-breaker
Z_1, Z_2, Z_3, Z_e = Impedances of the three phases and earth wire, from the breaker to the fault
Z_1', Z_2', Z_3', Z_e' = Impedances of the three phases and earth wire, from the fault to the end of the line
a, a′ = Three-phase earth faults in solidly earthed and unearthed systems
b, b′ = Three-phase short circuits in solidly earthed and unearthed systems
c, c′ = Two-phase earth faults in solidly earthed and unearthed systems
d, d′ = Interphase short circuits in solidly earthed and unearthed systems
e = Single-phase earth fault in a solidly earthed system

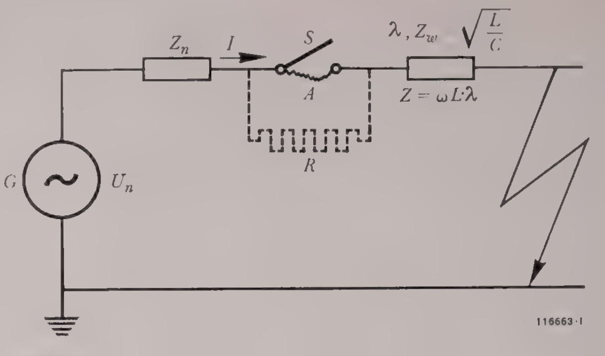
Z_n
I
S
$\lambda, Z_w \sqrt{\frac{L}{C}}$
A
$Z = \omega L \cdot \lambda$
R
G
U_n
116663 I
BROWN BOVERI

Fig. 2. – Simplified single-phase diagram of the short-line fault

G = Source of power
U_n = System voltage
I = Short-circuit current
S = Circuit-breaker
A = Arc in the breaker
R = Resistance parallel to breaker
Z_n = Impedance of the feeding system
Z = Impedance of the line section
λ = Length of the line section
Z_w = Surge impedance of the line = $\sqrt{L/C}$
L = Inductance per km of line
C = Capacitance per km of line
ω = Angular service frequency

According to the laws of travelling waves this voltage returns to zero in the form of a damped saw-tooth oscillation, as illustrated by u_Z in Fig. 3. In contrast, the potential of the input terminal of the breaker, starting at the value given by formula (3), oscillates with the natural frequency of the system damped to the peak value of the driving service-frequency voltage (see curve u_n in Fig. 3). During this process the breaker experiences the difference between these two voltages, as shown by curve u_s in Fig. 3.

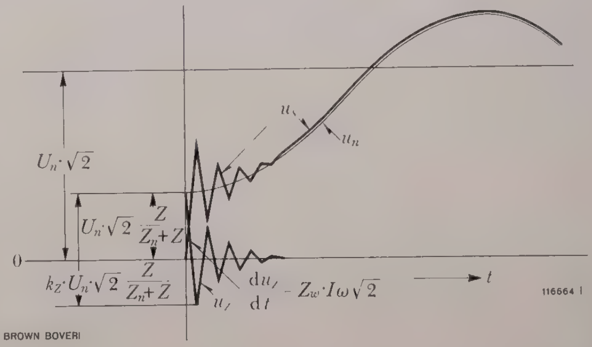

Fig. 3. – Curves showing the voltage to earth at the input terminal (u_n) and at the line terminal (u_z) of the breaker and the voltage across the breaker (u_s)

t = Time
k_z = Amplitude factor of the oscillation on the line side ($1 < k_z < 2$)
For other notation see Fig. 2.

Up to the reversal in the voltage its rate of rise at the line terminal of the breaker, according to well-known considerations, is given by

$$\frac{\mathrm{d}u_Z}{\mathrm{d}t} = Z_w \cdot \left(\frac{d_{\mathrm{i}}}{\mathrm{d}t}\right)_{t=0} = Z_w\, I\omega\,\sqrt{2} \qquad (4)$$

when $Z_w = \sqrt{L/C}$ is the surge impedance of the line and ω is the angular service frequency. If a resistance R is connected in parallel with the breaker, this rate of rise is approximately

$$\frac{\mathrm{d}u_Z}{\mathrm{d}t} = \frac{Z_w \cdot R}{Z_w + R} \cdot I\omega\sqrt{2} \qquad (5)$$

The magnitude of the voltage jump (between initial value and the first peak) of the line terminal will be between once and twice the value given by formula (3), depending on the damping. The surge impedance of an overhead h.v. line is of the order of 450 Ω, that of underground h.v. cables is 45 Ω. Hence the rate of rise at 50 c/s when the breaker is not fitted with parallel resistors and the r.m.s. value of I is in kA, is given by

$$\frac{\mathrm{d}u_Z}{\mathrm{d}t} = 0{\cdot}2 \cdot I \qquad \text{kV/}\mu\text{s for lines}$$

$$\frac{\mathrm{d}u_Z}{\mathrm{d}t} = 0{\cdot}02 \cdot I \qquad \text{kV/}\mu\text{s for cables.}$$

From the above it will be seen that the problem of short-line faults is far less serious in underground cable networks than in systems with overhead lines.

If, instead of the line in Fig. 2, we consider a different impedance, e.g. a reactor or a transformer with its secondary short-circuited, the conditions are similar. But then the voltage oscillation on the disconnected side is sinusoidal and not saw-tooth, as with the short-line fault. In particular the initial rate of rise of the voltage is zero, in contrast to the value given in (4) and (5). As will be demonstrated later, this may be important as regards the breaking capacity.

As mentioned earlier these remarks are only approximately true. In reality there are a number of other factors present, such as the effect of adjacent phases, travelling waves between the fault and the end of the line, the possible presence of voltage transformers, carrier frequency traps, and so on. The breaker also exerts an important influence on the phenomena occurring during the interruption of short-line faults, as will be demonstrated later.

II. Effect of the Circuit-Breaker and Breaking Capacity on Short-Line Faults

Tests with Airblast Breakers

(a) *The arc in the breaker*

Before the short-circuit current is interrupted, an arc A burns in the breaker (see Fig. 2). The arc voltage causes an increase in the potential to earth of both the input terminal and the line terminal of the breaker. During the half-wave of service-frequency current this increase is distributed between the breaker terminals roughly in the ratio of the impedances Z_n and Z; at the final moment, though, just as the arc voltage reaches its peak, the distribution can be quite different, depending on the capacitance on either side of the breaker. The increase is larger on the side with the smaller capacitance. In Fig. 4 the curve of the breaker voltage resulting from the arc voltage is compared with the "ideal" curve. During the ideal interruption (without allowing for arc voltage) the ionized break ought to

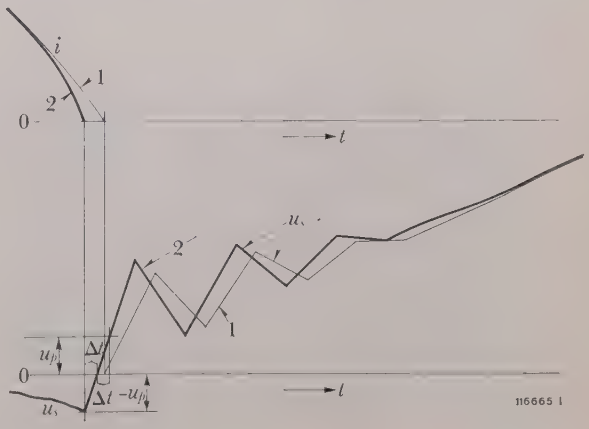

BROWN BOVERI

Fig. 4. – Curves of breaker current and voltage

1 = With an "ideal" breaker
2 = In the presence of arc voltage
i = Current through the breaker
u_s = Breaker voltage
$-u_p$ = Peak arc voltage before extinction
t = Time

withstand the rising restriking voltage immediately the current is interrupted. But due to the arc voltage the conditions of the break are much less severe. Admittedly the current drops more sharply to zero and the high-frequency part of the restriking voltage attains a higher peak value (compare curve 2 with curve 1). But the voltage across the breaker, having reached its peak $-u_p$ at which extinction occurs, first drops to zero in the time Δt. During this time the break can be partially deionized. When the voltage has passed zero it is impossible for the arc to restrike until the value $+u_p$ has been attained after another period of Δt; the striking voltage being notably higher than the arc voltage peak. From this it follows that, for certain short lengths of line and currents where the voltage drop on the line side is small, it is quite impossible for the breaker to fail as a result of a short-line fault. The numerous tests carried out confirm this.

(b) *Residual conductivity of the break*

As recent measurements have proved, every breaker develops a residual conductivity between its contacts immediately following the interruption. In the airblast breaker the duration of this residual conductivity is only a few microseconds, owing to the speed of the air blast. Since the voltage across the breaker during a short-line fault can equally rapidly rise to a value which can no longer be ignored, the residual conductivity is stressed by the residual current and the conducting zone is heated. Provided the amount of heat dissipated by the stream of air is greater than the amount generated, the interruption is successful. If not, it is possible for the arc to restrike thermo-electrically. Due to the presence of a residual current, the shape of the inherent restriking voltage is changed. The break, which is still capable of conducting, acts like a variable resistance in parallel with the breaker. It damps the rise of the restriking voltage. This can be seen in the oscillogram in Fig. 5, where the voltage (on the line side) in the first few microseconds no longer agrees with the theoretical inherent voltage. On the one hand, the measured change in voltage at the start is less than the inherent value. On the other hand, it can be seen that the envelope of the decaying voltage on the line side, when produced backwards, does not meet the initial value of the voltage. The very severe damping exhibited here during the first half-cycle of the line oscillation is mainly due to the residual conductivity of the break. The restriking voltage and residual conductivity are therefore closely related. The ionized break damps the restriking voltage, but is heated by it, thus changing its resistance.

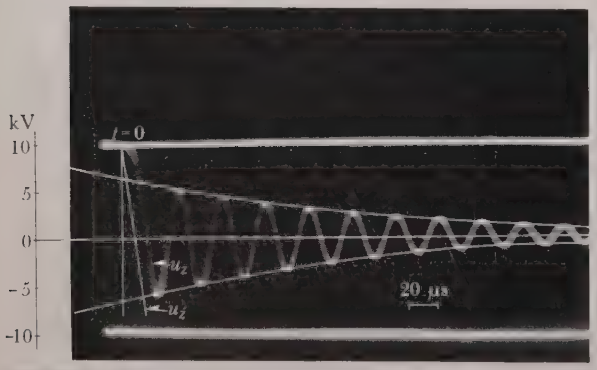

Fig. 5. – Oscillogram of the voltage on the line side of the breaker when interrupting a short-line fault of 14·8 kA at 52 kV with an airblast circuit-breaker

u_z = Measured voltage
u_z' = Calculated inherent voltage
$t = 0$: Arc extinguished

Distance to fault: 1·6 km

A much less regular voltage curve, in this case between the contacts, is illustrated by the oscillogram in Fig. 6, which corresponds to the interruption of a short-line fault with a current of 9·2 kA at a distance of 0·5 km from the breaker.

The characteristic oscillation caused by the line is heavily damped and distorted. In the current oscillogram (i) a residual current is visible between t_0 and t_1, which attains a peak value of 22 A [4]. At the moment t_1 when the residual current finally disappears, the oscillation on the line side is re-energized. This is easily explained by the fact that the residual current in this case drops to zero in a similar manner to the main current, although somewhat more slowly. This oscillogram shows how much the true conditions can deviate from the simplified theory laid down at the beginning of the article. The numerous measurements of this kind which have been carried out have produced a wide variety of voltage and current curves which cannot be expressed by simple formulae.

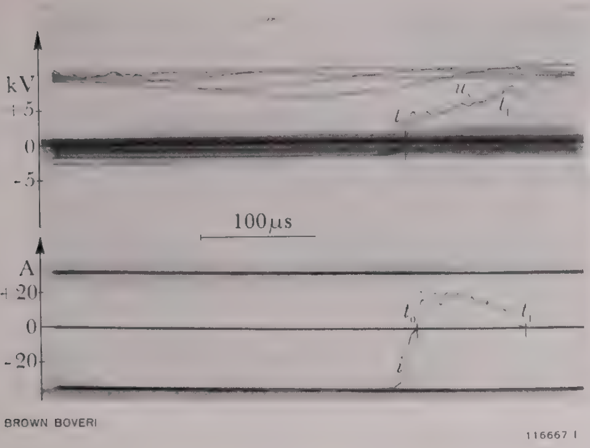

Fig. 6. – Oscillogram of the breaker voltage and current when a fault of 9·2 kA is interrupted on a line 0·5 km long by an airblast circuit-breaker

The cathode ray (controlled by a sweep generator for rapid flyback) covered the trace several times. The current oscillogram only shows the true values for the part close to zero. Higher momentary values are reduced by an amplitude limiter.

t_0 = Time at which current and voltage are zero
t_1 = Residual current disappears
u_s = Breaker voltage
i = Breaker current

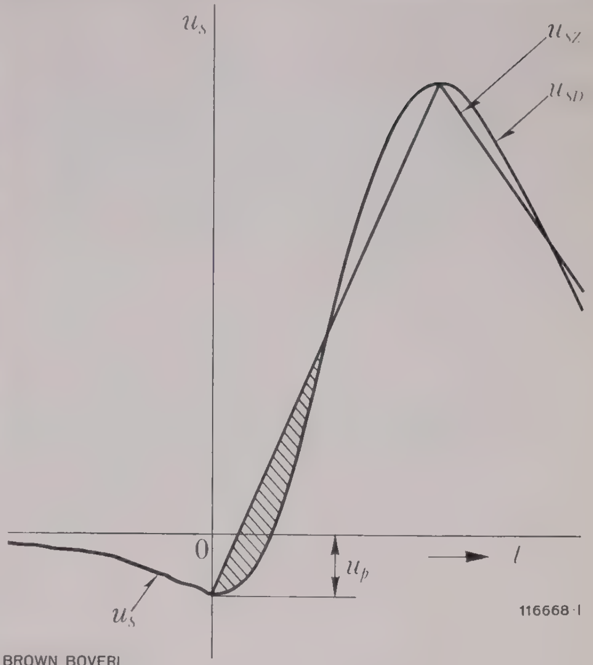

Fig. 7. – Curves of the breaker voltage in the case of a short-line fault (u_{sZ}) and when the short line is replaced by a concentrated reactance between the breaker and the fault (u_{sD}), without the residual conductivity of the breaker being taken into account

u_p = Peak arc voltage before extinction
u_s = Breaker voltage

Since the residual current retards the voltage rise, it simplifies the task of the breaker insofar as it renders restriking due to voltage breakdown very difficult. On the other hand, under certain conditions, on every breaker a critical residual current may cause restriking due to thermal breakdown, so it is impossible to conclude in every case whether a residual current will always be favourable or not. It may be pointed out that it is not only the magnitude and the duration of the residual current appearing under given conditions which depend on the properties of the breaker, but also the critical power of the residual current which causes thermal breakdown [4].

(c) *Comparison between the voltage oscillation on the line and a sinusoidal oscillation*

As already stated, the high-frequency component of the restriking voltage follows a similar curve if the line is replaced by a concentrated impedance, e.g. a reactor. In Fig. 7 these two are shown without paying any attention to the residual conductivity. Between these two, however, despite the assumption of equal natural frequency and equal peak voltages, there is an appreciable difference in the initial rate of rise of the restriking voltage, and after the arc voltage has reached its peak prior to extinction. In the case of concentrated reactance (u_{SD}) the break has more time to become deionized after extinction of the arc ($t = 0$) than it has with a short-line fault (u_{SZ}), i.e. there is less risk with the former. The truth of this has been confirmed in practice by a large number of tests. At equal natural frequency and with equal peak value it was possible to cope with considerably more power in a circuit with concentrated reactance, than was possible with a short-line fault.

(d) *Resistors parallel to the breaker*

Resistors in parallel with the breaker reduce the rate of rise and the first peak value of the voltage transient caused by the line. The time taken to

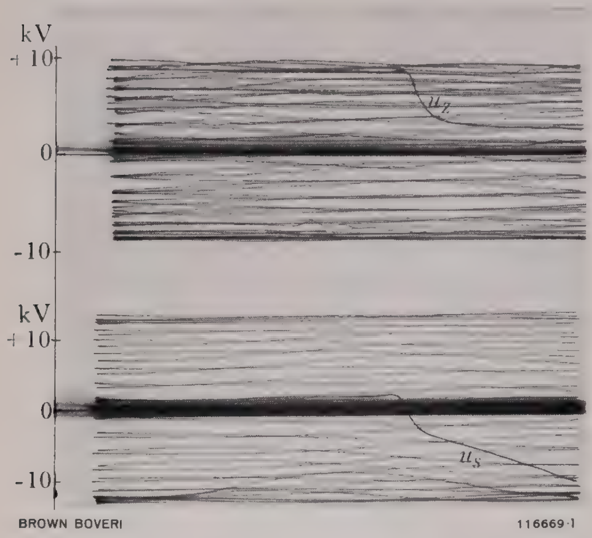

Fig. 8. – Oscillogram of the breaker voltage u_s and the voltage at the line terminal u_z when a short-line fault of 14·5 kA is interrupted on a line 0·5 km long, using an airblast circuit-breaker equipped with a parallel resistance of 100 Ω

reach the first voltage peak, or the first irregularity in the voltage rise, is in every case the same. If the ohmic value of the parallel resistance is equal to the surge impedance, the voltage on the line side falls with the initial gradient to zero and then stays equal to zero. If the resistance is smaller than the surge impedance, the zero line is not even reached with the initial gradient, the voltage changes direction beforehand and it approaches the zero line in a convex succession of straight lines. In Fig. 8 the junctions are somewhat rounded off.

(e) *Breakers with multiple interruption. Potential control. Stressing and testing individual interrupters. Breakers with parallel resistors*

It is a well-known fact that in breakers with multiple interruption the capacitances to earth of the series interrupters produce a non-linear voltage distribution across the breaker pole. For switching operations where the restriking voltage has a low or medium natural frequency, an improved or linear potential distribution is obtained by connecting control capacitors or resistors in parallel with the interrupters. With short-line faults the conditions during the steep initial rise of the restriking voltage are somewhat different. As mentioned before, the residual conductivity of the break becomes effective. To begin with, the voltage distribution is almost wholly determined by it. But it is not known whether the distribution is ideal. It may, however, be assumed to be so from the following considerations. If the residual conductivity, or resistance, is different from one interrupter to another, the rising voltage is distributed in proportion to these resistances. Since the current is the same in all the series arc chambers, the interrupter with the highest resistance will be heated most, thereby reducing the resistance, while in another interrupter with low resistance, the reverse takes place. In other words the resistance regulates itself to an equal value, thereby affording at least an approximately ideal voltage distribution. Tests performed to check this principle appear to confirm this argument. Fig. 9 shows the limiting breaking capacity of two arc chambers in series when clearing a short-line fault (distance 0·5 km) with various methods of potential control.

If a favourable means of potential control were not afforded by the residual conductivity, the breaking capacity in *b* ought to be less than in *a*. The test *c* shows, in comparison to *a*, that the residual resistances R_p in the two arc chambers must be roughly equal since the additional 1000 Ω in parallel provided for voltage control in case *c* exert a predominant influence and produce an ideal voltage distribution. Since the breaking capacity is practically the same in *a* and *c*, it may be concluded that with the arrangement *a* both interrupters are equally stressed by the restriking voltage, i.e. both possess the same resistance R_p. This state of affairs only applies to short lines, that is, so long as the residual conductivity is effective. As soon as the line exceeds, for example, 1·5 km in length, this control effect may only be present in the first part of the voltage rise, whereas in the subsequent part the other means of control gain the upper hand. However, the above tests should confirm that the residual resistances of the series arc chambers are approximately equal.

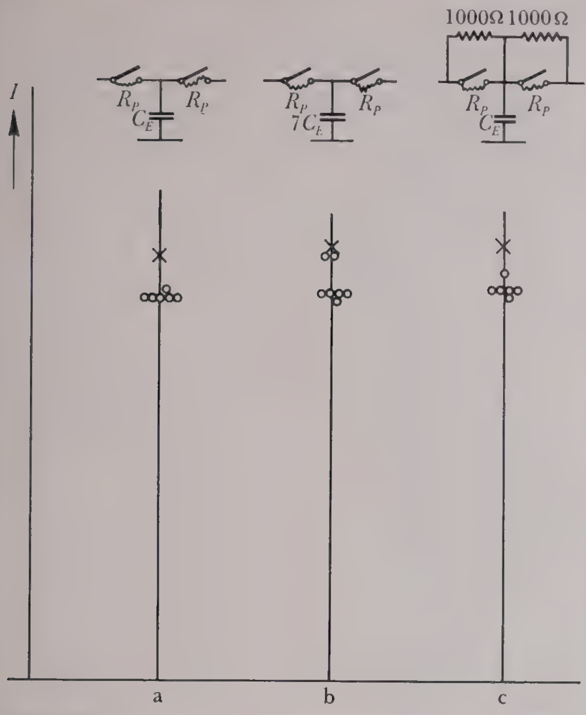

Fig. 9. – Breaking capacity of a breaker pole with two interrupters, with a fault situated 0·5 km from the breaker

a: Breaker pole without potential control

b: Potential distribution unfavourably influenced by artificially increasing the capacitance to earth

c: Potential distribution favourably influenced by adding 1000-Ω resistors in parallel with each interrupter

C_E = Natural capacitance to earth of the metallic parts between two interrupters

R_p = Resistance of the ionized gap between open contacts

I = Breaker current

○ = Successful interruptions

× = Limit of breaking capacity

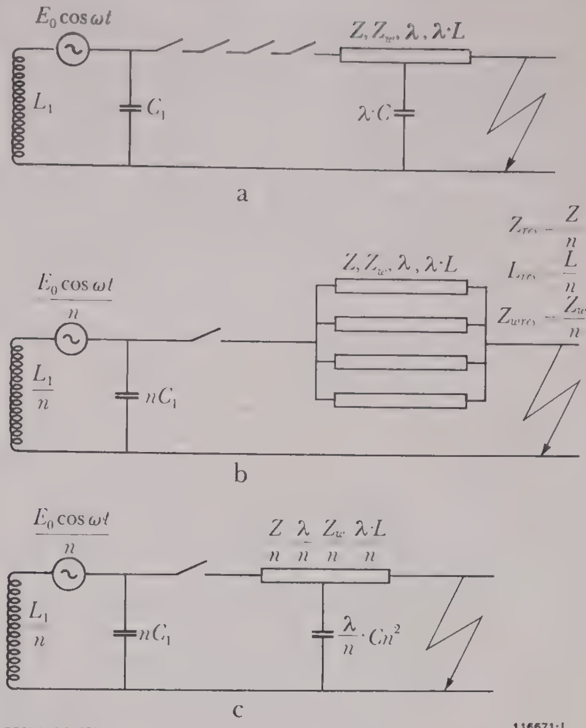
$E_0 \cos \omega t$
$Z, Z_w, \lambda, \lambda \cdot L$
L_1
C_1
$\lambda \cdot C$
a
$Z_{res} = \frac{Z}{n}$
$L_{res} = \frac{L}{n}$
$Z_{wres} = \frac{Z_w}{n}$
$\frac{E_0 \cos \omega t}{n}$
$\frac{L_1}{n}$
nC_1
b
$\frac{Z}{n}$ $\frac{\lambda}{n}$ $\frac{Z_w}{n}$ $\frac{\lambda \cdot L}{n}$
$\frac{\lambda}{n} \cdot Cn^2$
c
BROWN BOVERI
116671·I

Fig. 10. – Proposals for unit testing of breakers with multiple interruption having no parallel resistors and subjected to short-line faults

a: Short-line fault with complete breaker pole

b: Testing one interrupter with n parallel line sections short-circuited at their ends

c: Testing one interrupter with a line artificially changed by additional capacitance

C = Capacitance per km of line

L = Inductance per km of line

$E_0 \cos \omega t$ = Driving voltage

L_1, C_1 = Inductance and capacitance of the feeding system

n = Number of interrupters

For other notation, see Fig. 2

A single interrupter of a breaker pole having n interrupters is stressed as follows with ideal voltage distribution. The breaking current is the same throughout the breaker pole, the initial rate of rise and first peak value of the restriking voltage caused by the line are $1/n$ of the value for the complete pole. If we now denote the voltage share of one interrupter by u_{Z_1}, its first peak (amplitude) by $u_{Z_1 max}$, and the resultant amplitude factor by k_Z, it follows that

$$u_{Z_1 max} = \frac{k_Z U_Z \sqrt{2}}{n} = \frac{k_Z U_n \sqrt{2}}{n} \cdot \frac{Z}{Z_n + Z} \quad \text{[cf. eqn. (3)]} \qquad (6)$$

and

$$\left.\frac{\mathrm{d} u_{Z_1}}{\mathrm{d} t}\right|_{t=0} = \frac{1}{n} \cdot Z_w \cdot I \omega \sqrt{2} \quad \text{[cf. eqn. (4)]} \qquad (7)$$

Therefore to test a single interrupter with respect to a short-line fault, it is necessary for the corresponding curve of the system voltage to be realized.

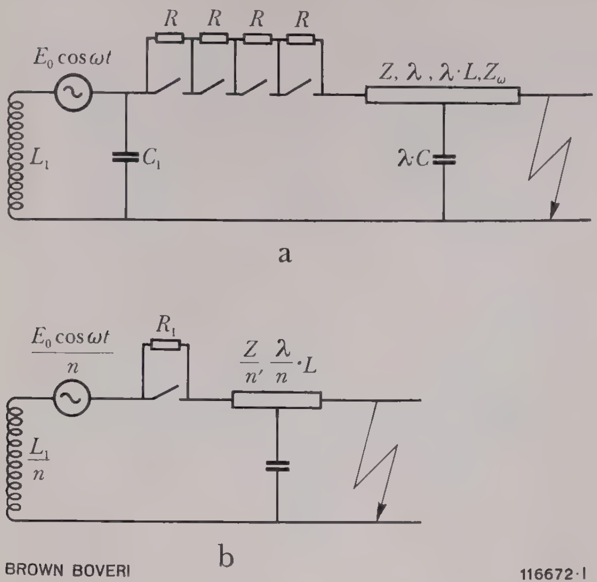
R R R R
$E_0 \cos \omega t$
$Z, \lambda, \lambda \cdot L, Z_w$
L_1
C_1
λC
a
$\frac{E_0 \cos \omega t}{n}$
R_1
$\frac{Z}{n'} \frac{\lambda}{n} \cdot L$
$\frac{L_1}{n}$
b

BROWN BOVERI 116672·I

Fig. 11. – Unit test of breakers with multiple interruption and parallel resistors, subjected to short-line faults

a: Short-line fault, the breaker being equipped with resistors, R per interrupter

b: Testing one interrupter with the equivalent resistance R_1

R = Parallel resistance per interrupter
R_1 = Equivalent parallel resistance when testing one interrupter

For other notation, see Fig. 10

But these two conditions are not sufficient. As stated before, the residual conductivity of the break is not only stressed by the rate of rise and the peak value of the restriking voltage but also by the oscillation energy of the line alone. Consequently $1/n$ of this energy must be provided when testing the single interrupter, namely

$$W_{Z_1} = \frac{1}{n} W_Z \tag{8}$$

The three conditions (6), (7) and (8) are fulfilled by the test circuits shown in Fig. 10. Circuit *b* for instance contains n parallel line sections shorted at their ends and having the same length and impedance as in the original case *a*, the voltage and impedance on the input side being only $1/n$ of the values in *a*, with the same natural frequency. Test circuit *c* consists of a line with $1/n$ of the original length, its surge impedance, however, being reduced artificially by capacitances which are distributed in such a manner that the character of the line, i.e. the characteristic form of the transient oscillation, is retained. The additional capacitances must be such that their total value per unit length is n^2 times the original capacitance per unit length.

Tests were carried out on breakers having two interrupters, using circuits *b* and *c*. The results confirmed that these tests are conclusive. The breaking capacity of a two-chamber breaker extrapolated from the results obtained with one chamber agreed in every case with the capacity obtained by testing a breaker with two chambers in series.

If the breaker is equipped with a total parallel resistance of nR, i.e. R to each interrupter, the unit test with the same current and $1/n$ the length of line represents approximately the same stress as a proper short-line fault, provided the interrupter is shorted by a resistance R_1, having the following value

$$R_1 = \frac{R \cdot Z_w}{R(n-1) + Z_w} \tag{9}$$

The circuit diagrams explaining this test are shown in Fig. 11. Formula (9) applies with reasonable accuracy provided the resistances R_1 are much smaller than the surge impedance Z_w of the line. In that case the greater part of the resonant energy of the line is dissipated in the resistance. In other words, the stipulation that the amount of resonance energy per interrupter must be maintained precisely is not of primary importance here. With high resistances, however, conditions are different; it is then not possible to establish a well-defined stipulation regarding the energy.

III. Tests in H.V. Systems

Results have been tabulated from numerous tests with short-line faults carried out in the Fontenay Testing Station of Electricité de France, in the Italian Electrotechnical Research Centre (CESI) in Milan, in the Mettlen substation in Switzerland, as well as on an experimental line attached to the

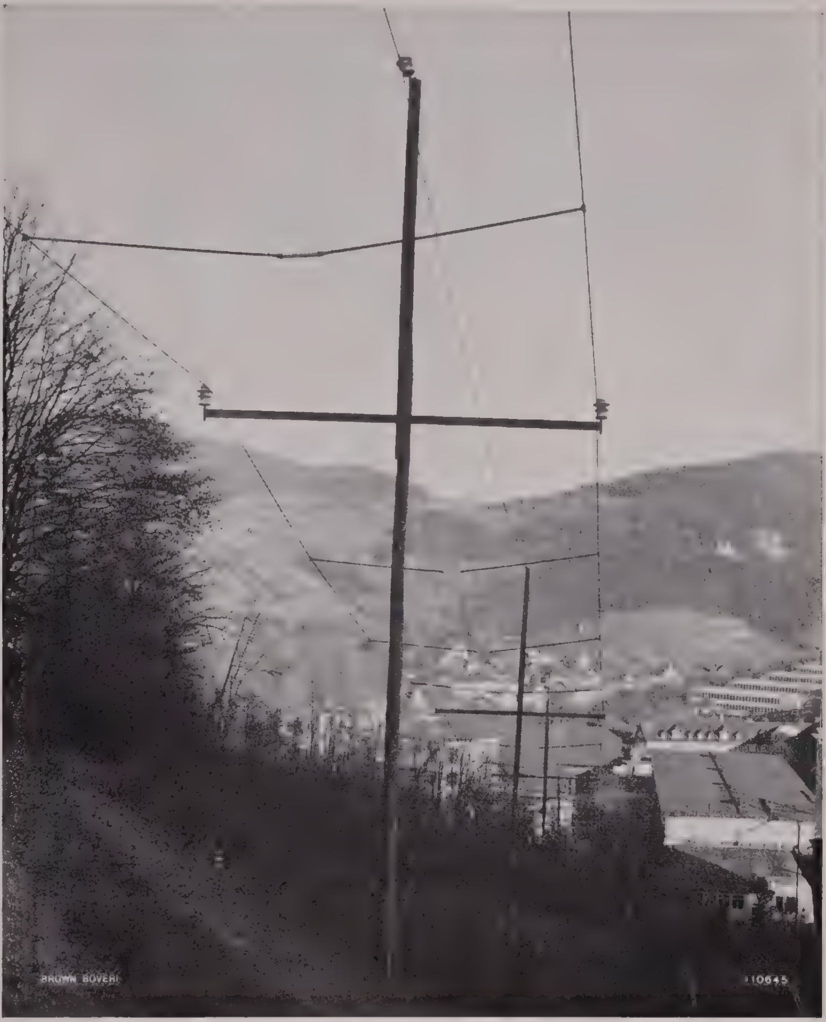

Fig. 12. – Experimental overhead line attached to the Brown Boveri Short-Circuit Testing Station, Baden

Length	1500 m
Height of lower phases from ground	8 m
Distance between phases	6 m
Conductor diameter	20 mm

To improve their resistance to electro-dynamic forces the outer conductors are braced through insulators, the earth-wire is buried in the ground.

Brown Boveri Short-Circuit Testing Station in Baden. At Fontenay it was possible for breakers with up to four arc chambers per pole, with and without parallel resistors, to be subjected to short-line faults of up to 26 kA (with very short lines and lines up to 1·6 km in length. At CESI, on a line 0–10 km in length, short circuits were interrupted with two interrupters, currents of up to 12 kA being supplied at a recovery voltage of 60 kV. At Mettlen a 150-kV breaker pole of normal design, with four interrupters, was tested with short circuits 3 and 6 km away from the breaker. The maximum short-circuit current thereby attainable in the system (9·5 and 8 kA at $150/\sqrt{3} = 87$ kV) was handled without difficulty. By far the largest number of tests were carried out on the experimental line attached to the Brown Boveri Short-Circuit Testing Station in Baden. A photograph of this 1·5 km long three-phase line is reproduced in Fig. 12. The lower phases are 8 m from the ground, the distance between phases is 6 m and the conductors are 20 mm in diameter. With these data the characteristics correspond to those of a normal overhead line.

One fact which these tests have clearly pointed out is that there is a critical length of line. For a breaker with two interrupters a critical line length between 1 and 2 km was established as shown by the curves in Fig. 13. If the breaker interrupts reliably when the short circuit is 1–2 km distant, it will function so much more reliably when the

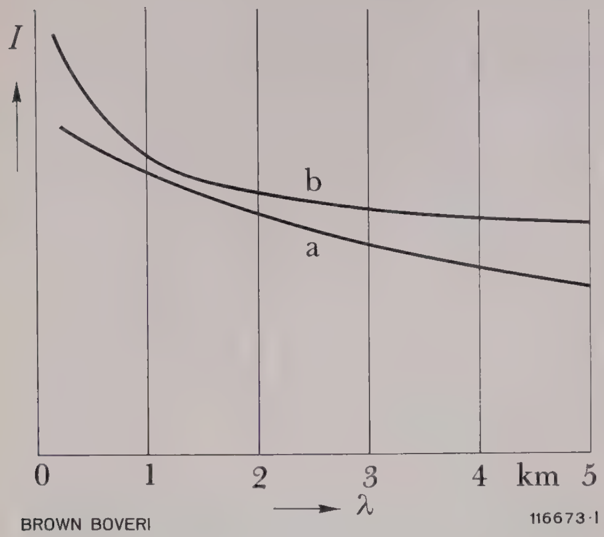

Fig. 13. – Critical length of line

a = Short-circuit current *I* due to system, in terms of line length, commencing at the breaker terminal

b = Breaking capacity of the circuit-breaker. A critical point occurs between 1 and 2 km from the breaker

distance is greater or less. The improved breaking capacity with shorter lengths may possibly be connected with the arc voltage mentioned earlier (see II a). With longer lines the circuit conditions become still less severe on account of the reduced current and the resultant smaller rate of rise of the restriking voltage.

Finally it may be mentioned that arcing short circuits and dead shorts produce almost identical transients and stress the breaker to an equal extent.

IV. Conclusions

The conventional single-phase diagram of a short-line fault is an approximation. To determine the inherent restriking voltage, at least the effect of adjacent phases and the length of line between the fault and the end must be taken into account. The ionized zone between the breaker contacts can considerably damp the inherent restriking voltage, while this voltage in turn heats up the ionized zone and changes its resistance. The reciprocal effect of breaker and the voltage curve, and the breaking capacity in the event of a short-line fault cannot be predicted numerically yet, but can only be determined by tests.

The experimental representation of a short-line fault by a concentrated impedance (instead of a length of line) may imply that the breaking capacity is greater than it really is. Conversion to the true short-line fault conditions is not feasible.

On account of the surge impedance being only one-tenth as great, short-line faults in cable networks are far less serious than on overhead lines.

There is a critical length of line at which the breaker is most severely stressed. For airblast-breakers with two and four interrupters, a critical length of 1–2 km has been established.

If a short-line fault stresses a breaker to the limit of its capacity, the conditions can be improved by fitting a parallel resistance.

In breakers with multiple interruption the residual conductivity affords a favourable initial voltage distribution. When this conductivity vanishes, the other means of potential control – capacitances, resistances – take effect. If there are no facilities available for testing a complete breaker pole with short-line faults, there are perfectly sound methods of testing the individual interrupters. Then the rate of rise and amplitude of the restriking voltage and the electrical oscillation energy of the line section should possess exactly the value which corresponds to the individual interrupter.

Brown Boveri circuit-breakers have been thoroughly tested regarding their capacity to interrupt short-line faults, both on an experimental length of line and in existing power systems. At the highest service voltages of over 300 kV, for which the breakers have eight or ten interrupters, short-line faults are cleared without any difficulty. At lower voltages and very heavy short-circuit currents the performance of the breaker can be improved if necessary by the addition of resistors, or other means.

(KME)

P. BALTENSPERGER
E. RUOSS

Bibliography

[1] M. Michel Pouard: Nouvelles notions sur les vitesses de rétablissement de la tension aux bornes de disjoncteurs à haute tension. Bull. Soc. franç. Elect. 7, Vol. 8, No. 95, p. 748–64.

[2] A. Hochrainer: Symmetrische Komponenten in Drehstromsystemen. Springer Verlag, Berlin/Göttingen/Heidelberg 1957.

[3] R. Petitpierre: Airblast circuit-breakers with relation to stresses which occur in modern networks, with particular reference to the interruption of short-line faults. CIGRE Report No. 115/1960.

[4] W. Rieder, J. Passaquin: On the decrease of the current to zero and the residual current in circuit-breakers. CIGRE Report No. 105/1960.

AIRBLAST CIRCUIT-BREAKERS FOR EXTREMELY HEAVY DUTY

621.316.57.064.45

Due to the lively development of high-voltage power systems, the duties of circuit-breakers become increasingly severe. Illustrated by the results of experiments, this article demonstrates that Brown Boveri airblast breakers will also be able to cope with the severe conditions which may be expected in the future.

Demands on Modern Circuit-Breakers

Owing to the steady rise in the demand for electricity, accompanied by increased generating capacity, conditions are continually changing in transmission systems. Large interconnected grids are being created employing extremely high voltages for transporting this energy in bulk. One consequence of this is that, in systems operating at high or medium voltage, the possible short-circuit powers often increase more rapidly than the installed generating capacity. This results in a heavy demand for circuit-breakers designed for increasingly severe duties. A point which must be borne in mind is that they must not only possess the high breaking capacity which is stipulated, but must also function reliably under a wide variety of other critical conditions. In modern interconnected systems the switchgear must at all times be relied upon to execute all possible operations correctly. The breakers, in addition to disconnecting lines and transformers at no-load, must also be able to open in the case of phase opposition. Having regard to the value of the protected object, as well as the requirement that interruption of the service should be avoided at all costs, increasing stress is laid on short break-times and automatic rapid reclosure. With the growth in the size of switching stations and the shortage of skilled operating personnel, it is preferable to use standardized equipment requiring a minimum of attention. Hence the most suitable breakers are those which operate equally reliably under the widest imaginable extremes of conditions, e.g. very frequent operation, or operation after a long period in the on or off position. Long life of the moving parts or those subject to mechanical stresses, and retention of the insulating capacity under all circumstances, demand quite as much attention as the breaking capacity.

In order to satisfy all these requirements, the designer must not only possess an extensive knowledge of test results, but must also have wide operational experience. He can only possess both of these if he planned his development work on a long-term basis, so that any new designs are founded on firmly established principles. Units, whose development constantly followed this golden rule, and indeed continues to follow it, are the Brown Boveri airblast circuit-breakers, which have been steadily improved to cope with increasing severity of the duties. The first breakers of this type came on the market about

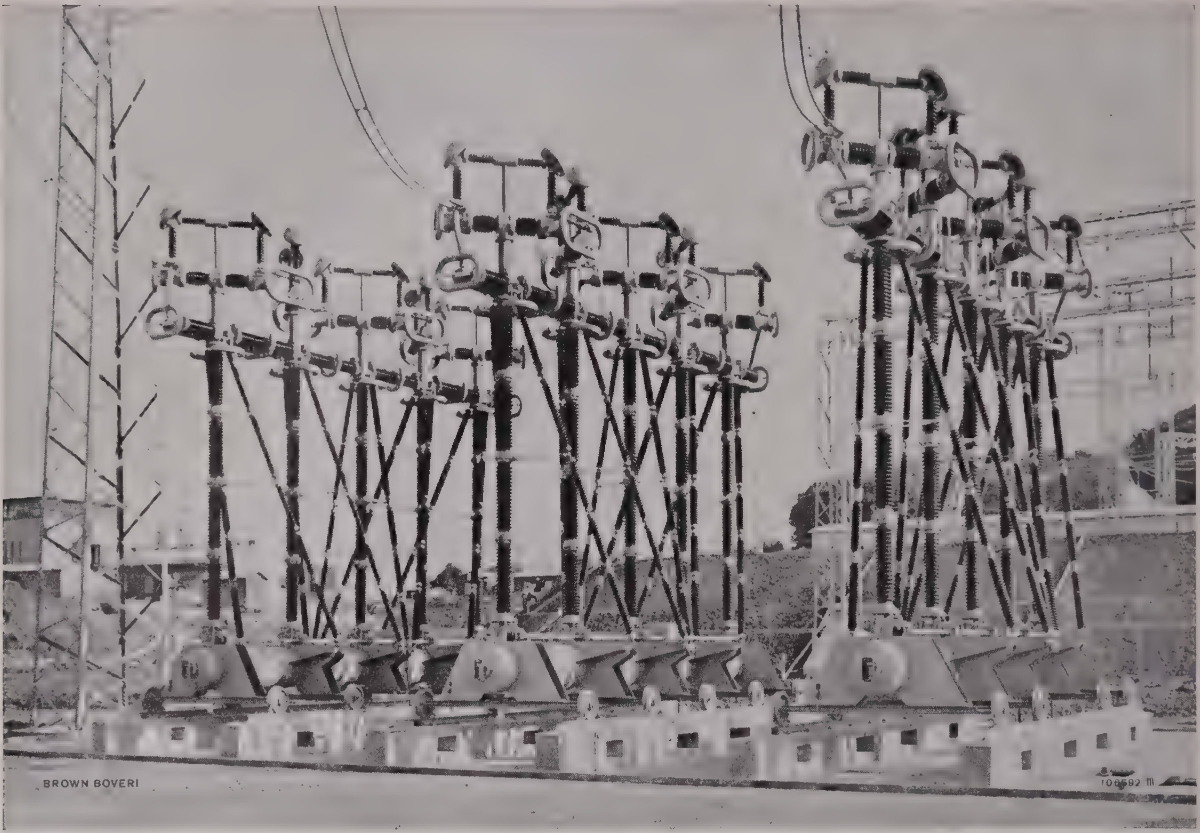

Fig. 1. – 400-kV airblast circuit-breaker which satisfies extremely severe conditions as regards breaking capacity, insulation and freedom from corona

This is one of the breakers supplied to the Rheinisch-Westfälisches Elektrizitätswerk AG. for the first e.h.v. system in Central Europe.

25 years ago. Even then, an attempt was made to provide properties which are nowadays becoming generally stipulated, such as short break-time and automatic rapid reclosure. Outdoor and indoor breakers for heavy duties have been continuously developed since then [1].[1] Modern products are now bearing the fruits of years of experience in operation and are rendering excellent service under extreme climatic and operational conditions [2, 3, 4]. Tests

---

[1] The figures in brackets refer to the bibliography on p. 344.

Fig. 2. – Oscillograms of six interruptions by one arc extinction chamber of a 400-kV airblast breaker at the Fontenay testing station of Electricité de France

U = Restriking voltage between the terminals of a chamber
I = Breaking current
i = Current in trip coil
a = Command given
b = Contacts part
c = Arc extinguished
t_a = Duration of arc
t_t = Total break-time
U' = Recovery voltage
f_1, f_2 = Transient frequencies (Hz = c/s)
U_1, U_2 = Amplitudes of transients
1–6 = Recorded with normal oscillograph
6 R = Recorded with fast-sweep oscillograph

During the six interruptions the restriking voltage followed the same course each time. The six successive interruptions, which represent a breaking capacity for the whole breaker of 20 000 MVA at 455 kV, were all performed correctly.

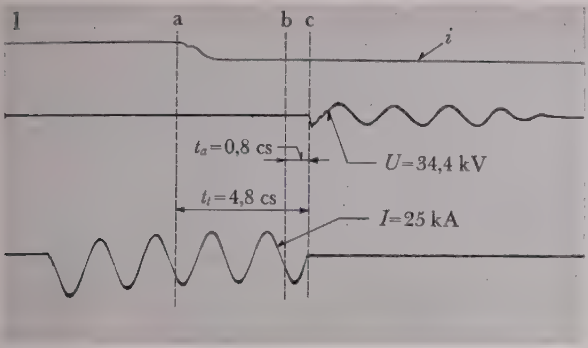

BROWN BOVERI 116556-I

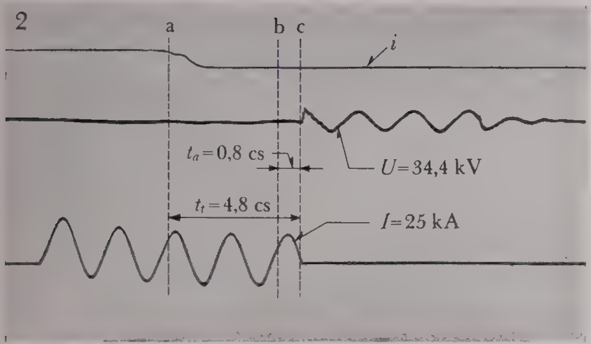

BROWN BOVERI 116557-I

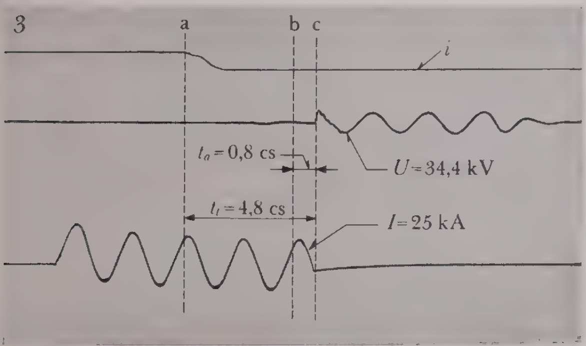

BROWN BOVERI 116558-I

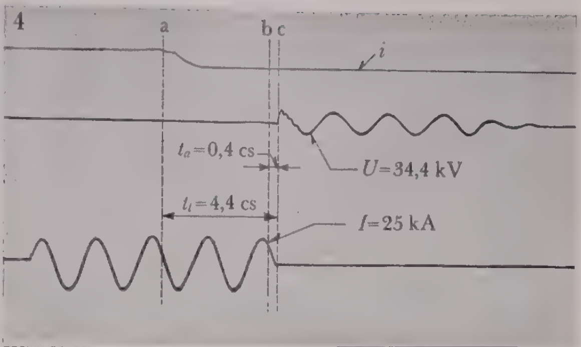

BROWN BOVERI 116559-I

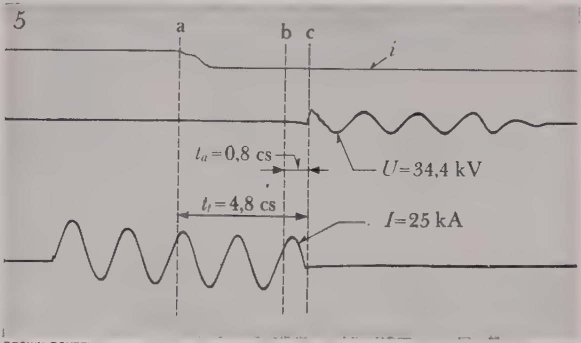

BROWN BOVERI 116560 I

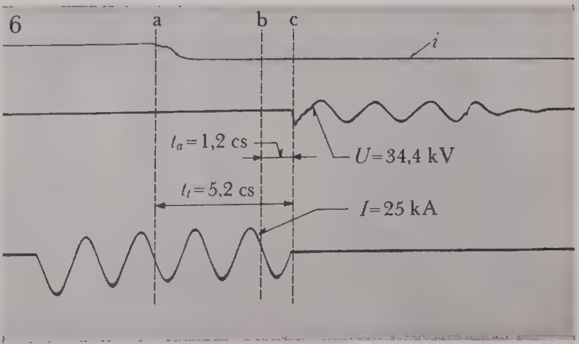

BROWN BOVERI 116561-I

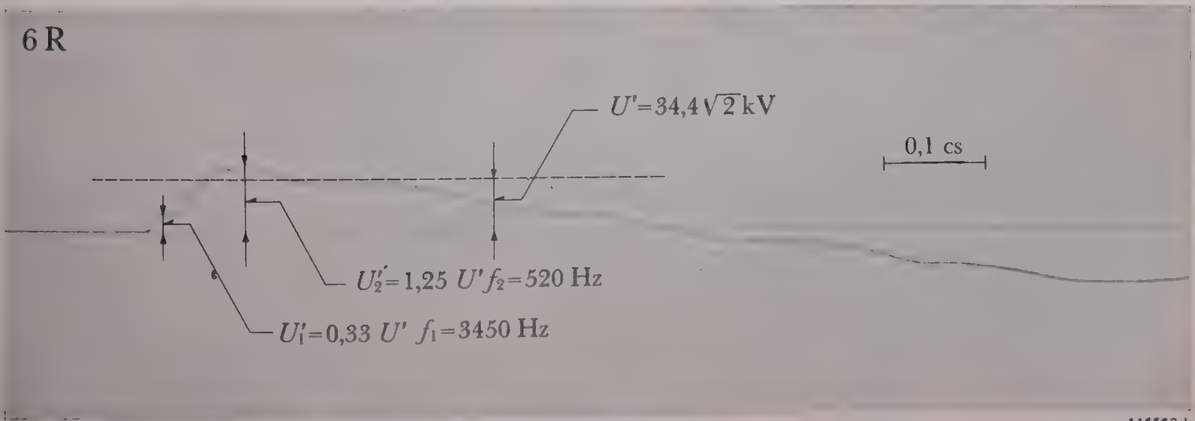

BROWN BOVERI 116562-I

in power systems are observed to determine whether and to what extent switchgear duties in critical conditions change with the growth of the system, and how the breakers behave in such circumstances [5, 6, 7, 8]. In conjunction with tests in the high-capacity testing station, these investigations yield valuable information for further development. With the aid of some test results, the next chapter will show that the principle of the airblast circuit-breaker will in future continue to satisfy the severest requirements.

Airblast Circuit-Breakers Handle Heavy Loads

Airblast circuit-breakers for 400 kV were placed in service some ten years ago in the first 400-kV transmission line in Sweden [9,10]. Their performance has been first-class in every respect. Tests in the system proved their outstanding properties under all kinds of critical conditions. Numerous airblast breakers for service voltages above 300 kV have since been supplied for e.h.v. systems in Canada, Finland, Germany and the United States [11,12]. This type of breaker is also visualized for the projected 400-kV system in Switzerland. From these successes it may be stated that the principle of multiple interruption with potential control has proved ideal. The standardized arc extinction chambers connected in series are not over-stressed even at the highest service voltages and loads, and can be thoroughly tested individually.

Fig. 1 shows a 400-kV airblast breaker with a very high breaking capacity. During tests at the Fontenay testing station of the Electricité de France, the arc extinction chamber of a breaker of this kind was

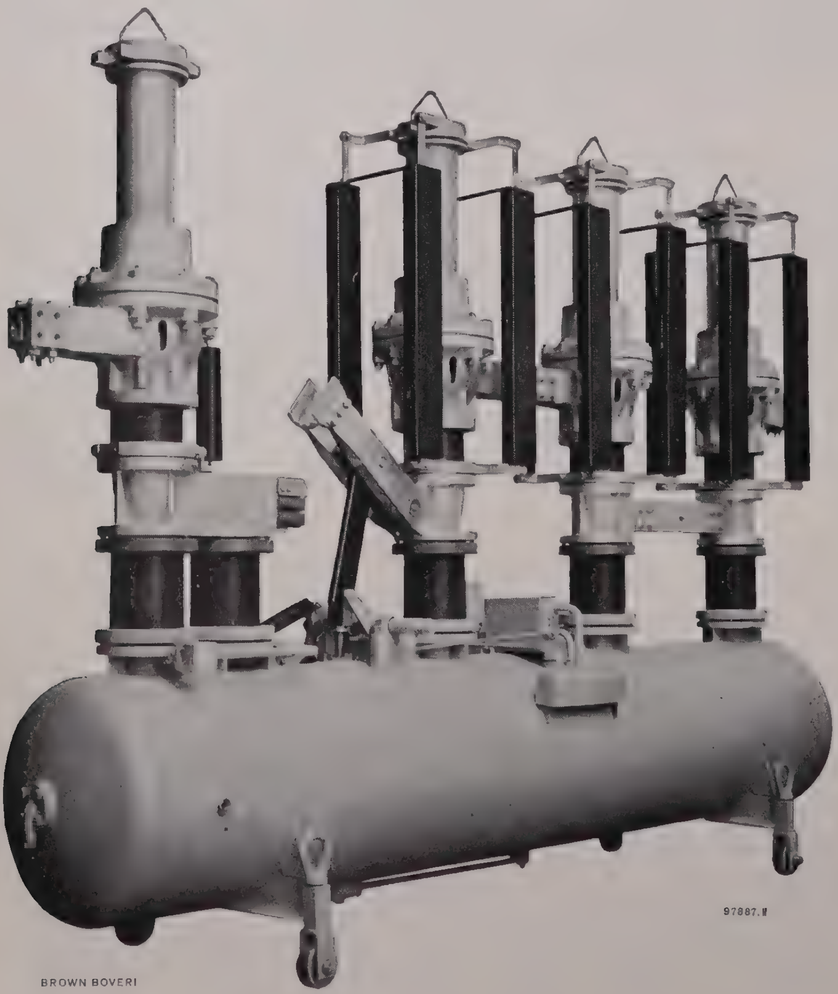

Fig. 3. – Pole of an airblast breaker for interruption of a symmetric current of 130 kA at 11 kV

Two triple-pole breakers of this design are installed as safety breakers for the extended testing station of KEMA in Holland.

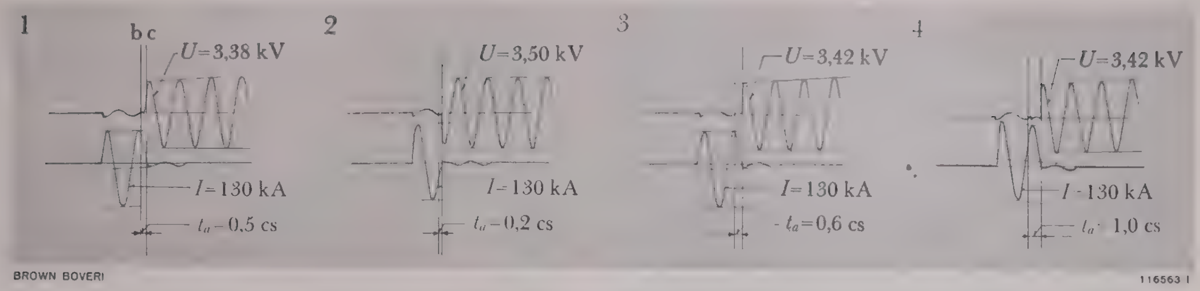

Fig. 4. – Four oscillograms from a series of interruptions by one arc extinction chamber of the breaker in Fig. 3

U = Restriking voltage I = Breaking current b = Contacts operated c = Arc extinguished t_a = Arc duration

No matter at what point of the half-wave the contacts parted, the arc was always extinguished at the next current zero.

stressed over the full range of its properties. The oscillograms in Fig. 2 were obtained during these tests. They show the behaviour of the breaker during six interruptions, carried out successively and without overhauling the contacts. Since the high resistances ensure a linear potential distribution across the ten chambers of a breaker pole, the restriking voltage of 34·4 kV for one chamber represents a value of 344 kV for the entire pole. In solidly earthed 400-kV systems it is usual to allow a phase factor of 1·3. Therefore the above figure represents a three-phase line voltage of $344 \frac{\sqrt{3}}{1 \cdot 3} = 455$ kV, and the proved breaking capacity 20 000 MVA. No matter at what point of the half-wave the contacts part, the arc is always extinguished positively and regularly. In spite of the relatively large distance between the control gear and the active parts (during these tests the breaker was equipped with a longer insulator column than is usual for 400-kV breakers, to allow for still higher service voltages), the break-times were remarkably short. A comprehensive investigation of the dielectric porperties of breakers for high insulation requirements showed that there are no fundamental reasons why airblast breakers should not be built for higher voltages than 400 kV [13].

Nowadays it is not only important to develop breakers for the highest service voltages in use, but also units for very heavy short-circuit currents at lower voltages. Due to the erection of larger power plants and distribution substations, as well as the close meshing of the h.v. systems, the short-circuit powers are greatly increased in m.v. installations. In this range airblast breakers are likewise ideal. As proof of this, the results obtained with the new safety breaker for the KEMA[2] testing station may be quoted.

Fig. 3 shows one pole of this breaker. It comprises four arc extinction chambers in series which are operated simultaneously. Three of them have fixed low resistances in parallel, while the fourth interrupts the residual current in the resistances. The oscillogram in Fig. 4 was recorded during a group of four tests on one chamber of this breaker. The symmetrical current of 130 kA is reliably interrupted each time. The low voltage at the beginning of the short-circuit current is due to the considerable voltage drop in the busbars of the station. For these tests the residual current was interrupted by a separate auxiliary breaker, whereas the whole breaker interrupts this current at the first zero.

Fig. 5 shows the state of the contacts after this group of tests. The amount of erosion was very small and the breaker was quite capable of carrying out further interruptions. Particularly noteworthy is the reliability with which the severe natural frequency conditions prevailing during these tests were mastered with the aid of the low resistances.

---

[2] Keuring van Electrotechnische Materialen, Arnhem, Holland.

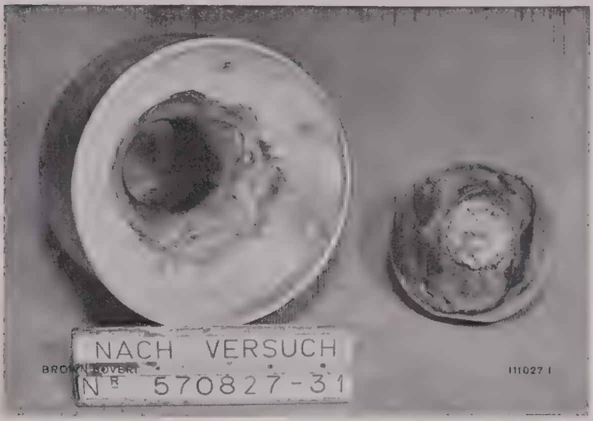

Fig. 5. – State of the contacts after the series of operations in Fig. 4.

In airblast breakers the erosion of the contacts is very slight, even when very heavy short-circuit currents are interrupted.

Conclusions

Tests with extremely heavy duties demonstrate that the principle of the airblast circuit-breaker as employed by Brown Boveri can be relied upon to meet future demands imposed by system development. At the highest service voltages the severest conditions can also be mastered, owing to the adoption of multiple interruption with potential control. The very heavy short-circuit currents which are experienced at lower service voltages are also reliably interrupted. In this range the ideal solution with respect to the rate of rise of restriking voltage has proved to be low resistances in parallel with the arc extinction chamber. The demands at present made on circuit-breakers, and to be expected in the future, are not expressed merely by the rated performance, but also by the wide variety of duties. It is therefore most valuable that the Company possesses a design of breaker which has proved its qualities during many years. Wide experience in design and operation is the best guarantee for the successful development of breakers for increasingly severe duties.

(KME) R. PETITPIERRE

Bibliography

[1] H. THOMMEN: Recent progress in the field of air-blast circuit-breakers. CIGRE Report No. 119/1956.

[2] P. LAUENER: Brown Boveri Airblast Circuit-Breakers—World-wide Favourites. Brown Boveri Rev. 1958, Vol. 45, No. 9, p. 397–407.

[3] R. PETITPIERRE and W. REUTERCRONA: High-Capacity Indoor Airblast Circuit-Breakers. Brown Boveri Rev. 1957, Vol. 44, No. 12, p. 539–57.

[4] A. LEUTHOLD: Brown Boveri Airblast Circuit-Breakers in Canadian Power Systems. Brown Boveri Rev. 1955, Vol. 42, No. 11/12, p. 443–64.

[5] C. L. KILGORE, A. C. CONGER and W. WANGER: Ultra-High-Capacity Field Tests on 230-kV Airblast Circuit-Breaker at Grand Coulee Power Plant. Brown Boveri Rev. 1951, Vol. 38, No. 12, p. 375–90.

[6] P. BALTENSPERGER: Line-Dropping and Reactor-Load Interruption Tests with a Brown Boveri 220-kV Airblast Circuit-Breaker in the Stadsforsen Power Station (Sweden). Brown Boveri Rev. 1951, Vol. 38, No. 12, p. 391–410.

[7] A. AMSTUTZ and H. MEYER: Field Tests on High-Voltage Airblast Circuit-Breakers. Brown Boveri Rev. 1950, Vol. 37, No. 4/5, p. 136–43.

[8] P. BALTENSPERGER: Disconnection of an Unloaded Transformer at Bottmingen Substation by a Modern Brown Boveri 150-kV Airblast Circuit-Breaker. Brown Boveri Rev. 1952, Vol. 39, No. 8/9, p. 335–41.

[9] H. MEYER: Der Brown Boveri Druckluftschalter für das 380-kV-Netz. Bull. schweiz. elektrotech. Ver. 1953, Vol. 44, No. 4, p. 157–62.

[10] P. BALTENSPERGER: The Brown Boveri 380-kV Airblast Circuit-Breaker. Brown Boveri Rev. 1954, Vol. 41, No. 9, p. 319–26.

[11] H. BAATZ et al.: Die deutsche 380-kV-Übertragung. Elektrotech. Z., Edn. A, 1958, Vol. 79, No. 7, p. 263–7.

[12] F. PARSCHALK, E. RUOSS and K. SCHLOSSER: The First 380-kV Power System in Germany. Brown Boveri Rev. 1958, Vol. 45, No. 3, p. 128–36.

[13] A. GOLDSTEIN and W. FREY: Power Transmission at Extremely High Voltage. Brown Boveri Rev. 1959, Vol. 46, No. 4, p. 227–49.

CARRIER TRANSFER FOR HIGH-SPEED DISTANCE PROTECTION

621.316.925.45.052.63

For short circuits occurring within a space of about 15% from the ends of a power line, automatic rapid reclosure demands the provision of a coupling between the circuit-breakers and the distance relays of the opposite ends, in order that tripping and reclosure may be effected in perfect synchronism. The article describes the means available, allowing the power line itself to be utilized for the transmission of tripping signals modulated on carrier frequencies, despite the disturbance in transmission caused by the short circuit. Many years' experience gained from over 200 installations equipped with rapid reclosure have shown that the principle of carrier transfer and the equipment developed for this purpose meet all practical requirements regarding reliability and tripping times.

Duties of Distance Protection with Carrier Transfer

THE INCREASING interconnection of high-voltage networks and the unceasing growth in installed capacity have resulted in a tremendous increase in the short-circuit energy, especially in the power distribution centres. But the stipulation that the reliability of the distribution stations be maintained at the highest possible level is undiminished. This necessitates not only quick-acting high-voltage circuit-breakers with adequate breaking capacity, but also places exacting demands on the protective system with regard to the exact location of the fault and determination of its character in the shortest possible time.

One of the methods which has been specially adapted to the present-day conditions is the principle of the distance relay combined with automatic rapid reclosure of the breakers. This is not the place to describe the principle in detail, but it is advisable to explain why carrier transfer is necessary for rapid reclosure. The graduation of the times of a distance protection system is illustrated schematically in Fig. 1. To prevent unselective tripping in a neighbouring line section to the protected section, the elements which measure the impedance are so adjusted that, for 85% of the line, tripping takes place in the basic time, while for the remaining 15% it is in the second time step. But this is incompatible with rapid reclosure because, if the reclosing action of the breakers at each end of the line is not synchronized, it is possible for power to be fed back into the short-circuit arc, thus leading to lock-out by the breakers.

It is the task of the carrier transfer in such cases to ensure synchronous operation by the breakers at both ends of the protected line section. In practice this means that the tripping impulse imparted by the distance relay situated nearest to the fault must also be communicated to the other breaker at the

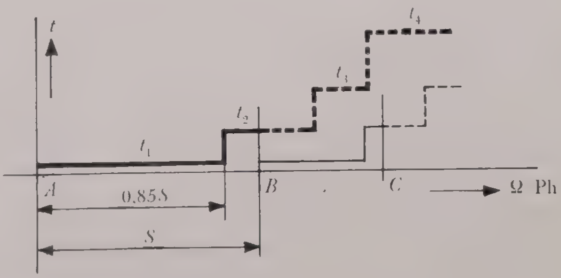

BROWN BOVERI 95084·II

Fig. 1. – Time graduation characteristic of the distance relay

The characteristic of the distance relay shows its tripping time in relation to the distance to the fault. The stepped characteristic allows faults on the protected line section or on adjoining sections to be cleared in the shortest possible times. The times and impedance values of the four steps are adjustable. The first step is normally set to 85–90% of the length of the protected line.

S = Protected section

t_1, t_2, t_3, t_4 = Tripping time steps (t_1 = basic time for first step)

A, B, C = Stations

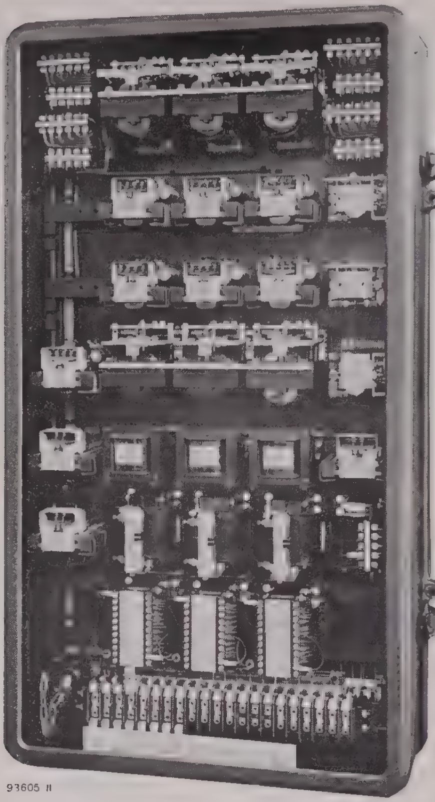

Fig. 2. – One-cycle distance relay type L6f for solidly earthed e.h.v. lines equipped for single or three-phase, or single and three-phase rapid reclosure

This relay is supplementary to the rotating-field distance relay.

far end, as well as to its own breaker. As stated above, the distance relay at the far end would give the impulse to its breaker in the second time-step. This method of communicating a tripping signal is commonly known as "transfer tripping", in contrast to another method in which the carrier channel merely has the passive task of transferring a blocking signal to the breaker ("transfer blocking").

Fig. 2 shows the standard model of a one-cycle distance relay, the operating time of which does not exceed 1 cycle at 50 c/s, even under the most unfavourable circumstances. With the rapid action of modern airblast circuit-breakers it is possible for a breaker to be tripped in 70–80 ms, including the relay time, even under adverse conditions. The transmission time of the carrier link must then not exceed half a cycle at 50 c/s.

Properties of the Power Line as Communication Channel

The carrier transfer of the tripping signal of the distance relay utilizes the power line itself as the communication path. This kind of solution appears most expedient; provided the line is capable of fulfilling the specified requirements, it is usually the shortest possible route between the associated distance relays.

The conditions governing the propagation of carrier frequencies along a power line are taken to be known, so that it is only necessary to consider the differences between normal operating conditions and short-circuit conditions.

The short circuit may be between phases or it may involve earth. From experience it is known that polyphase shorts occur much less frequently than earth faults, but must nevertheless be cleared reliably by the protective system. To a first approximation, an earth fault or short circuit can be likened to a metallic connection. In this case the attenuation of the line, to which the carrier is coupled either phase-to-phase or phase-to-earth, in relation to the distance of the fault from the end of the line, has already been investigated by a number of authors. Fig. 3 shows typical attenuation curves for lines with single- and two-phase coupling, on which the short circuit was simulated by a metallic connection. However, it should be pointed out that the curves are envelopes of the actual attenuation, because the latter fluctuates between maxima and minima at intervals of half the wavelength, due to reflections. The actual attenuation occurring with a short circuit is, on the average, smaller because the arc possesses an impedance of 5 to 20 ohms, depending on the magnitude of the short-circuit current. This attenuation is additional to that experienced by the carrier when the line is operating normally. From the attenuation curves it will be observed that the additional attenuation increases considerably when the fault is near the ends of the line. Furthermore, the curves also show that it is noticeably less with two-phase coupling than with single-phase coupling.

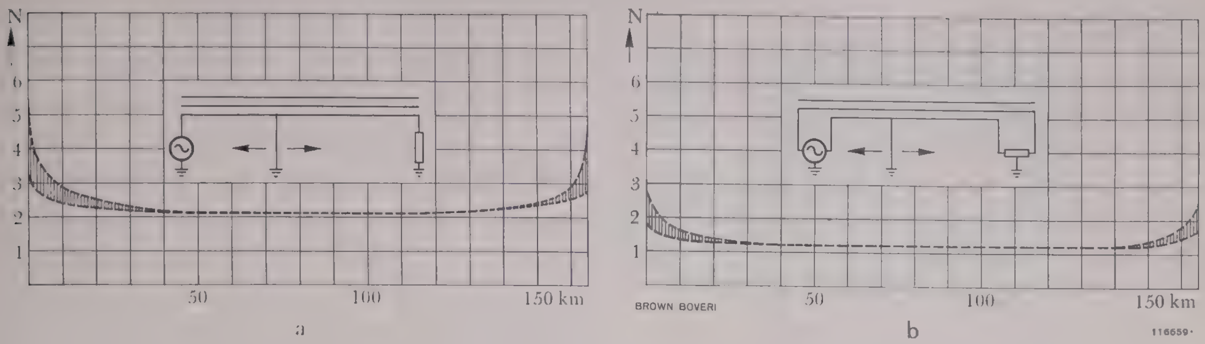

Fig. 3. – Attenuation of a power line carrier link in terms of the position of a dead short along the line

a = Phase-to-earth coupling, coupled phase earthed b = Phase-to-phase coupling, one of the coupled phases earthed

(Taken from: H. KUNJEWSKY, CIGRE Report No. 309/1948)

The reason for this is clear when the manner in which propagation of the carrier frequencies along the line takes place with single-phase coupling is considered.

Fig. 4 depicts this propagation process schematically. Owing to the severe attenuation by the earth, the asymmetric wave between phase and earth which was present at the start has completely disappeared after about 10 to 20 km and the phases which were not coupled act as the return path. At the middle of a long line the conditions are very similar to those with two-phase coupling, but not towards the ends of the line. If a short circuit occurs on the coupled phase, near the end, the establishment of the return path through the non-coupled phases will also be affected. To try to explain the action of the attenuation in the event of a short circuit near the end of the line would be exceeding the scope of this article. The circumstances become at least qualitatively understandable if we imagine that a power line in the case of a short circuit may be treated as a group of inductively and capacitively coupled and very badly terminated aerials. With two-phase coupling, on the other hand, the conditions are much more favourable because there is now no asymmetric wave between phase and earth, as was the case with single-phase coupling. It will of course be obvious that conditions for coupling will be bad, i.e. the additional attenuation will be large, as soon as these aerials differ widely in length. This is particularly true when the short circuit occurs near the end of the line. For this reason two-phase coupling is preferred for the transmission of protective signals. The lower attenuation per kilometre with this method of coupling is not the deciding factor in this case. As very approximate values for the increase in attenuation in the event of a short circuit near the end of the line (800 m), the following apply for two-phase coupling (short-circuit current 3500 A):

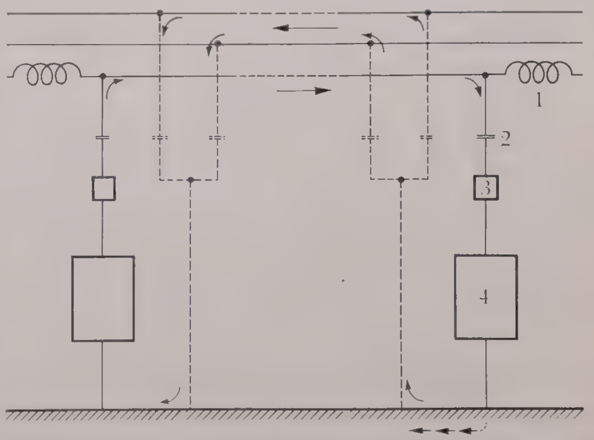

Fig. 4. – Diagram to illustrate the propagation process with single-phase coupling

1 = Carrier frequency trap
2 = Coupling capacitor
3 = Line matching unit
4 = Carrier set

Owing to the capacitance to earth of the non-coupled phases, the carrier circuit employs the line as return path. Due to the heavy losses the return path via earth is non-existent in practice.

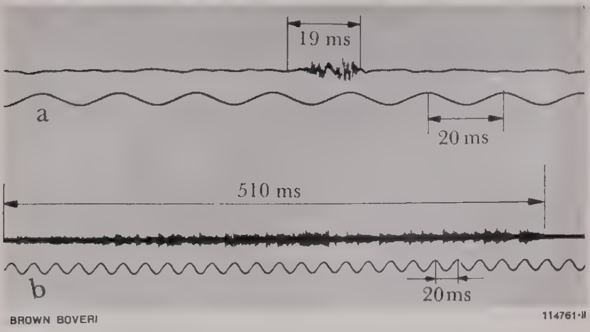

Fig. 5. – Disturbance spectra produced by switchgear

a: Disturbance spectrum of a h.v. circuit-breaker. The relatively large amplitude decays in a very short time.

b: Disturbance spectrum of an isolating switch. The "cold" discharge caused by the capacitive effect when an isolator is opened and closed lasts considerably longer and produces a spectrum similar to corona, with a high energy content.

Earth fault	*Additional attenuation (approx.)*
Single-phase, non-coupled phase	1·7 db
Single-phase, in one of the coupled phases	4·3 db
Two-phase, including one of the coupled phases	3·5 db
Two-phase, affecting both of the coupled phases	13 db

In contrast, with single-phase coupling and a two-phase earth fault affecting the coupled phase, the attenuation under similar conditions is about 22 db or more. The increase in attenuation is, however, not the only factor which renders transmission more difficult; the short-circuit arc itself is also a source of high-frequency disturbance. Fortunately the disturbance power in the highly ionized arc is quite small and does not severely affect the signal-to-noise ratio.

Disturbance effects independent of short circuits

A further group of disturbance effects, which are unrelated to the short circuit and therefore affect the healthy line too, are the disturbance spectra produced by the opening and closing of circuit-breakers and isolating switches. These disturbances will primarily affect the transmission channels of adjacent lines (an isolator of a protected line is never opened on-load). This kind of disturbance is particularly pronounced in large substations with extensive busbar systems and a large number of feeders at different voltages. Switching operations are fairly frequent in such stations, which usually also contain a concentration of carrier communication links.

Fig. 5, which shows typical disturbance spectra of a breaker and an isolator, proves that the brief, powerful action of the high-voltage circuit-breaker is far less disturbing than the relatively slow opening and closing of an isolating switch, in spite of the much lower current involved. The explanation for this is that, with a typical heavy-current arc, the ionized gas envelope does not collapse once it has struck, so that once the arc is established, it produces a continuous disturbance spectrum, decaying rapidly towards the higher frequencies. This, as already stated, applies to the short-circuit arc. Conversely, the low-current opening and closing of an isolator has the drawback that the already ionized gas in the break collapses at each voltage zero, so that flashover must take place afresh every time the voltage rises again. This leads to steep wave-fronts in the disturbance voltage and therefore a large proportion of the disturbance frequencies are in the carrier band. The effect of corona on badly dimensioned power lines is fundamentally the same.

Worth special mention at this point are certain designs of circuit-breakers, whose disturbance spectra can occur when interrupting long lines at no load, due to backfires. The disturbance energy can attain values many times greater than an on-load interruption.

Measures to Improve Transmission

From the foregoing considerations it is evident that two distinct groups of measures are necessary to improve the dependability of transmission:

Optimum utilization of the transmission power in order to counteract any deterioration in the signal-to-noise ratio in the event of a fault.

Optimum design in accordance with the conditions regarding the reliability of transmission in the face of disturbance effects caused by the operation of switchgear.

Compromises are unavoidable in both these groups. In view of the restrictions imposed on the maximum power output of carrier equipment by the postal authorities, the transmission power cannot rise above definite values, which will differ from one country to another. These values vary between 10 and 100 W. In some countries it is permissible for the output to be increased above the normal steady value, when tripping signals have to be transmitted.

Still more difficult to fulfil are the conditions with regard to the immunity from disturbance effects. The two effective measures, i.e. reduction of the bandwidth of the communication channel and coding the signals, affect the transmission time and can therefore only be used to a limited extent.

As a result of exhaustive investigations and many years' experience, technically mature solutions are now available, which can be employed in a wide variety of operational conditions, and have already been adopted for over 200 installations. For very long lines and extreme transmission conditions—such as in the presence of hoar-frost, which causes serious disturbance—and for one-cycle distance protection, single-purpose carrier sets have been provided. These units, which employ the principle of frequency shift and are used solely for transmission of protective signals, have a carrier output of 20 to 150 W.

Fig. 6 shows a carrier transfer set with an output of 150 W. The transmitter and receiver are combined into a single unit.

For short and moderately long lines it is still possible to use the well-established multi-purpose sets which, in addition to transmitting tripping signals, are also used for telephony, telemetering, remote control, and so on. These sets are obtainable with single or double-sideband modulation. They permit optimum utilization of the equipment and of the carrier-frequency spectrum, without any of the reliability having to be sacrificed. The frequency-shift protection channel is modulated on the carrier as partial channel. If tripping becomes necessary, the other partial channels are briefly interrupted and during this short time the tripping channel transmits at full power. In single-sideband sets, provided

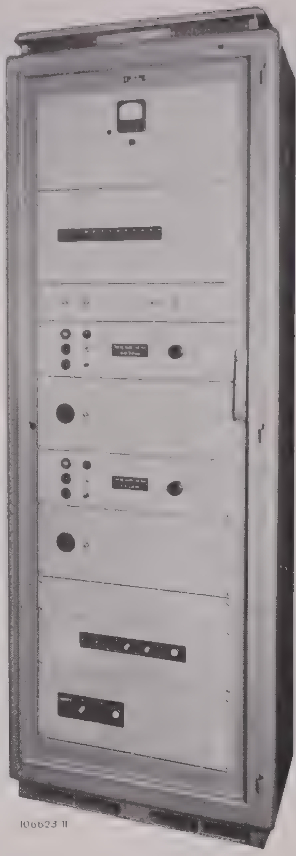

Fig. 6. – Carrier transfer unit for use with the distance protection of a two-circuit line system

This unit is specially designed for service on long lines in conjunction with distance relays equipped with a supplementary one-cycle relay.

Characteristic data:

Transmission time: approx. ½ cycle at 50 c/s

Maximum range: 400 km; for one system alone approx. 600 km

Output power of the common output stage: 100–150 W

The sub-units for testing and time measurement can be recognized by their labels.

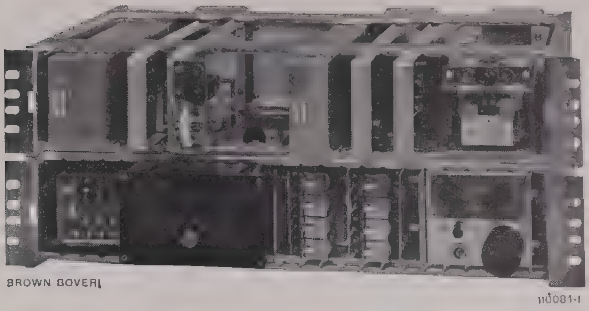

Fig. 7. – Transistorized a.f. transfer unit for distance protection signals, for use with pilot wire or in combination with a multi-purpose carrier set

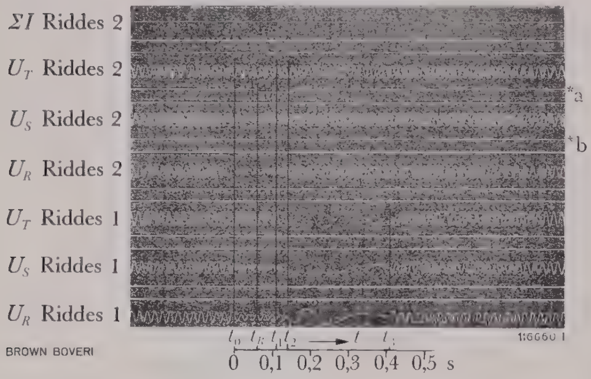

Fig. 8. – Short-circuit tests on the two-circuit line between Mühleberg and Riddes

The carrier transfer is coupled to phases R and S of circuit 1. It transmits the tripping signals for both circuits over a common transmitter-receiver unit, i.e. in the event of a fault on one circuit, there is no possibility of the carrier transfer for the other circuit picking up. The oscillogram obtained with a Masson-Carpentier fault recorder illustrates the correct clearance of this interphase short circuit on the phases employed for the carrier transfer. (Monitoring the emission of the tripping signals to the carrier transfer unit in Mühleberg.)

a = Impulse over circuit 1
b = No impulse over circuit 2

Being unaffected by the fault, this circuit is not interrupted.

t_0 = Occurrence of the fault in Mühleberg
t_R = Response time of the distance relay of circuit 1 in Mühleberg
t_1 = Breaker trips in Mühleberg
t_2 = Breaker trips in Riddes
t_3 = Reclosure

it is permitted by the authorities, this output can be raised appreciably above its normal value for a brief period. Fig. 7 shows a transistorized carrier transfer unit combined with monitoring equipment in a multi-purpose set.

Certain additional requirements may also be mentioned as they improve the reliability of such channels and may be considered essential:

The operational state of protective channels must be constantly supervised by monitoring the carrier and by further intensive monitoring.

It must be possible for functional tests to be performed at any time on the entire channel; during such tests all manipulations which might lead to the breaker being tripped must be excluded.

Behaviour of the Carrier Transfer Link in the Event of a Short Circuit

Interest is mainly centred on the sequence of events from the occurrence of the short circuit until the line breaker has reclosed. These conditions can best be illustrated by a typical case chosen from a series of tests. These were single-phase and polyphase short circuits simulated on the two-circuit 220-kV line of the Bernese Power Co. between Mühleberg and Riddes. The length of the line is 120 km, the distance of the short circuit from the Mühleberg end of the line was about 800 m. The protection of a two-circuit line poses still more exacting conditions regarding the reliability with which the tripping signal is transmitted. On the other hand, the two-circuit arrangement can be treated as the usual form in many cases today. The communication channel is provided by a single-sideband carrier link with an output of 10 W, which is normally used to transmit telephony, telemetering and frequency shift channels for the protection of both systems of conductors in service. Carrier transfer of distance relay signals by single-sideband multipurpose sets is nowadays almost standard practice. The carrier is coupled to the two phases R and S of circuit 1. Fig. 8 shows the variation of the phase voltage on the two circuits 1 and 2, recorded by a Masson-Carpentier fault recorder in Mühleberg. The short circuit having been initiated between phases R and S, i.e. the coupled phases of circuit 1, at the moment t_0, the voltage collapses in phases R and S.

Owing to the nearness of the short circuit to the end of the line (800 m), the phase voltages R and S on circuit 2 were also affected. At the moment t_R the distance relay gives the command to the carrier set to trip the breaker at Riddes, the opposite end of the line. The tripping command for the breaker at the near end of the line is given a few ms later.

At the moment t_1 the breaker at Mühleberg trips as a result of the evaluation by the distance relay of circuit 1 in Mühleberg, followed 30 ms later by the breaker tripping at Riddes as a result of the command transmitted by carrier transfer from the distance relay at Mühleberg. In the meantime (t_2-t_1) the voltage on circuit 2 recovers because the short circuit has now become completely isolated from this circuit due to the opening of the breaker in Mühleberg. On circuit 1, however, the short-circuit arc continues to burn till t_2, due to its being fed from the other side. In the interval t_2 to t_3 circuit 1 is dead, following which normal operation continues.

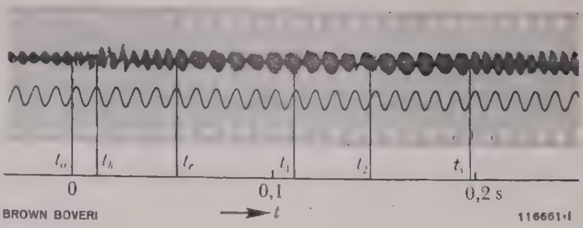

Fig. 9. – Oscillogram of the a.f. signals received in Riddes over the two-circuit line from Mühleberg

Two-phase short circuit between phases R and S of circuit 1 in Mühleberg.

t_0 = Occurrence of the fault in phases R and S of circuit 1
t_h = Output power stepped up to 100% due to minimum-impedance relay picking up
t_e = Tripping signal for the breaker of circuit 1 received in Riddes
t_1 = Breaker trips in Mühleberg
t_2 = Breaker trips in Riddes
t_s = End of the tripping signal for circuit 1. The increased output continues for about 100 ms beyond this point.

It is interesting to study the action of the carrier transfer link within the scope of this well-known time schedule of a reclosure cycle. Fig. 9 shows an oscillogram of the audio-frequency voltage at the output of the receiver in Riddes, i.e. at the point where the tripping command must be evaluated. To simplify understanding of this oscillogram, one or two remarks regarding evaluation would be useful: to transmit the signals from the distance relays belonging to the two line circuits frequency-shift units are employed, whose audio frequency is used to modulate the carrier. With the frequency-shift system the carriers are modulated with steady-state frequencies during the time that no tripping signals have to be transmitted. In the oscillogram in Fig. 9 the envelope of these two steady-state frequencies is visible as an apparent frequency difference. If one of the channels changes its frequency from the steady-state to the tripping frequency, this immediately becomes visible in the oscillogram as the frequency difference assumes another value. On the one hand, this envelope only occurs when there are two tripping channels; on the other hand its presence greatly simplifies the determination of the instant at which the tripping command was given. The times t_0, t_1 and t_2 in Fig. 9 are identical with those in Fig. 8. With the aid of these reference points it is quite easy to follow the course of the tripping action. At point t_0 when the two-phase short circuit was initiated in Mühleberg, the reception signal in Riddes is slightly disturbed. At point t_h the tripping signal is emitted at increased power in Mühleberg, i.e. the other channels are interrupted and the maximum power of the carrier set is concentrated in the tripping signal. An important point is that this increase in transmitter output at Mühleberg takes place before the actual tripping signal is emitted—t_R in Fig. 8. At t_3 the tripping signal appears at the output terminals of the receiver, whence it is conveyed via the carrier transfer set to the tripping circuit of the breaker in Riddes. The tripping of the breakers at Mühleberg (t_1) and Riddes (t_2) are apparent in the oscillogram as disturbance spectra superposed on the tripping signal. The end of the tripping signal is marked by t_s, the increased output continuing for 10 ms after this. A point worth noting is that the tripping signal arrives at the far end of the line (t_e) before the breaker at the end nearest the short circuit has opened (t_1). Since the receiver is automatically blocked as soon as the tripping signal has been received, the disturbance spectra produced by the operation of the breaker cannot affect the carrier link.

Summarizing, it may be said that the disturbance effects of a short circuit on the line, as far as the arc is concerned, are rendered ineffective by increasing the power at which the tripping signal is emitted, as well as by the other measures visualized in the set, while the possibility of the switchgear operation causing a disturbance is prevented from taking effect by a skilfully arranged race against time. These are the reasons why transfer tripping using carrier channels may be considered every expedient and reliable solution to one of the most important problems of power system protection.

A. DE QUERVAIN
(KME) C. HAHN

MICADUR, A NEW INSULATION FOR THE STATOR WINDINGS OF ELECTRICAL MACHINES

621.315.613.1:621.313.045

The article describes the development of a new system of insulation, referring to experiments and endurance tests, and the results obtained. These resulted in a continuous insulation impregnated in vacuum with a specially developed synthetic resin containing no solvent. Tests and operational experience prove that this insulation fulfils the severest requirements. It has already been used for a number of large machines (turbo-alternators and hydro-electric generators).

FOR OVER 30 years Brown Boveri have used asphalt micafolium for insulating the stator windings of high-voltage machines. Some years ago a start was made with the development of a completely new system, now known as Micadur, the need for which was dictated by certain manufacturing and design considerations. For some machines—an extreme case is the short-circuit generator, for example—it is necessary to lay down minimum plastic (in particular thermoplastic) deformation, not only for the active part of the winding but also for coil-ends. It was decided that the junction between the pressed slot insulation and the taping of the ends should be eliminated, in order to reduce the projection of the coil-ends and to improve the resistance to creepage.

From the manufacturing point of view it is rather difficult to press the folium round the bars, especially when the iron is very long and the bars high, due to the twisting of the bars while being wrapped. The familiar disadvantage of the thermoplastic insulations commonly used hitherto should be avoided, with the general attainment of adequate resistance to ageing, conforming to the severest requirements. These requirements automatically led to continuous wrapping of the bars and coil-ends, and thus to vacuum impregnation with a polymerizable synthetic resin containing no solvent. But before the new system could be considered ripe for production, numerous tests had to be carried out. These began with the selection and testing of the various materials and their different combinations, according to the purpose for which they were required. Then trial bars were wrapped and subjected to endurance tests before the manufacturing procedure was decided upon and production could commence.

Choice of Suitable Materials

In order to select the most suitable material from those available, it was necessary to get to know their different properties. Therefore investigations had to be performed to determine their electrical, thermal, mechanical and technological properties, and their

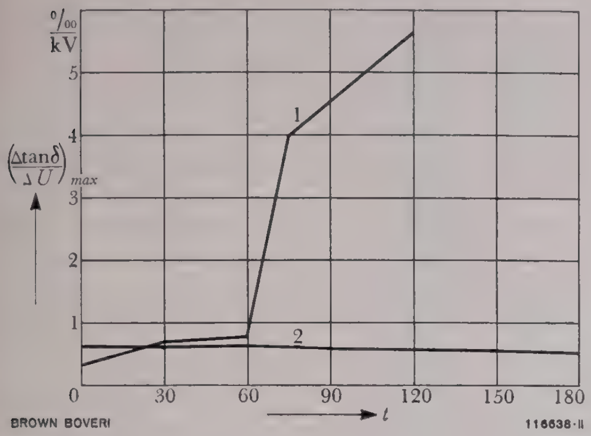

Fig. 1. – Variation of the dielectric properties with respect to time at 135 °C

1 = Insulation system based on paper
2 = Insulation system based on glass fabric
$(\Delta\tan\delta/\Delta U)_{max}$ = Maximal rate of rise in loss factor, expressed in 0·1 % per kV

Both systems are impregnated with modified epoxy resin 'A'. The glass-based system 2 is post-polymerizing at 135 °C and continues to achieve better values. The paper-based insulation, on the other hand, deteriorates after about 2 months at this temperature, due to decomposition of the paper. Measurement carried out at 20 °C.

t = Ageing time in days

behaviour in conjunction with other materials. In some cases the method of testing, corresponding to the stresses expected, had to be devised first.

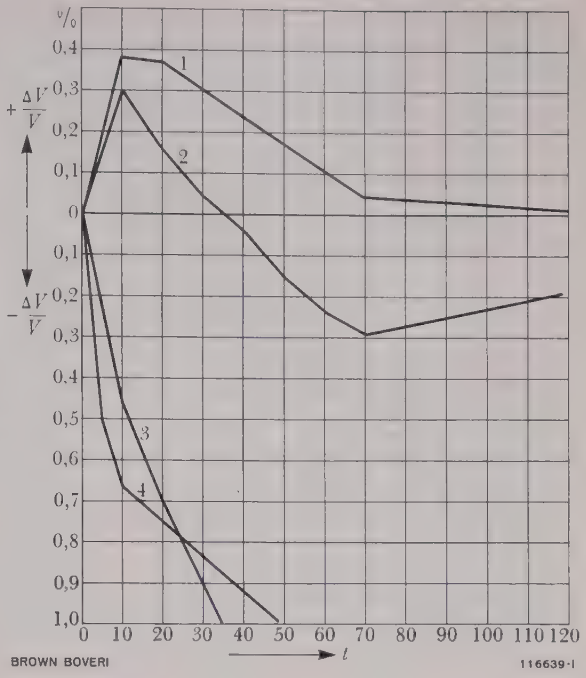

Fig. 3. – Change in volume plotted against the ageing time at 160 °C

1 = Modified epoxy resin 'A' (as used for the vacuum impregnation of Micadur insulation)
2 = Epoxy resin
3 = Polyester resin
4 = Modified epoxy resin 'B'
t = Duration of ageing in days
$\Delta V/V$ = Change in volume

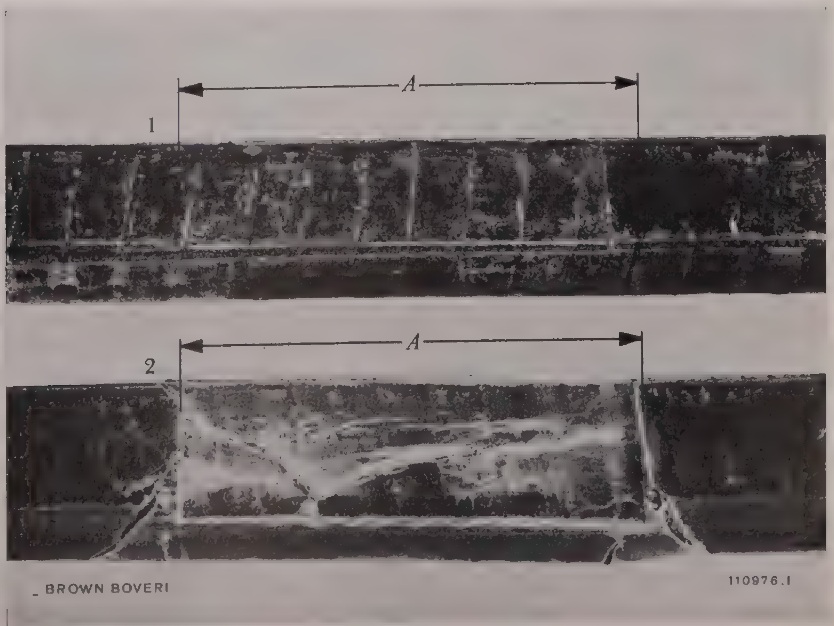

Fig. 2. – Resistance to compression of Micadur insulation at 120 °C

1 = Bar insulated with Micadur (glass-based), appearance after subjection to a pressure of 2000 kg/cm²
2 = Bar insulated as 1, but with paper base, state after a pressure of 700 kg/cm²
A = Loaded area

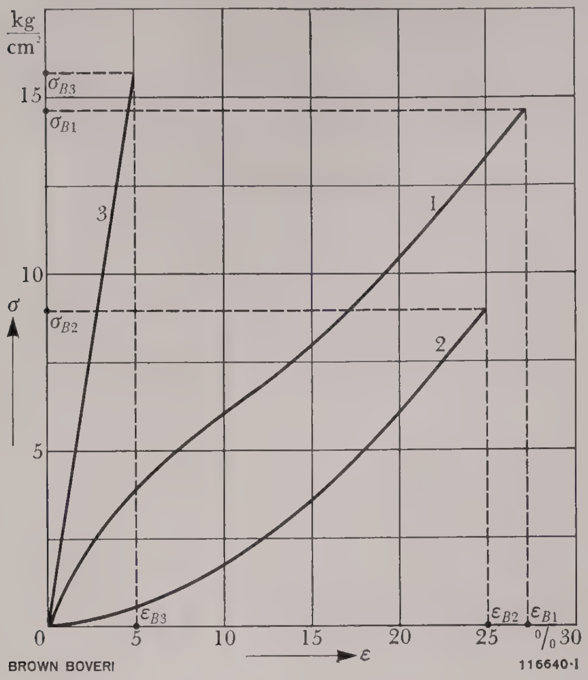

Fig. 4. – Curves of elongation against load at 110 °C for various resins

1 = Modified epoxy resin 'A'
2 = Epoxy resin
3 = Polyester resin
σ_B = Load at fracture
ε_B = Elongation at fracture

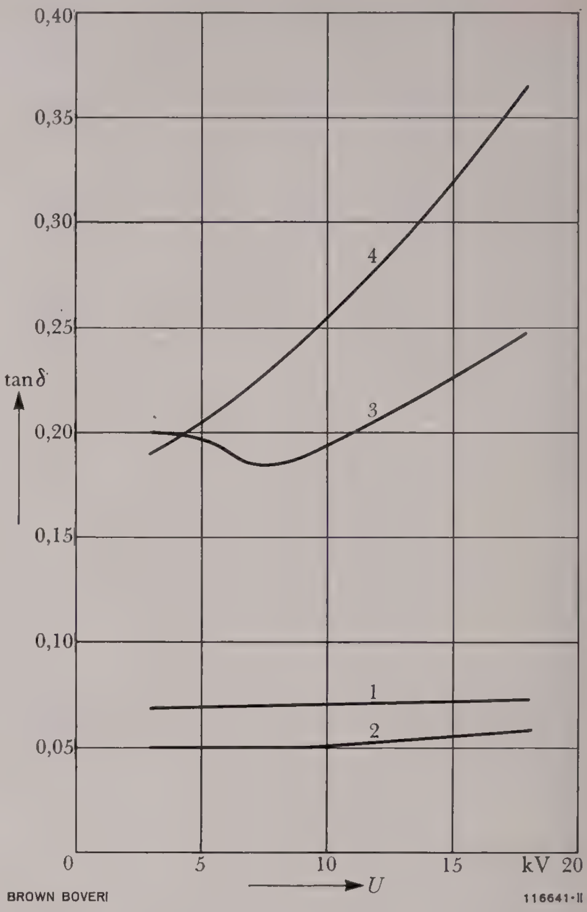

Fig. 5. – Loss factor tan δ in terms of the voltage

Measured at 130 °C on test plates 200 × 200 × 1·5 mm

Insulation system: Glass-Mica paper impregnated with:

1 = Modified epoxy resin 'A'
2 = Epoxy resin
3 = Polyester resin
4 = Modified epoxy resin 'B'

For checking the changes which take place in an insulation system during ageing under the influence of temperature, the best results have been obtained by plotting the loss factor tan δ* in terms of the voltage at regular intervals. The maximum rate of change $(\Delta \tan \delta / \Delta U)_{max}$, expressed in 0·1% per kV, is defined as a measure of the change in the quality of the insulation.

The main insulation material used for electrical machines is still mica. In addition to splittings which are commonly used, a number of mica papers (100% mica) are also available.

In addition to glass fabric and papers there are now a number of plastic materials in the form of foil which can be used as a carrier or base for the main insulating medium. The difference in the behaviour of a synthetic resin insulation with normal paper as base, and one with high-grade glass fabric can be seen by comparing Fig. 1 and 2. Even within the various categories of materials there are quite appreciable differences. For glass fabrics the type of glass, the thickness of the fibres, the weave, and the finish are all important factors, particularly as regards its compatibility with the impregnating resin.

The adhesive or bonding medium is the most awkward part of the insulation. Although the choice of synthetic resins containing no solvent, which may be considered suitable for a new insulation system, is large, only one modification, developed by Brown Boveri, has so far been found to satisfy all requirements.

---

* tan δ is also sometimes called "power factor".

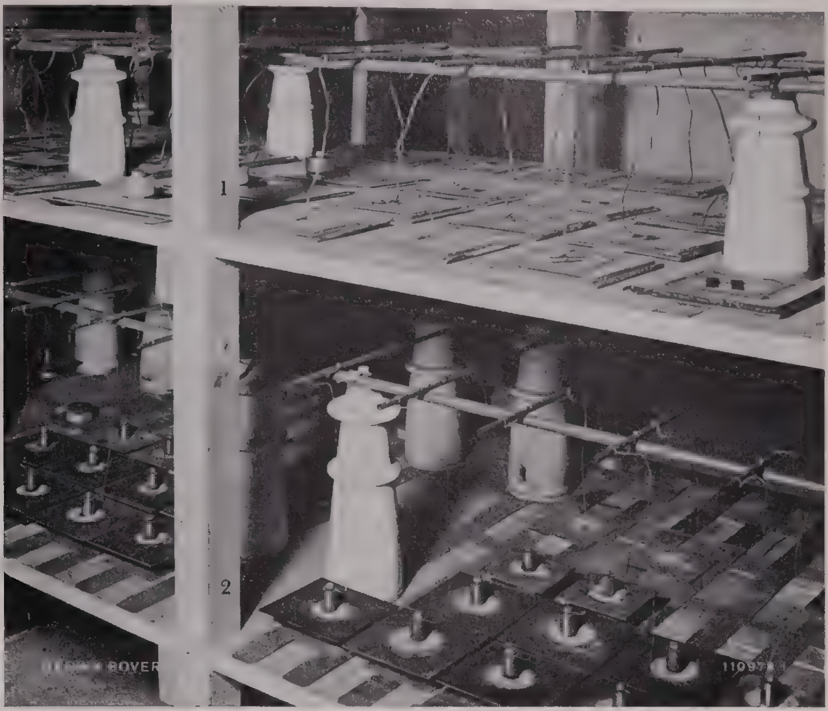

Fig. 6. – Test cells for investigating the effect of corona discharge

1 = Cell as per French proposal
2 = Conventional cell

Since it was stipulated from the start that the wrapping should be impregnated with resin under a vacuum, a number of resins had to be discarded for technological reasons. Only the polyester and epoxy resins remained. The former offer certain advantages from the technological aspect, the latter from the mechanical and electrical aspects. The selected modification enjoys the main advantages of both groups.

A very important factor is the resistance of the resin to deformation at elevated temperatures. To determine this the following were measured and plotted against the ageing time: Loss in weight, voluminar stability, flexural strength and impact strength. Fig. 3 and 4 show some of the results of investigations of this kind, carried out with typical resins. Fig. 3 shows that the chemical action of resins 1 and 2 is practically finished when the material has solidified, in contrast to resins 3 and 4. In Fig. 4 it can be seen that, by suitable modification, the elongation on fracture of an epoxy resin can be improved.

The fundamental investigations into the behaviour of the combination of resin, base and mica were performed with test plates before trial bars were wrapped. The dielectric and mechanical strengths were measured at different temperatures

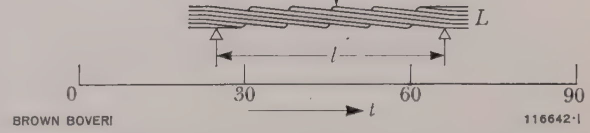

Fig. 7. – Change in flexural strength of Roebel bars aged at 160 °C

F = Force needed to bend the bar by 2 mm
F_3 = Force needed to bend bar 3 by 2 mm in its brand-new condition
l = Distance of support

The conductors were insulated and bonded as follows:

1 = Glass-wrapped, bonded with resin I
(new standard Brown Boveri conductor insulation)
2 = Glass-wrapped, bonded with resin II
3 = Bare copper with intermediate insulation bonded with zinc oxide-bakelite cement

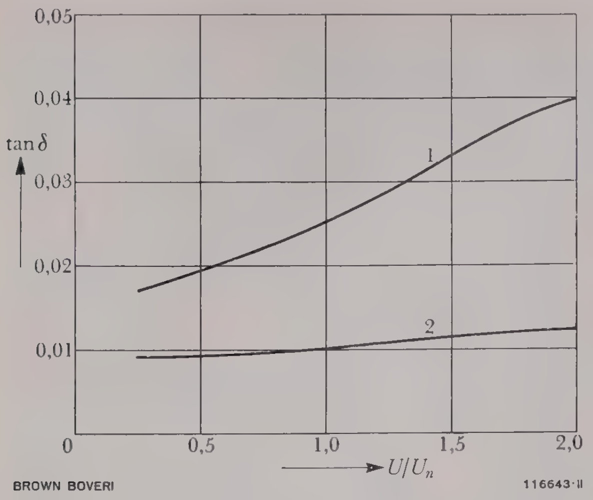

Fig. 8. – Effect of curing temperature on the dielectric properties of a synthetic resin insulation

Loss factor of the insulation plotted against voltage; measured at 20 °C

1 = Cured at 140 °C 2 = Cured at 110 °C

U_n = Rated voltage

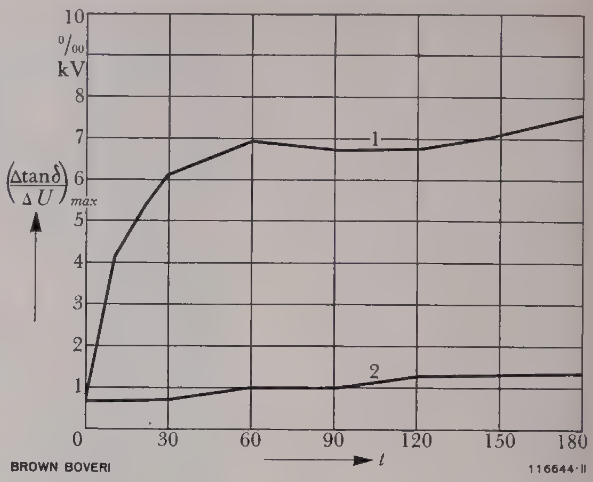

Fig. 9. – Effect of ageing on insulations impregnated with different resins

The maximum rate of rise of loss factor is plotted against the ageing time t in days. Ageing temperature 160 °C, measurement at 20 °C.

1 = Polyester resin, mica paper with glass fabric as base

2 = Modified epoxy resin 'A', mica paper with glass fabric as base

and plotted in terms of the ageing time. Fig. 5, for example, shows the curve of the loss factor tan δ against the voltage. The observations also include the effect of corona discharge on the arrangement, as shown in Fig. 6.

In addition to developing the main insulation, other parts of the system had also to be devised from scratch. Fig. 7, for instance, shows the results of testing the adhesion between conductors after ageing for different lengths of time. Conductors wrapped with glass-based insulation and impregnated with a suitable resin gave the best results in every test.

Investigation of Test Bars

Having selected the best materials, as described above, a number of test bars were made up in the laboratory. Apart from testing the material, investi-

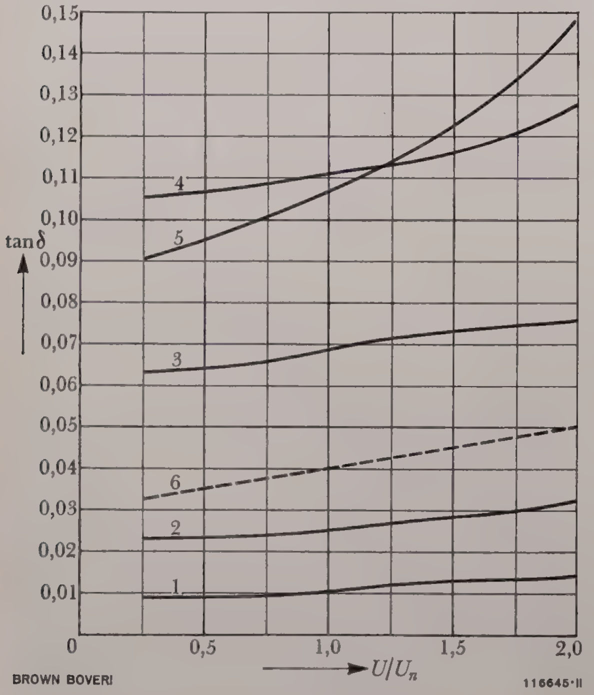

Fig. 10. – Comparing the effect of temperature on the variation of tan δ with voltage for Micadur insulation and asphalt micafolium

1–4 = Micadur

5 = Asphalt micafolium at 90° C.

6 = Reference value: rate of rise of loss factor ($\Delta \tan \delta / \Delta U$) = 0·1% per kV

Temperatures:

1 = 20 °C

2 = 110 °C

3 = 130 °C

4 = 150 °C

U_n = Rated voltage

The test bars were heated and measured without any means of compression (dummy slot)

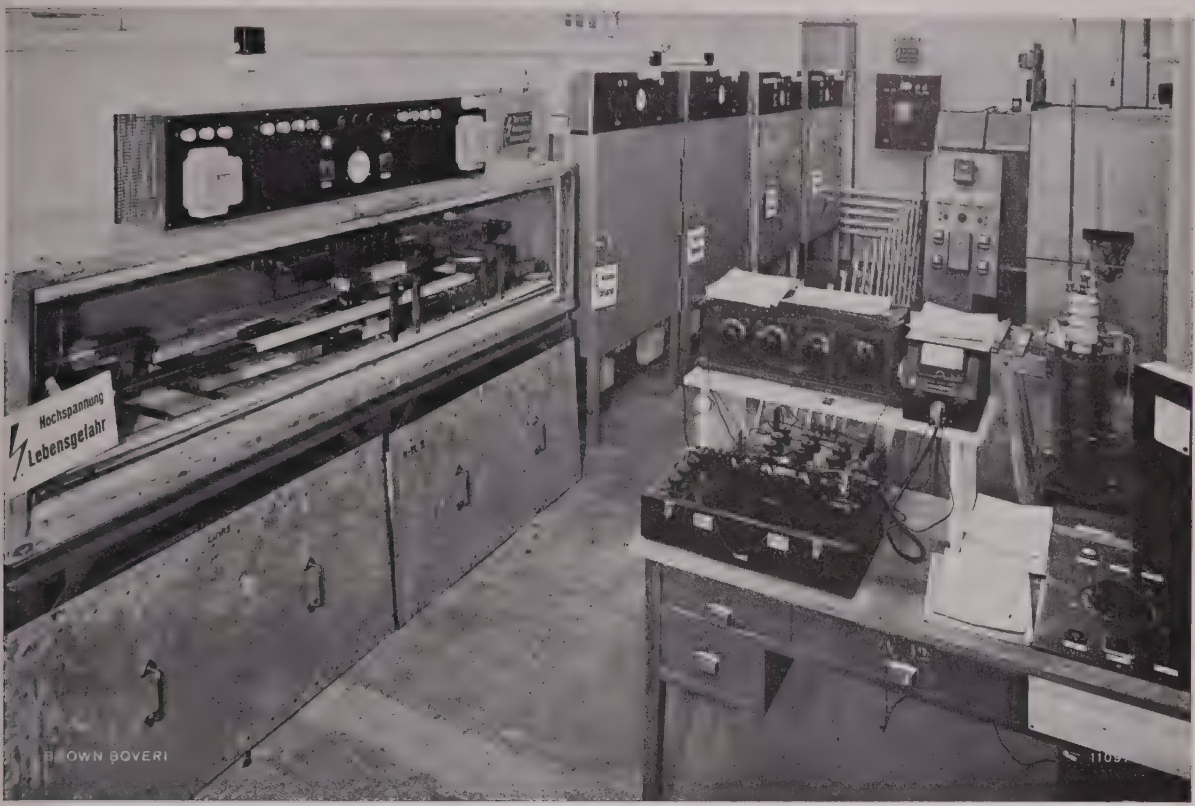

Fig. 11. – Ageing tests on various insulation systems

Showing the oven used for ageing tests on bars at temperatures between 80 and 160 °C. During these tests some of the bars were also subjected to a continuous stress of 50% in excess of the rated voltage. To aggravate the conditions, the insulation was not held in any means of compression (dummy slot).

In the foreground: the equipment for measuring the loss factor in terms of the voltage at various temperatures up to 150 °C.

gations were also carried out regarding factors affecting production, e.g. the best vacuum pressure, the curing temperature (Fig. 8), and so on.

Various methods of measurement were tried out apart from tan δ measurements, especially those which allow the precise nature of changes to be investigated. These include measurement of the insulation resistance, the polarization index, corona intensity and the dielectric strength on d.c.

Every test bar was first tested with regard to its properties when brand new and, if these were satisfactory, was then subjected to endurance tests. As

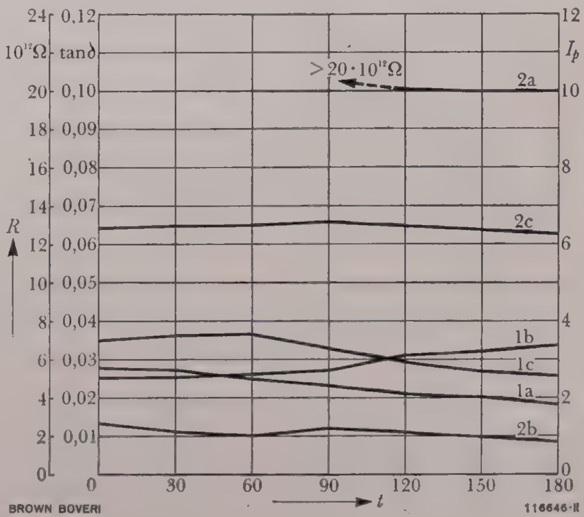

Fig. 12. – Change in dielectric properties of an insulating system with respect to time

Constant temperature 40 °C, constant relative humidity 80%

1 a–c = Asphalt micafolium
2 a–c = Micadur
1 a, 2 a = Resistance R in ohm measured at 500 V d.c.
1 b, 2 b = Loss factor tan δ measured at 1·2 times the rated voltage
1 c, 2 c = Polarization index I_p at 500 V d.c.

preliminary tests had already shown, the bonding resin exerts a deciding influence. The results of tests on bars whose insulation was impregnated with different kinds of resin are shown in Fig. 9. The effect of temperature on the loss factor (up to 150 °C) and the rise of tan δ with voltage is shown in Fig. 10. By way of comparison, the figures are also plotted for asphalt micafolium (measured at 90 °C) which for many years was the standard insulation for machines with service voltages up to 36 kV.

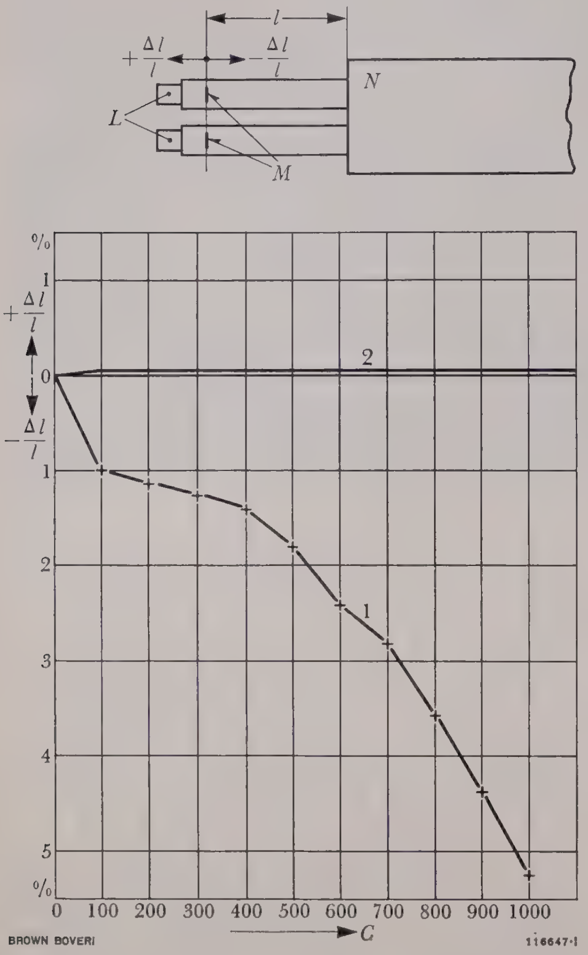

Fig. 13. – Endurance tests with heating and cooling cycles performed on long bars made under factory conditions

Showing the creeping of the insulation into the slot (−) and out of the slot (+) as a function of the number of cycles. The bars were alternately heated to 155 °C by passage of current and cooled to 20 °C by fans. The dummy slots were water-cooled in order to attain the desired temperature gradient in the insulation.

L = Test bar
N = Dummy slot
C = Number of heat/cool cycles
M = Reference mark a distance l from the end of the slot
1 = Asphalt micafolium
2 = Micadur

In order to determine the effect of temperature on the insulation, the test bars were aged at different temperatures. For insulation exposed to severe thermal stresses (class B) the figure of 160 °C proved to be a good temperature for assessment of the insulation, while for less severely stressed insulation (e.g. as used in oil- or water-cooled stator windings) 135 °C is sufficient.

For a number of bars the thermal ageing tests were aggravated by simultaneous voltage stresses. Fig. 11 shows the equipment used for such endurance tests, which were also extended to include the effect of a relative atmospheric humidity of 80% on the insulation at 40 °C. Fig. 12 shows the difference between asphalt micafolium and the almost non-hygroscopic Micadur insulation.

Investigation of Complete Bars

Despite comprehensive and conscientious tests during the development of the new system of insulation, these alone are not sufficient. An unambiguous verdict can only be obtained by carrying out endurance tests on complete bars, produced under factory conditions. During these tests the bars were submitted for several months to the same sort of conditions as they would experience in service, the stresses being somewhat aggravated in order to accelerate the ageing process. For typical arrangements the endurance tests are depicted in Fig. 13 and 14.

Owing to the difference between the coefficients of expansion of iron and copper, changes in the load on the machine can cause the insulation to expand or contract, thus leading to cracking, swelling, loss of adhesion by the resin, or creeping by the insulation. The insulation systems were tested in this respect during a thousand heating and cooling cycles, at the same time being subjected to a voltage 50% in excess of the rated value. Dielectric and mechanical check measurements were taken every

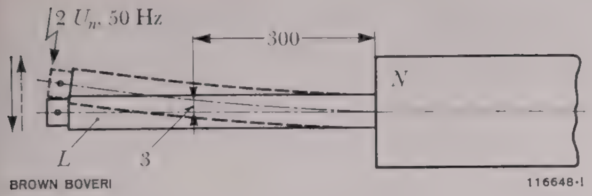

Fig. 14. – Endurance tests with bending stresses performed on long bars made under factory conditions

L = Test bar N = Dummy slot

The insulation is stressed with twice its rated voltage and bent until breakdown occurs.

Hz = c/s

250 cycles. Fig. 13 shows the relative extents of the creeping of asphalt micafolium and Micadur insulation.

On account of the mechanical stresses to which the insulation is exposed when the bar is being inserted in the stator slot, and the stress on the coil-end in the event of a short circuit, the insulation must not be brittle. Fig. 14 shows the results of bending tests, in the course of which the bars were bent several thousand times. The results are listed in the Table below, showing the relative qualities of insulating systems containing glass and different resins.

Insulation system	Deflection of bar 300 mm from end of slot	Number of times bent before breakdown occurred
Glass-based fabric impregnated with polyester resin	3 mm	⩽ 20 000
Micadur glass-based fabric impregnated with modified epoxy resin A	3 mm	⩾ 50 000

A further important factor is the electric strength of an insulation. With a thickness previously employed for 10-kV machines, Micadur does not break down until 100 kV when brand new. After ageing for 6 months at 160 °C this figure is only reduced by about 15%. Another important test is the measurement of the breakdown voltage in terms of the duration of the applied voltage.

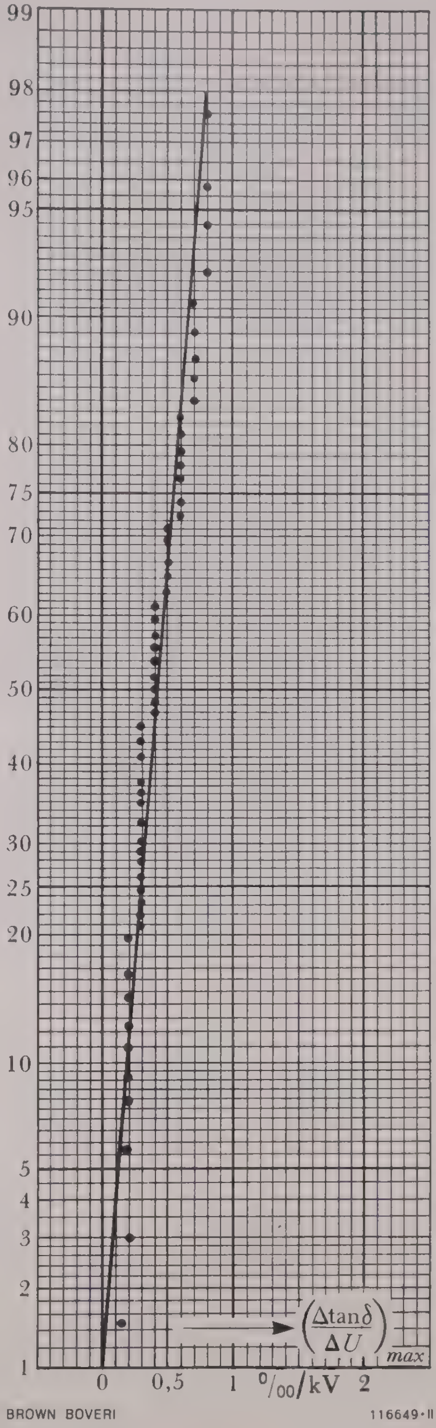

Fig. 15. – Illustrating the effect of the voltage on the loss factor tan δ

Cumulative frequency of measurements plotted as a function of the rate of rise of tan δ between 0·4 and 0·8 times the rated voltage. Measurements carried out on individual bars of a hydro-electric generator.

Production

The method of manufacture and the choice of material are closely linked. Any change in the manufacturing process, or in the material, demands new endurance tests. The notable improvement in quality attained with vacuum-impregnated continuous Micadur insulation was made possible by the use of ideal materials. Compared with micafolium bonded with asphalt or shellac, the new insulation necessitated the development of completely new manufacturing methods.

The stator windings of a number of new machines, some already in service, have been equipped with this new insulation. Others are in the course of manufacture. They include the turbo-alternator illustrated on the front cover, in which the stator winding and iron are both oil-cooled; the rating of the machine is 218 MVA at 12 kV and it has an iron length of 4 m. Other machines are: a short-circuit generator for a rated voltage of 11 kV (iron length 6 m), two hydrogen-cooled turbo-generators with an iron length of 3·4 m, rated 87 MVA at 13·2 kV and 96 MVA at 10·5 kV, respectively. The fact that a high standard of uniformity has been attained in the quality of the insulation of such machines is borne out by the results of acceptance tests on a large hydro-electric generator (Fig. 15).

Conclusions

The exhaustive investigations carried out have led to an insulation impregnated in vacuum with a synthetic resin containing no solvent, using glass fabric as base for carrying the mica.

Now that operational experience has also been gained with this new insulation, in addition to the results of endurance tests, it is being adopted for all machines whose iron length exceeds 3·5 m. The most impressive machines for which it will be employed in the near future, all having an iron length of 5·4 m, are two turbo-alternators rated 270 MVA each at 18 kV and a pair of generators with a combined output of 611 MVA at 24 kV, driven by a cross-compound steam turbine.

(KME)

O. Wohlfahrt
M. Moravec
B. Doljak

TESTS ON VARIOUS METHODS OF VOLTAGE CONTROL FOR USE WITH LARGE GENERATORS

621.316.722:621.313.322

In Piottino power station (owned by ATEL) extensive tests were performed to compare various static voltage controllers with the conventional high-power regulator type KC. The present article discusses the variants used and the results obtained with them, as illustrated by oscillograms. This is followed by a qualitative comparison of the different systems.

THE DEVELOPMENTS in the generation and transmission of electric power impose increasingly severe demands on the equipment regulating the generator voltage. On the one hand, the excitation power needed for machines with high unit ratings can attain values beyond the capacity of the well-tried high-power regulator type KC. On the other hand there are cases in which the stipulations regarding the dynamic behaviour of the control system are most exacting, thus necessitating the replacement of the electro-mechanical regulator by some other system.

An obvious step is for the various modern elements which have proved successful in other spheres to be employed for controlling synchronous machines. The deviations of the controlled voltage from the desired value are then detected at a very low power level and the control signals so derived are conveyed through amplifiers to the exciter field. We have the choice of magnetic amplifiers and amplifiers employing electron tubes or transistors. Since the primary aim, as before, is for its output to be at a high power level so that, if possible, it can be applied direct to the field of the exciter, the controller—i.e. the static part of the control circuit—has to consist of a cascade of amplifiers. Obviously there are many feasible combinations.

The ideal output or power amplifier is the magnetic amplifier because it can easily be constructed for quite high outputs with a very short response time. The Brown Boveri programme now includes magnetic amplifiers with outputs up to 200 kW with which, as far as can be visualized, the largest exciters likely to be built can be controlled direct.

Likewise, as pre-amplifier and, in some cases, intermediate amplifier it is possible to use magnetic amplifiers or alternatively tube or transistor amplifiers (Fig. 1a). In this case the control function is

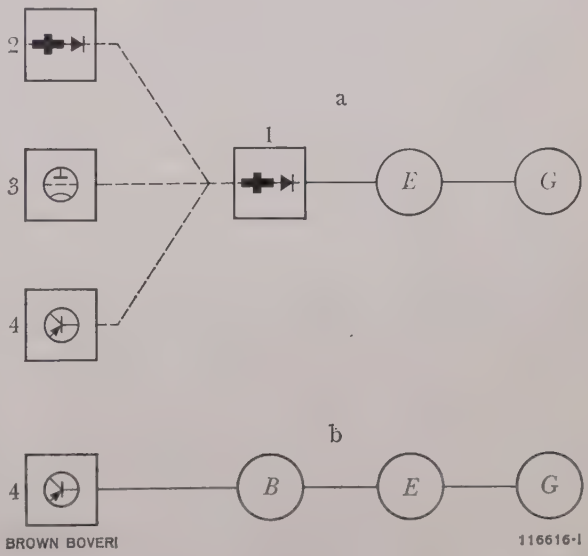

Fig. 1. – Alternative fundamental control systems

G = Generator
E = Exciter
B = Intermediate exciter
1 = Transductor power amplifier
2 = Transductor controller
3 = Controller employing electron tubes
4 = Transistorized controller

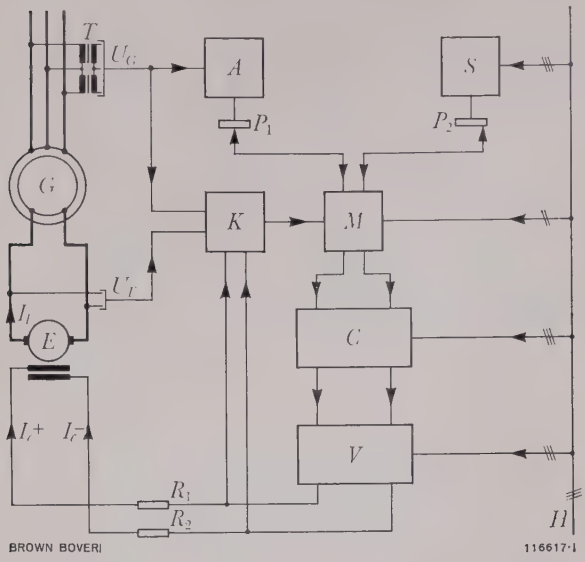

Fig. 2. – Circuit diagram of voltage regulation with magnetic amplifiers

G = Generator
E = Exciter
T = Voltage transformer
R_1, R_2 = Resistors
A = Actual-value element
S = Desired-value element
P_1 = Setting resistor ±10%
P_2 = Coarse control resistor 20–100%
K = Feedback element
M = Magnetic amplifier regulator
C = Intermediate magnetic amplifier
V = Power amplifier
H = Auxiliary supply
U_G = Generator voltage
U_E = Exciter voltage
I_E = Rotor current
I_e+, I_e- = Output currents of controller

actually performed by the pre-amplifier. These different variants have all been tested experimentally in order to find out which is most suitable under given circumstances.

In addition, a control cascade was also developed consisting of a transistorized controller with two-step action and an intermediate exciter (Fig. 1b). This exciter is a single-stage rotating amplifier with a very rapid response.

By kind courtesy of the Aare-Tessin Electricity Co. (ATEL) a rare opportunity was granted for carrying out comprehensive tests in their Piottino power station, where the static control systems could be compared with the type KC high-power regulator. The various methods of excitation (separate, series, shunt) were also compared at the same time. This article, however, is confined to the comparison of the different control systems. These tests, for which the exciter was always separately excited, mainly involved the shedding of leading and lagging reactive loads.

The available machines had the following data:

Generator: 23 MVA, 8·2 kV, 1620 A, 750 rev/min
$X_d = 131\%$, $X'_d = 30\%$, $X''_d = 17\%$,
$T_{d0} = 5{\cdot}3$ s

Exciter: 125 kW, 250 V, 500 A, 2940 rev/min
Voltage at rated generator output 175 V
Ceiling voltage 375 V
$T_E = 0{\cdot}35$ s, Response ratio $= 3{\cdot}25\ \text{s}^{-1}$

Voltage Control Using the Transductor Controller

The design and principle of the magnetic amplifier were amply dealt with in a previous article [1] and do not need to be repeated here. It is sufficient to say that these amplifiers are very robustly constructed and have extremely good dynamic characteristics. These reliable units contain neither moving parts nor contacts and are therefore completely static.

Circuit with Transductor Pre-amplifier

This arrangement of this circuit is shown in Fig. 2. The voltage controller comprises the three-stage magnetic amplifier cascade M, C and V, the desired-value element S, the actual-value element A and the feedback element K. S is a high-grade voltage stabilizer. Its output voltage (d.c.) is almost completely independent of input voltage, frequency or temperature. The element A measures the generator voltage three-phase and, by rectification and addition, produces a d.c. voltage corresponding to the mean of the three phase-to-phase voltages. Following each of these elements there is a potentiometer, one for coarse and the other for fine setting of the generator voltage. In the first magnetic amplifier

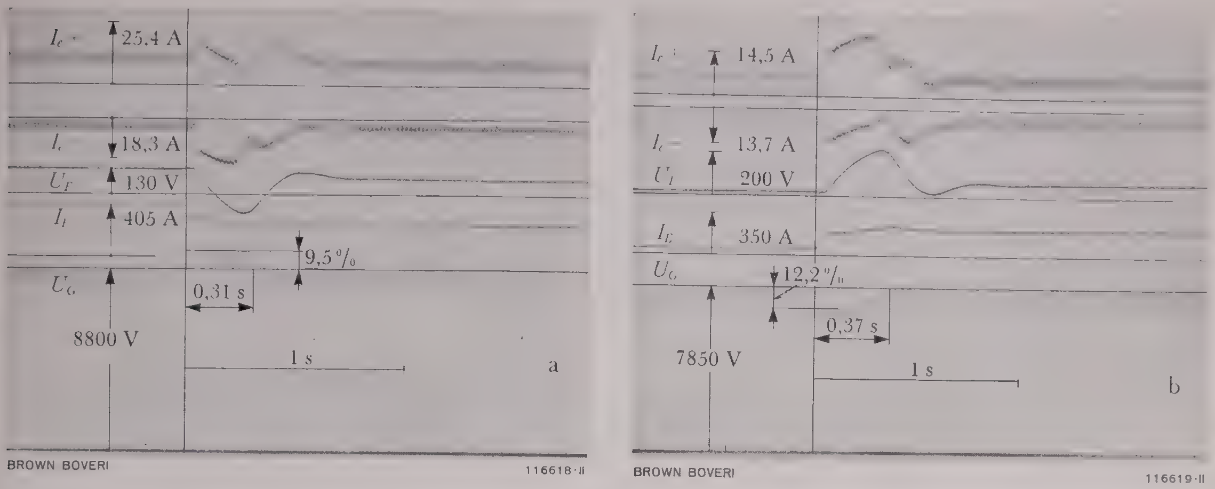

Fig. 3. – Oscillograms of test with the transductor controller

(a) Shedding 50% lagging reactive load

(b) Shedding 50% leading reactive load

Notation as in Fig. 2.

stage *M*, which is the comparison element, the actual value of the voltage is compared with the setting (desired value), the difference between them influencing the pre-amplifier *M* and the succeeding amplifier stages *C* and *V*. The entire amplifier cascade operates in push-pull, the output currents flowing in opposite directions through the two field windings of the exciter *E*. The controller has a proportional action. The circuit is stabilized by three differential feedbacks, i.e. from the generator, the exciter and the two output voltages of the power amplifier *V*. It would have been possible to give the controller a PID (proportional-integral-derivative) action, thereby eliminating the feedbacks. Such PID controllers are standard Brown Boveri components [1]. With equivalent stabilization the results would be very similar.

During the tests the power stage had an output of 5·5 kW per half. The gain was made such that the error in proportionality between no-load and full-load was about 0·5%, thus being comparable with the values normally stipulated for voltage regulation. The total time constant of the amplifier cascade, including dead time, was only about 45 ms for sudden small changes on the linear part of the characteristic.

The oscillogram in Fig. 3a shows the effect of shedding 50% lagging reactive load. The two upper curves show the output currents of the controller I_e+ and I_e-, which flow in opposite directions through the field windings of the exciter. Due to the magnetic coupling of these windings, the currents influence one another. A rapid change in one current produces a peak in the opposite direction in the other current, as may be observed very clearly at the beginning of the control process. Appropriate series resistors are incorporated to avoid the resultant increase in the time constant of the exciter. A notable feature is the rapid decrease in the exciter voltage U_E, the initial gradient of which is around 1600 V/s; it becomes zero after only 0·13 s. The outcome of this is that the generator voltage U_G hardly rises at all after the first jump caused by the data of the generator. The time taken to regain the desired value (henceforth referred to as "settling time") is only 0·31 s. After this there is a slight underswing of about 20% of the maximum deviation before the steady state is completely restored. Therefore the stability is also very good.

An oscillogram showing the effect of shedding 50% leading reactive load is shown in Fig. 3b. In this case the settling time was 0·37 s.

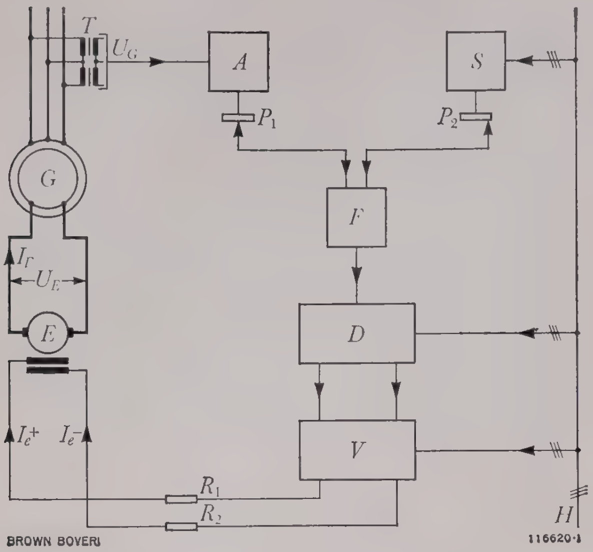

Fig. 4. – Circuit diagram for voltage control by a controller employing electron tubes with a transductor power amplifier

G = Generator
E = Exciter
T = Voltage transformer
R_1, R_2 = Resistors
A = Actual-value element
S = Desired-value element
P_1 = Fine setting resistor
P_2 = Coarse setting resistor
F = Filter
D = Controller (tubes)
V = Transductor power amplifier
H = Auxiliary supply

Other notation as in Fig. 2.

As regards stability, it may be pointed out that this can naturally be set differently. If the oscillation is to be more heavily damped, a longer settling time must be expected. It is therefore quite an easy matter to allow for customers' requirements in this respect.

Circuit with Instantaneous Pre-amplifier Stage

With this variant the intention was to examine the effect of reducing the response time of the controller on the dynamic behaviour of the whole circuit. To do this a controller containing electron tubes was connected before the power amplifier. Since tubes and transistors have the same properties from the control point of view, the results of these tests may also be applied to transistorized pre-amplifiers.

The block diagram in Fig. 4 shows the version with the tube pre-amplifier and a transductor power stage. For formation of the desired and actual values the same elements *S* and *A* were used as before. Through a stabilizing filter *F* which has a PID action, the difference voltage influences the push-pull tube controller *D*. This controls the power amplifier *V* direct; the outputs of the latter again feeding the two fields of the exciter *E*. The com-

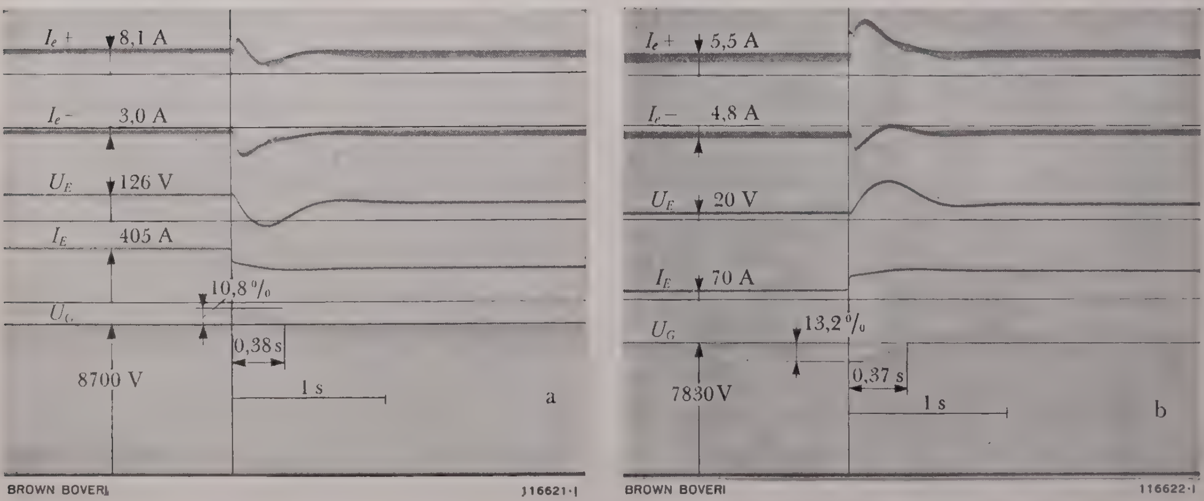

Fig. 5. – Oscillograms of tests with an electron tube controller and transductor power amplifier

(a) Shedding 50% lagging load

(b) Shedding 50% leading load

Notation as in Fig. 4.

parison element was a normal type of regulator of the kind frequently used for heavy drives, in particular for rolling mills. The control circuit is stabilized by the filter F alone, therefore no feedback is required.

Oscillograms showing the effect of shedding 50% lagging and leading load are reproduced in Fig. 5a and 5b. Here the short dead time is particularly pronounced. Since the tube controller is instantaneous in its action, there remains only the dead time of the magnetic amplifier stage, which measured 12 ms. The settling times are slightly longer than, or equal to the circuit consisting wholly of magnetic amplifiers. Nevertheless control is somewhat more stable, as indicated most forcibly by the curve of the exciter voltage.

With equivalent settings of the stability the settling times would probably be shorter, but the differences between the two systems are insignificant when the whole control circuit is considered. It is therefore almost impossible to improve the dynamic behaviour by reducing the response time of the comparison element. This is obvious, when it is considered that the time constants of the controlled object, i.e. the exciter and the generator, differ by several orders of magnitude from that of the controller.

Having established this fact, and knowing that there is no demand for controllers employing electron tubes for use with synchronous alternators, this system was discarded in favour of the solution employing only transductors.

Transistorized Controller with Intermediate Exciter

Owing to their excellent properties transistors have become extremely popular in recent years, especially for control applications. With their instantaneous action and freedom from wear they combine the dynamic advantages of electron tubes with the long life of the transductor. Since the permissible power dissipation in the transistors at present obtainable is relatively low, they are preferably employed as switches. In this case the power which can be controlled is not governed by the power dissipated, but by the maximum admissible values of collector current and collector voltage. Thus transistorized controllers can be constructed for outputs up to several hundred watts.

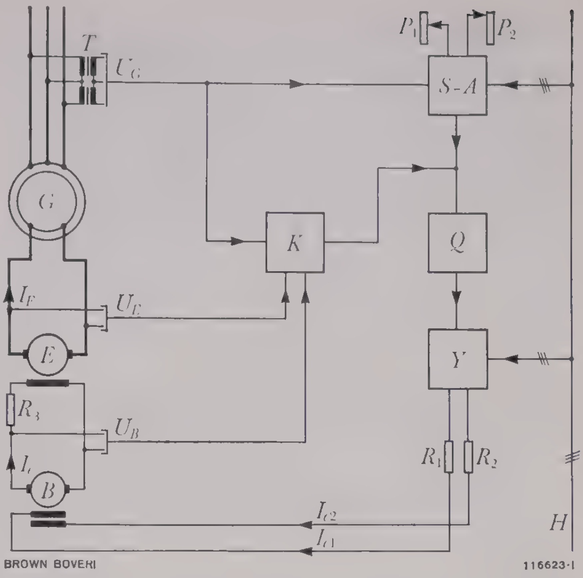

Fig. 6. – Circuit diagram for voltage regulation with a transistorized controller with two-step action and an intermediate exciter

G = Generator
E = Exciter
B = Intermediate exciter
T = Voltage transformer
S–A = Comparison of desired and actual values
P_1 = Fine setting resistor
P_2 = Coarse setting resistor
K = Feedback element
Q = Trigger stage
Y = Transistorized amplifier
H = Auxiliary supply

Other notation as in Fig. 2.

The transistorized voltage controller developed by Brown Boveri consequently has a two-step action. As a result of the high output power which is thereby made available, there is no need for more than one intermediate excitation stage, thus realizing the view held by Brown Boveri, namely that the controller output should be at the highest possible power level.

The block diagram in Fig. 6 shows the layout of the control circuit. The controller consists mainly of a bridge circuit $S-A$ (in which the desired and

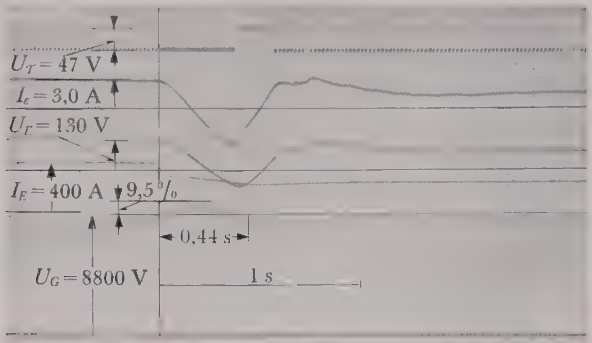

Fig. 7. – Oscillogram showing the effect of shedding 50% lagging load when using a transistorized controller with two-step action

U_T = Voltage across output transistor
Other notation as in Fig. 2.

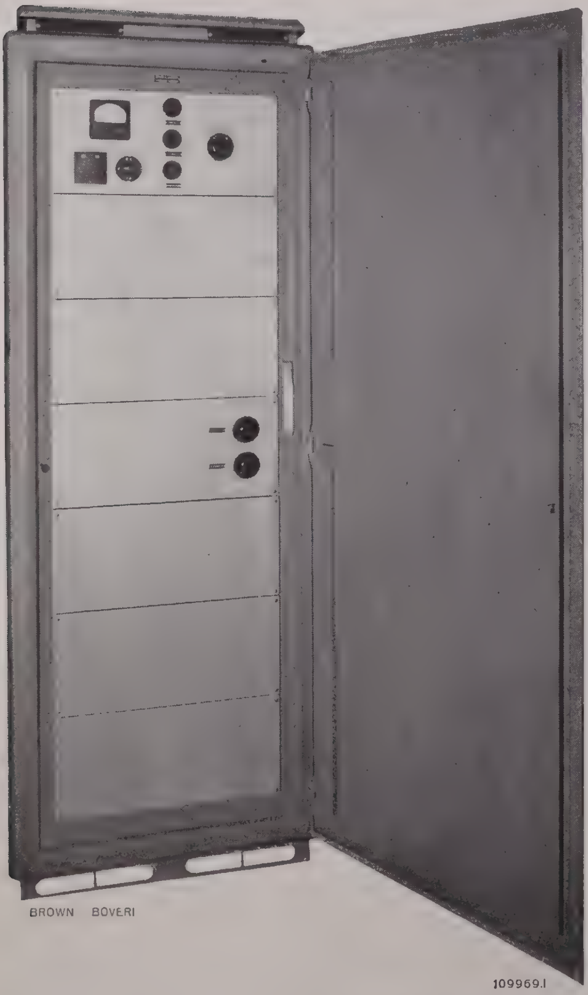

Fig. 8. – Front view of a transistorized controller with two-step action and push-pull output

The various sub-units are mounted on separate chassis attached to a hinged frame and are therefore easily accessible.

actual values are compared), a feedback element K, a trigger stage Q (timer), and the transistorized amplifier Y. The controller used for the tests at Piottino, in contrast to the transductor variant, did not operate in push-pull. Only the positive field of the quick-acting exciter B was controlled; the negative field being fed at constant voltage. While the positive ceiling voltage and the time constant of the main exciter E were the same as for the other variants, the maximum negative voltage was only 80% of the ceiling value.

The oscillogram in Fig. 7 shows the effect of shedding 50% lagging reactive load. At the top is U_T, the voltage across the output stage of the transistorized amplifier. It can be seen that the controller oscillates continuously between two definite points. The mean value of the output value depends on the ratio of the pulse duration to the length of the pause. The transistor only stays open or blocks for any length of time when the deviation of the generator voltage is fairly large. But blocking or opening is instantaneous, i.e. there is no dead time or time constant involved. The controller is extremely sensitive, so that hardly any offset can be detected. Its output current naturally contains a considerable amount of ripple but this is completely smoothed by the time constants of the subsequent machines. The exciter voltage U_E has already lost all the ripple.

The decrease in the exciter voltage is less rapid in this case than it was with the transductor variant; consequently the settling time is increased to 0·44 s. This is partly due to the relatively high time constant of the intermediate exciter (110 ms) and partly to the use of a reduced negative ceiling voltage. The time constant of the intermediate exciter is largely dependent upon its output and its gain. If it is designed to have a very rapid response, the values attained are generally below 100 ms.

From the control point of view it is also desirable for the maximum negative voltage of the exciter to be as high as possible; it would be ideal for it to equal the positive ceiling value. But for the circuit described this would increase the output which the

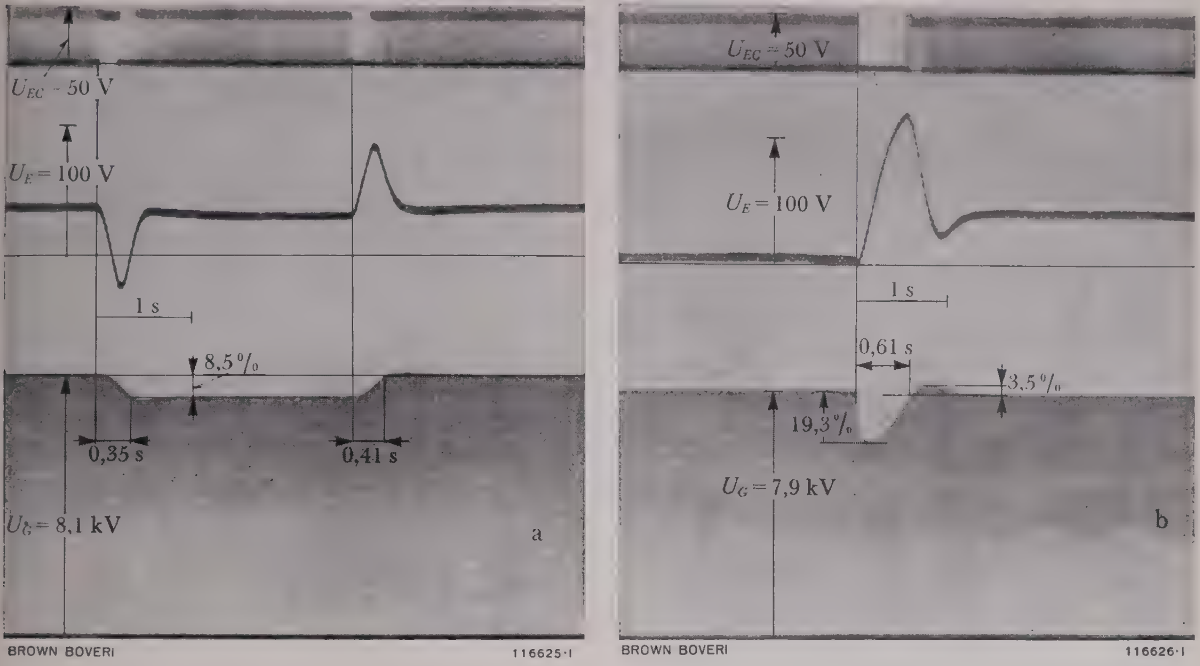

Fig. 9. – Oscillograms of tests with a transistorized controller with two-step action and push-pull output

(a) Sudden displacement of desired value of voltage with generator at no-load

(b) Shedding 60% leading reactive load

U_G = Generator voltage
U_E = Exciter voltage
U_{EC} = Voltage across an output transistor

controller has to produce. This can be avoided by adopting the push-pull system. With a corresponding arrangement, the circuit was left the same as far as the trigger stage. Now this element not only controls the positive amplifier but, through a reversing stage, it also controls a negative amplifier.

Fig. 8 is the front view of a controller of this kind. The various sub-units are mounted on separate chassis in a hinged frame, making them easily accessible.

Using this controller operational tests were carried out with a turbo-alternator in the Company's works in Baden. The data of the machines were as follows:

Generator:	1875 kVA, 8 kV, 135 A, 3000 rev/min	
Exciter:	Voltage at rated generator output	92 V
	Ceiling voltage	150 V
	Time constant (unsaturated)	0·56 s

The oscillograms in Fig. 9a and b were recorded during these tests. The first of these shows the effect of suddenly altering the setting of the desired-value potentiometer at no-load. The second oscillogram shows the effect of shedding 60% leading reactive load. Both oscillograms illustrate the good stability of the control system. Despite the much smaller output of the controlled generator the settling times were considerably longer than the corresponding results obtained at Piottino. This is due to differences in the exciter data.

High-Power Regulator Type KC with Supplementary Device

The comparative tests at Piottino power station were also extended to the high-power regulator type KC, of which about 1000 are in service in many parts of the world. For these tests the regulator was augmented by a supplementary device with a derivative action (it is therefore known as the D-device) (see Fig. 10). The arrangement of the circuit is shown in Fig. 11. At the top is the type KC regulator 4, represented by its main components, the

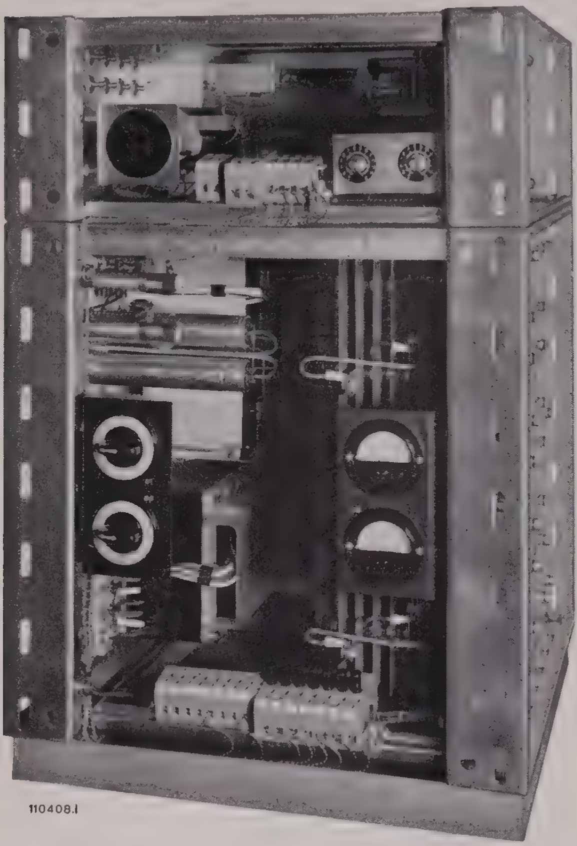

Fig. 10. – Supplementary unit with derivative action (D device) without its casing

This device augments the high-power electro-mechanical regulator type KC. It provides a derivative component which can be superposed on the voltage measuring circuit of the regulator, thereby rendering control more sensitive and quicker.

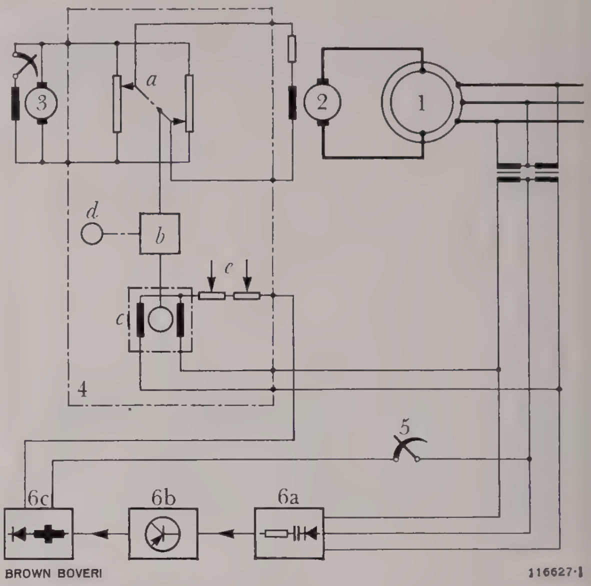

Fig. 11. – Simplified circuit diagram of the high-power regulator type KC with a D device

1 = Generator
2 = Exciter
3 = Pilot exciter
4 = Regulator type KC
  a = Rheostat
  b = Servo-motor
  c = Control element
  d = Pump motor
  e = Setting resistor for stabilization and compounding
5 = Resistor for setting voltage
6 = D device
  a = Differentiating element
  b = Transistorized amplifier
  c = Magnetic amplifier

commutator with regulating resistors *a*, the servo-motor *b*, and the control element *c*. In the D device 6 the generator voltage is rectified, differentiated and amplified. Ignoring a slight time-lag, the output voltage is proportional to the rate of change of the generator voltage and is superposed on the measuring circuit of the KC regulator. The magnitude of the influence and the time constant of the differentiating element can be adjusted separately and the best possible match with the control circuit obtained.

As a result of the derivative action of this supplementary device it is possible to increase the rate of response of the KC regulator [2]. It has been proved that the effect of the D device is particularly favourable when the change in voltage is small. It is possible to improve the settling time by up to 30% on the average. In the event of larger voltage changes, e.g. resulting from shedding full rated load, the effect of the D device on the settling time is not so great because the regulator then runs back to its end position at maximum speed of its own accord.

The maximum output currents of the regulator were symmetrical and produced the same positive and negative ceiling voltages as the transductor variants. The maximum time constant of the exciter was also roughly equal. But here it must be mentioned that this time constant varies with the position of the brushes under the influence of the bridge

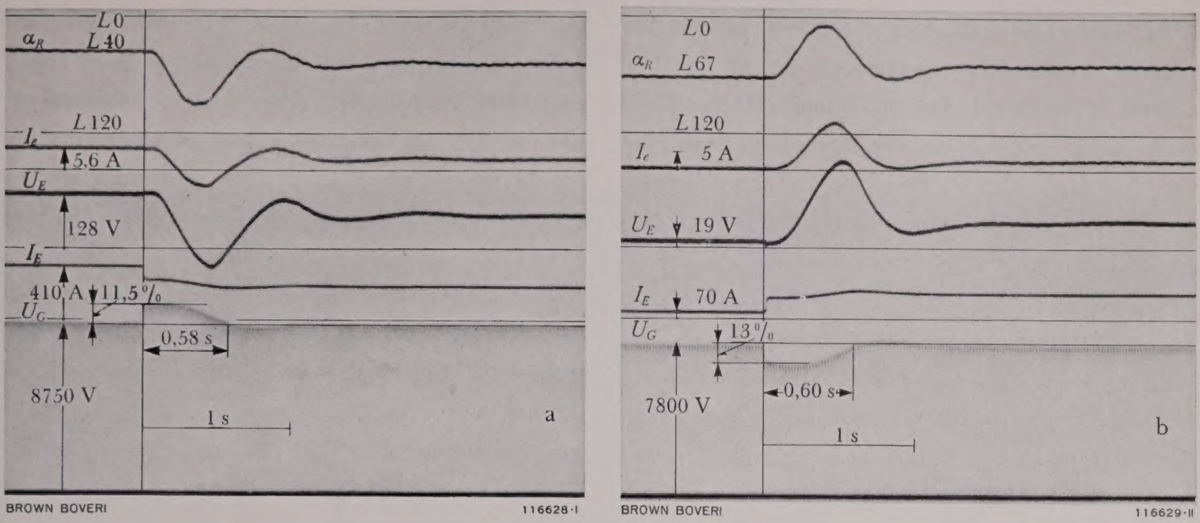

Fig. 12. – Oscillograms of tests with a high-power voltage regulator type KC augmented by a D device

(a) Shedding 50% lagging reactive load
(b) Shedding 50% leading reactive load
α_R = Position of regulator
I_e = Field current of exciter
U_E = Exciter voltage
I_E = Rotor current
U_G = Generator voltage
L (with suffix) = Segment of the commutator

resistance of the regulator. One of the advantages of the type KC regulator is that its natural time constant only applies to the two end positions, while for intermediate positions it is reduced accordingly. During the tests, the time constant was reduced to about ¼ at no-load, for instance.

It is often contended that mechanical regulators are insufficiently sensitive, due to friction. This is hardly true of the type KC regulator, the dead band of which amounts to only ±0·1 to 0·2% and is not noticeable at all in operation.

The oscillograms (a) and (b) in Fig. 12 once more show the effect of shedding 50% lagging and leading load. The settling times are respectively 0·58 and 0·60 s with roughly the same stability as before. They are therefore some 75% slower than the transductor variants. But it must be borne in mind that for all these tests the settling times are, generally speaking, very short due to the favourable data of the exciter, so that the difference appears quite large when expressed as a percentage. But this soon changes when an exciter is used which has a lower ceiling voltage and longer time constant. Here very little can be gained by inserting a quicker-acting regulator.

Conclusions

During the tests, steps were taken to ensure that the various control systems could be compared on a common basis as regards their dynamic behaviour. To achieve this the ceiling voltage and time constant of the exciter, as well as the stability of the control circuit was made practically equal in each case. Thus the comparison can be made on the basis of the settling times measured. The settling times of the transistor variant are slightly longer than the transductor variant, the main difference being due to the time constant of the intermediate exciter. When the latter was reduced to about 50 ms, the settling times became approximately equal.

Control system	Settling time in s	
	Shedding 50% lagging load	Shedding 50% leading load
Transductor controller	0·31	0·37
Transistor controller + intermediate exciter	0·44	0·44
KC regulator + D device	0·58	0·60

As was to be expected, these two systems are superior to the KC regulator, as far as speed of control is concerned; but the actual differences are quite small and only assume any significance in a very few cases. The results prove that the KC regulator also belongs in the category of controllers with rapid response. As already mentioned, it will generally prove more effective to design the main exciter for an adequate ceiling voltage and reduce its time constant than to use a quicker controller. It has already been proved on numerous occasions that the KC regulator is capable of an excellent performance under difficult circumstances. It is sufficient to mention the stability tests at Piottino, where the generator ran steadily with a load angle of 117°el., and even reached 120° for a short period [3].

The expansion of the Company's manufacturing schedule in the sphere of voltage regulation for large machines, by the addition of transductor and transistor controllers, makes it possible for all customers' requirements and wishes to be taken into account, and the most expedient solution put forward in every case. Owing to its good technical qualities, its simplicity and favourable price, the high-power electro-mechanical regulator type KC will also prove to be the most suitable solution to many future problems. Where improvement of its dynamic behaviour appears desirable it can be augmented by the D device. Static controllers will primarily be considered when difficult operating conditions make it essential for control to be as rapid as possible; this of course does not include the cases where a customer declines to accept an electro-mechanical regulator on principle or where the power required for the field of the exciter exceeds the capacity of the KC regulator. Finally it may be pointed out that in extremely difficult cases, it is still possible to put forward excitation by mercury-arc rectifiers [4].

(KME) A. DUDLER

Bibliography

[1] G. HANKE: Brown Boveri Magnetic Amplifier Units. Brown Boveri Rev. 1957, Vol. 44, No. 11, p. 497–504.

[2] Brown Boveri Rev. 1959, Vol. 46, No. 1/2, p. 37–8.

[3] Brown Boveri Rev. 1959, Vol. 46, No. 1/2, p. 39–40.

[4] R. NOSER and W. FREY: Recent developments in the excitation and control of synchronous machines. CIGRE Report No. 127/1958.

Machine room of the Riddes high-head hydro-electric generating station in Valais, Switzerland, with five Brown Boveri alternators rated 67 MVA each at 500 rev/min. The station thus has an aggregate output of 335 MVA

Published by Brown, Boveri & Company, Limited, Baden, Switzerland. Printed by Kreis & Co. AG., Basle, Switzerland
Obtainable direct from the publishers